



Review article

A tectono-stratigraphic review of continental breakup on intraplate continental margins and its impact on resultant hydrocarbon systems

Tiago Alves^{a,*}, Marcos Fetter^b, Cathy Busby^c, Rogerio Gontijo^b, Tiago A. Cunha^d, Nathalia H. Mattos^{a,e}

^a 3D Seismic Lab – School of Earth and Ocean Sciences, Cardiff University – Main Building, Park Place, Cardiff, CF10 3AT, United Kingdom

^b Petrobras-E&P, Av. República do Chile 65, Rio de Janeiro, 20031-912, Brazil

^c Department of Earth and Planetary Sciences, University of California, Davis, CA, 95616, USA

^d Integrated Geochemical Interpretation Ltd., The Granary, Hallsannery, Bideford, Devon, EX39 5HE, United Kingdom

^e Applied Geophysics Group, Institute of Geosciences - Universidade Estadual de Campinas Rua Carlos Gomes, 250 Campinas, 13083-855, Brazil

ARTICLE INFO

Keywords:

Continental margins
Continental breakup
Subsidence
Sedimentation
Structure
Hydrocarbons

ABSTRACT

Intraplate Continental Margins comprise fully rifted areas of continents and cratons recording the tectonic events associated with plate breakup and subsequent continental drift. In contrast to extensional basins, this tectonism post-dates the initial stages of continental rifting of tectonic plates and is specifically associated with the breakup and ‘drifting’ of continents. Seismic and outcrop data from eight (8) Intraplate Continental Margins are reviewed in this work and tectonic-subsidence models are compiled to highlight their large-scale structural and depositional variability. Specific geological aspects that enhance the hydrocarbon potential of Intraplate Continental margins include: a) syn-rift strata that are strikingly thicker, and presumed older, than previously assumed on vintage seismic profiles, b) an important control of basement type and fabric on tectonic subsidence and subsequent reactivation after continental breakup is achieved, and c) widespread extensional collapse accompanying the continental breakup process to generate a phase of important sediment bypass into relatively deeper, distal depocentres. There is evidence on seismic data that the continental breakup process per se overprints older syn-rift structures to create a complex mosaic of uplifting and subsiding basins that may not coincide in location and extent with early syn-rift depocentres. This character has the potential of generating vast amounts of reservoir strata during tectonically active periods, at the same time enhancing the influx of organic matter to basins distant from point-sources of sediment during continental breakup. As a corollary, a classification of *breakup sequences* is presented in this work and a new case-study from South California is developed to acknowledge the varied hydrocarbon-generating settings of Intraplate Continental Margins when continental breakup is established.

1. Introduction

Continental rifts formed on new cratons and tectonic plates can evolve into nascent ocean basins bordered by Intraplate Continental Margins that obey four main configurations: shelf-slope-rise, transform, embankment and halokinetic (Ingersoll, 2011; Busby and Azor, 2012). Continental rifts that do not evolve into oceans become fossil rifts, important regions rich in hydrocarbons that later become sites for development of intracratonic basins and aulacogens. If all plate boundaries within and around an ocean basin become inactive, a dormant ocean basin develops, underlain by oceanic crust and surrounded by continental crust (Dietz, 1961; Busby and Azor, 2012). Intraplate Continental Margins thus record important tectonic movements

whenever older crustal structures are reactivated in association with far-field crustal stresses (Sykes, 1978; Sibson, 1994; Hand and Sandiford, 1999; Sandiford and Egholm, 2008; Holford et al., 2011; Pinet, 2016; Craddock et al., 2017). Such a tectonism post-dates the initial stages of continental rifting of tectonic plates and is specifically associated with the breakup and ‘drifting’ of continents (e.g. Davison et al., 2015; Kukla et al., 2018). Magmatic events during the continental breakup and drift stages, together with regional stress ‘readjustments’, are additional phenomena capable of imposing important changes in plate motion and near-field tectonic stresses (Koptev et al., 2016; Cavazza et al., 2015).

With such a complex setting in mind, the term Intraplate Continental Margins, or ICMs as used herein, was recently introduced to

* Corresponding author.

E-mail address: alvest@cardiff.ac.uk (T. Alves).

<https://doi.org/10.1016/j.marpetgeo.2020.104341>

Received 9 August 2019; Received in revised form 28 February 2020; Accepted 2 March 2020

Available online 20 March 2020

0264-8172/© 2020 The Authors. Published by Elsevier Ltd. This is an open access article under the CC BY license (<http://creativecommons.org/licenses/by/4.0/>).

Location of data sets analysed in this review

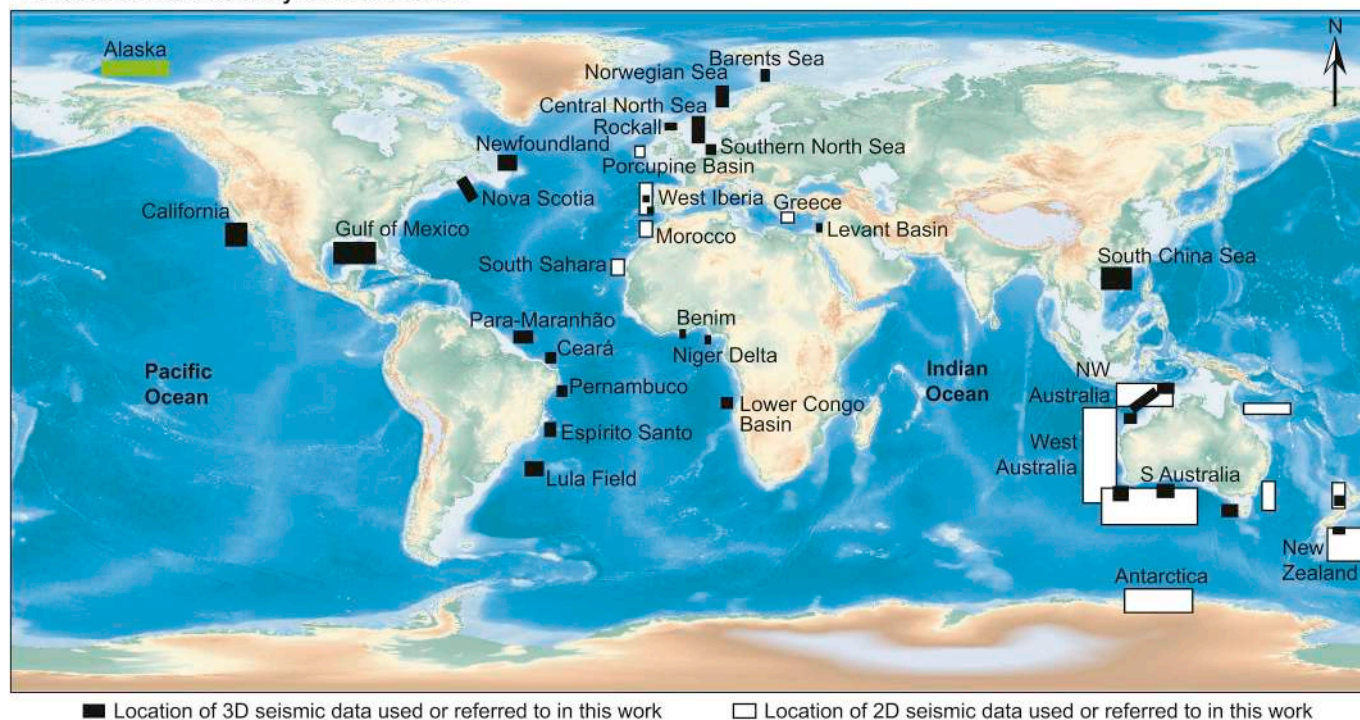


Fig. 1. Location map of the studied 3D seismic volumes and outcrop locations referred to in this paper. Outcrop analogues in this work are from Crete and Portugal, in the areas where Greece and West Iberia are indicated in the figure. According to their definition, ICMs are generated during the last tectonic events leading to continental breakup, developing fully during continental drifting. This character excludes aulacogens such as the North Sea, Gulf of Corinth, East African Rift or interior basins in Central Asia from being ICMs.

represent the wide spectrum of tectonic settings previously mentioned in the scientific literature (e.g. [Ingersoll, 2011](#); [Busby and Azor, 2012](#)). Three fundamental characteristics differentiate ICMs from other margins. First, ICMs solely refer to the fully rifted margins of tectonic plates and continents regardless of the styles (and geometries) of continental rifting and breakup they record through time. The definition of ICMs does not include aulacogens, plate interior basins and intraplate rifts such as the North Sea, Gulf of Corinth, East African Rift or interior rift basins in Central Asia. ICMs are formed during the last tectonic events leading to continental breakup, developing fully during continental drift ([Fig. 1](#)).

Second, the definition of ICMs considers ‘passive’ or ‘rifted’ margins as representing oversimplified terms for regions that are, in all effects, tectonically active well after continental breakup is achieved ([Hillis et al., 2008](#); [Sandiford and Egholm, 2008](#); [Ebinger and Belachew, 2010](#)) ([Fig. 2](#)). The margins of tectonic plates are thus the source of most tectonism in intraplate areas due to extensional, lateral (strike-slip) and convergent movements between tectonic plates, or due to a combination of the three latter processes ([Storti et al., 2003](#); [Bayona et al., 2011](#); [Whitney et al., 2016](#); [Dias et al., 2018](#)). Another cause of tectonism in Intraplate Continental Margins is ridge push by newly formed, and also relatively old, mid-ocean ridges ([Fig. 2](#)). Ocean ridge push marks a dramatic change from plate-normal extension to compression as continental breakup is achieved ([Lundin and Doré, 2002](#); [Salomon et al., 2015](#); [Gac et al., 2016](#); [Ulvrova et al., 2018](#)).

Intraplate Continental Margins comprise areas of relatively moderate seismicity when compared to convergent plate boundaries (e.g. [Schulte and Mooney, 2005](#); [Illsley-Kemp et al., 2017a, 2017b](#); [Stein et al., 2017](#)). Yet, earthquakes reaching $M > 7$ in magnitude may occur in response to variable stress regimes that are far from negligible. World Stress Data ([Heidbach et al., 2016](#)) have shown ICMs to be affected by a wide range of stress regimes at present, from shelf-parallel strike-slip

movements imposed by far-field tectonic stresses (California, New Jersey and Nova Scotia; [Mount and Suppe, 1987](#); [Zobach and Zobach, 1989](#); [Wolin et al., 2012](#)), local extension resulting from gravitational collapse above salt and shale (South Atlantic; [Demercian et al., 1993](#); [Mauduit et al., 1997](#); [Rouby et al., 2002](#)), thermal relaxation of young ICMs (Red Sea; [Corti et al., 2015](#); [Segev et al., 2017, 2018](#)), to compressional stresses in basins dominated by local tectonic inversion (Northern Norway, Ireland, Greenland; [Pascal, 2015](#); [Andreasen et al., 2016](#); [Svennevig et al., 2016](#); [Janutyte and Lindholm, 2017](#); [Demuth et al., 2019](#); [Rodríguez-Salgado et al., 2019](#)) ([Fig. 3](#)). Adding to the presence of contiguous transform and transcurent faults, tectonic compression and strike-slip movements induced by mid-ocean ridges (e.g. ‘ridge-push’) become important controls on ICMs’ structural evolution as one approaches their abyssal areas ([Heidbach et al., 2016](#); [Alves et al., 2017](#); [Janutyte and Lindholm, 2017](#)). These characteristics have consequences when selecting distinct hydrocarbon production strategies prior to, during, and after drilling ([Meier et al., 2015](#); [Ma and Chen, 2015](#); [Ma et al., 2015, 2017](#)). Time-dependent stress variations, and the tectonic events behind them, are also capable to control the migration of oil, gas and NSO compounds into subsurface prospects ([Rullkötter et al., 1988](#); [Bonini, 2012](#); [Lee et al., 2016](#)).

A third final aspect of ICMs concerns the complex magmatic histories these margins reveal as hydrocarbon exploration extends into deep-water regions. Such a complexity is known to affect, and relate to, distinct subsidence histories during late rifting and continental breakup ([Geoffroy et al., 2015](#); [Hartz et al., 2016](#); [Alves and Cunha, 2018](#)). In fact, [Franke \(2013\)](#) has recently reviewed the concept of magma-poor and magma-rich continental margins in [White et al. \(2003\)](#) to propose a wide spectrum of geometries and magmatic evolutions for ICMs. As shown at the end of this work, we go a step forward from [Franke \(2013\)](#) to propose typical tectonic evolutions for ICMs, and that magmatism is expressed in different ways, in distinct zones, and following different

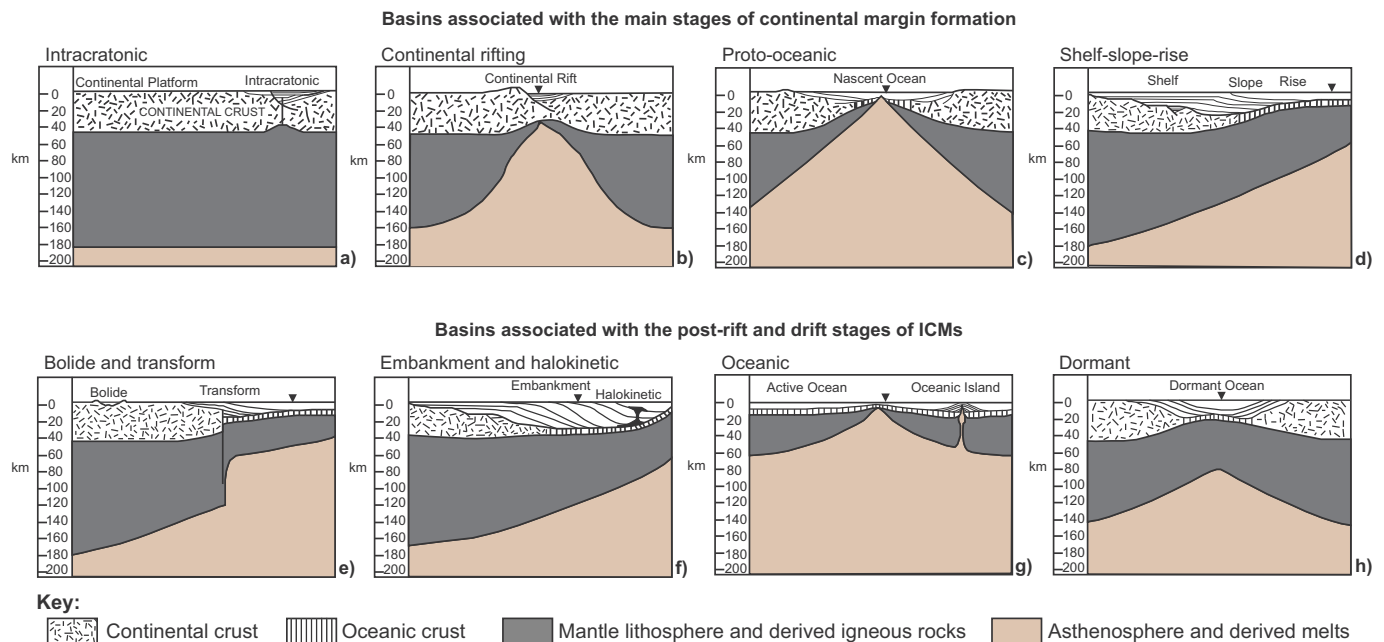


Fig. 2. Schematic representation (in true scale) of sedimentary basins associated with continental margin formation (divergent) and the post-rift and drift stages (intraplate) stages of ICMs. Cartoons a) to c) refer to the types of basins formed prior to the establishment of a fully rifted continental margin, shown in d) as a shelf-slope-rise configuration. Bolide basins (e) may occur at any time after ICMs are formed. Halokinetic basins (f) usually relate to embankment configurations, which load the salt to induce widespread halokinesis. Oceanic basins (g) occur far from ICMs, in old oceanic crust fed by pelagic and volcanoclastic sediment from oceanic islands. Dormant basins (h) occur when ocean spreading ceases and a proto-oceanic basin continues to be filled by erosional products of two aborted ICMs. This work focuses on the four (4) main structural configurations on ICMs: a) shelf-slope-rise, b) transform, c) embankment, and d) halokinetic. Figure modified from Busby and Azor (2012).

timings, as ICMs are rifted from their conjugate tectonic plates.

This paper is divided in specific sections addressing particular aspects of ICMs (Fig. 1). After the methodology section, two-dimensional (2D) and three-dimensional (3D) seismic data introduce key structures and features of ICMs (Figs. 1 and 2). Their regional structures are explained using high-quality seismic data, tectonic subsidence models and outcrop information from exposed rift basins in the Eastern Mediterranean Sea (Figs. 1 and 3). An attempt is made throughout this work to present examples of the four (4) key margin configurations in Busby and Azor (2012) (Fig. 2). In addition, tectonic subsidence models are presented for all ICMs considered here. Hence, this review will focus on the key geological characteristics of ICMs, and their economic potential using state-of-the-art seismic data. It will address three key research questions:

- 1) What are the effects of variable subsidence and magmatic histories on ICMs' hydrocarbon potential in distinct parts of the world?
- 2) What are the structural and magmatic evolutions 'typical' of the continental breakup process, and of ICMs in general, and how the deposition of resulting *breakup sequences* alters the economic potential of such margins?
- 3) Can outcrop analogues from ancient and modern areas of continental breakup (such as South California) record the full sequence of continental breakup on ICMs?

2. Database and methods

Two- (2D) and three-dimensional (3D) seismic data from eight (8) distinct regions were selected to document the evolution of ICMs (Figs. 1 and 2). In addition, outcrop data from Crete (Eastern Mediterranean) and West Iberia (North Atlantic Ocean) are used to illustrate the key structures and depositional units interpreted on the selected seismic data (Fig. 1).

2.1. Seismic interpretation

Seismic interpretation was based on the recognition of key stratigraphic boundaries on 2D seismic profiles, together with the compilation of seismic-attribute maps on 3D volumes (Brown, 2011). Seismic attributes of interest, used in our interpretation workflow, include root-mean-square (RMS) amplitude and coherence slices, all capable of highlighting structural and depositional features on ICMs. Root-mean-square amplitude maps depict the average squared amplitude from individual samples within a defined interval (Brown, 2011). Coherence attributes convert a seismic volume of continuity (normal reflections) into a volume of discontinuity so that faults and stratigraphic boundaries are emphasised (Marfurt and Alves, 2015). Faults were identified on both seismic attribute maps and vertical profiles. Depositional systems were mapped and characterised by combining borehole, seismic attributes and profile data in their analysis. Data artefacts or other pitfalls are highlighted in our data whenever necessary (see Marfurt and Alves, 2015). The locations of the seismic surveys used in this study are shown in Fig. 1.

2.2. Well and pseudo-well backstripping

Tectonic subsidence and uplift histories were estimated at borehole and pseudo-well locations along ICMs (Fig. 1) by 1-D Airy backstripping techniques, where backstripping uses information on the lithologies, ages and depths of deposition of the stratigraphic units to sequentially decompact and unload the sediment and water loads and thus recover the contribution from the tectonic forces that shaped a basin through time (e.g. rifting, thermal sagging, basin inversion or wrenching). At a given well (or pseudo-well) location the tectonic subsidence (TS) is given by a simple mass balance assuming local (Airy) isostatic compensation (Watts and Ryan, 1976; Steckler and Watts, 1978):

$$TS = S \frac{\rho_m - \rho_s}{\rho_m - \rho_w} + Wd - \Delta sl \frac{\rho_m}{\rho_m - \rho_w}$$

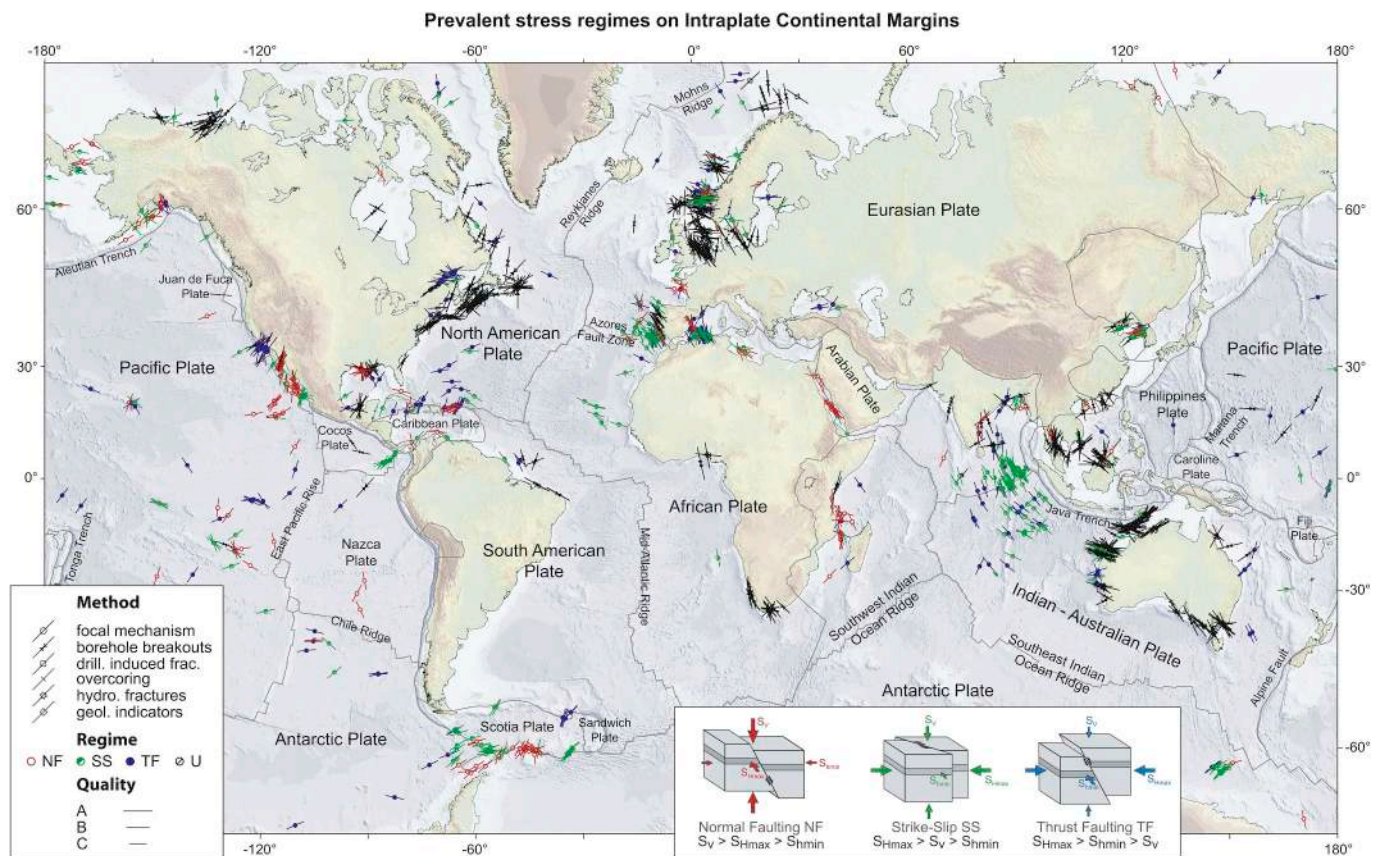


Fig. 3. World-stress map highlighting the prevalent stress regimes acting on ICMs at present. The figure shows only the stress orientations and regimes of ICMs and nearby seamounts where stress measurements were acquired. ICMs are affected by a wide range of stress regimes at present, from shelf-parallel strike-slip movements imposed by far field stresses, local extension resulting from gravitational collapse above salt and shale, thermal relaxation of young ICMs, to compressional stresses in basins dominated by local tectonic inversion. Sets of arrows with no interpreted stress regime refer to areas where such a regime was not unequivocal. Figure modified from [Heidbach et al. \(2016\)](#).

where S is the decompacted sediment load, Wd the water depth and the Δsl the sea-level at a given period of the basin evolution.

The tectonic subsidence-uplift histories were calculated for four (4) industry wells and eight (8) pseudo-wells, based on well-log information and the regional seismic stratigraphy. Whenever possible, we also used the available palaeoenvironmental data and published palaeogeographic reconstructions, to provide constraints for the palaeo-water depths. For the eustasy term of the backstripping equation, the [Stecker and Watts \(1978\)](#) sea-level curve is assumed, and the default sediment compaction curves provided by the Genesis petroleum systems modelling software Zetaware Inc. are used throughout ([Supplementary Tables 1 and 2](#)).

2.3. Outcrop analogues from SE Crete (Eastern Mediterranean)

Data from SE Crete was used as an analogue of a marine rift basin. On Crete, an Upper Sequence occurring above a basal detachment comprises non-metamorphic rocks and younger sediments ([Ring et al., 2001](#)). The Upper Sequence comprises non-metamorphic Upper Cretaceous–Eocene rocks that are part of the highly faulted Tripolitza unit, above which Neogene strata fills a series of extensional (supra-detachment) basins ([Ring et al., 2001](#)) ([Fig. 4a and b](#)). Branches of this basal detachment (*Cretan detachment*) outcrop in parts of Crete as highly tectonised metamorphic slates and marbles comprising fragments of supradetachment rocks ([Fig. 4c to g](#)). Above the Cretan detachment, [Postma and Drinia \(1993\)](#) subdivided the regional stratigraphy of [Meulenkamp \(1979\)](#) into facies associations documenting proximal (continental) to distal (marine) environments.

2.4. Outcrop analogues from West Iberia (Lusitanian Basin)

In West Iberia (Lusitanian Basin), field analogues were studied to focus on uppermost Jurassic-lower Cretaceous syn-rift strata and overlying breakup sequences ([Alves and Cunha, 2018](#)). In this region, two pre-Oxfordian rift phases (Rift 1, Late Triassic; and Rift 2 in the Sinemurian–Pliensbachian) preclude a rift-climax phase in the Late Jurassic–Early Cretaceous ([Stapel et al., 1996](#); [Rasmussen et al., 1998](#)). At this time, rifting and continental breakup in the Tagus Abyssal Plain, SW Iberia, resulted in significant subsidence south of a large ESE-trending structure, the Nazaré fault ([Rasmussen et al., 1998](#); [Alves et al., 2009](#)). Distinct sectors of the basin were then filled with mixed continental-marine deposits that show complex depositional facies distributions ([Wilson et al., 1989](#); [Leinfelder and Wilson, 1998](#); [Alves et al., 2003](#)).

The field analogue used in this work comprises marine carbonates deposited at the end of rift-climax phase on a shoulder area of the Lusitanian Basin, and were intruded by post-rift magma related with the intrusion of a granite batholith. Other magmatic sills and dikes occur during the pre-rift stage south of the Lusitanian Basin, in association with the Central Atlantic Magmatic Province (CAMP), and during the syn-rift events that led to (or immediately precede) to continental breakup ([Neres et al., 2013](#); [Pereira et al., 2017](#); [Merle et al., 2018](#)).

3. State-of-the-art

3.1. Types of rifted continental margins

The past decade has witnessed the publication of multiple models

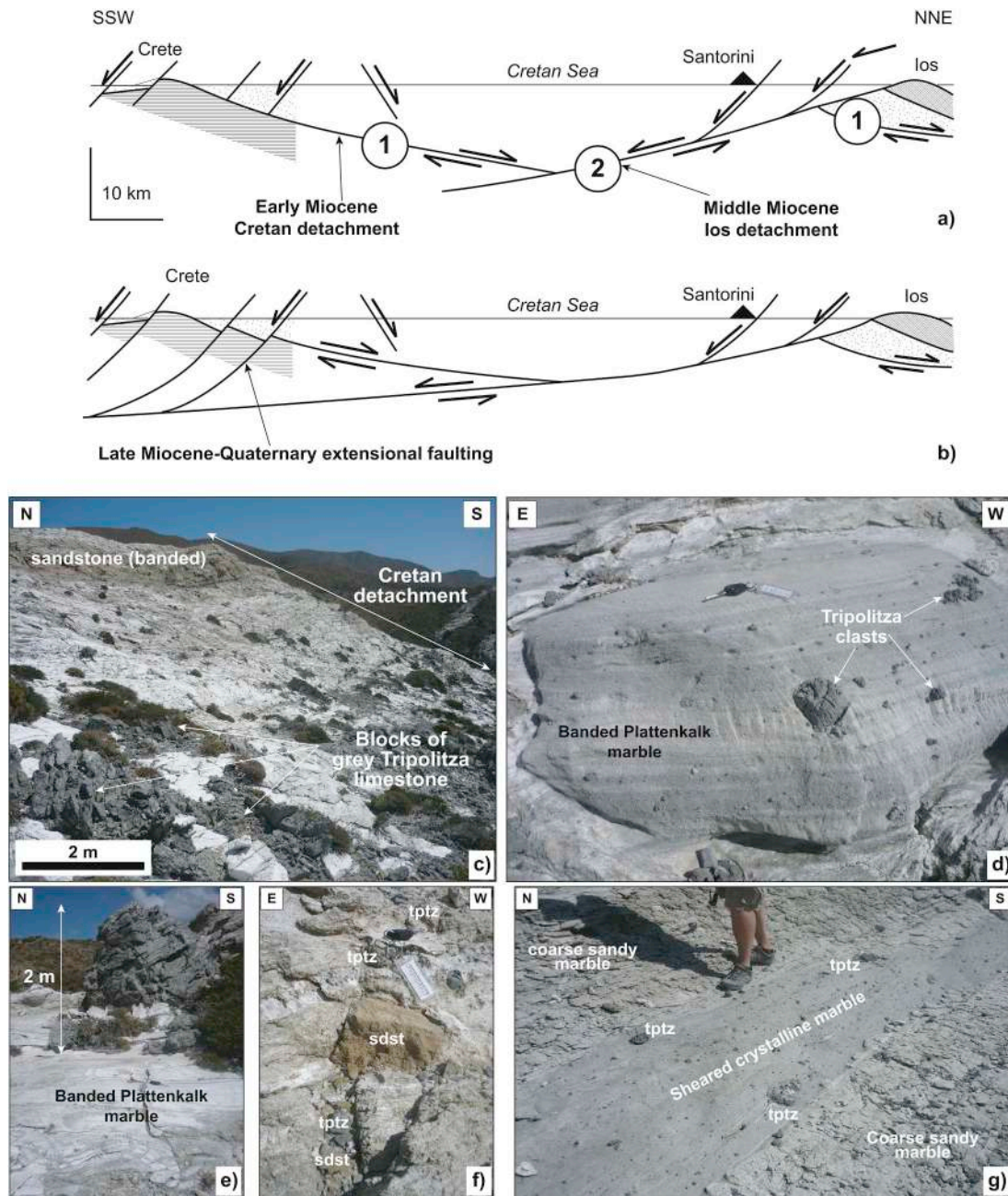


Fig. 4. a) and b) Sketches summarising the Early and Middle Miocene evolution of the South Aegean Sea (Greece). a) The Early and Middle Miocene were dominated by widespread extension over basal low-angle detachment faults, the *Cretan Detachment*, which resulted in the translation of Crete's lowermost units some 150 km south, from Ios to the island's current position. b) By the end of the Miocene, until the Quaternary, extensional tectonics concentrated on what is now the island of Crete, and in adjacent basins to the south. Extensional tectonics has been compounded, after the Pliocene, by transtension to the south of the island and local transpression associated with the tectonic rise of Crete. c) Field photograph of part of the Cretan Detachment in SE Crete. The photo shows the uppermost part of the detachment fault as a white, banded marble, highly sheared, comprising large blocks of Tripolitza limestone (supradetachment units) and a highly tectonised sandstone. The thickness of this tectonised marble is ~200 m. d) Zoomed in photo showing the presence of polymictic fragments of supradetachment rocks in the marble matrix of the Cretan Detachment in this area. Tripolitza clasts are, nevertheless, predominant in this location. e) Example of 2-m tall block of dark Tripolitza limestone involved in the marble matrix of the Cretan Detachment. f) Example of sandstone and Tripolitza fragments enclosed in the marble matrix of the detachment. g) Highly sheared interval of a microcrystalline marble that includes fragments of supradetachment rock of distinct lithologies and sizes. Above and below the sheared interval the marble's crystalline composition of coarser and larger blocks of Tripolitza limestone are observed above and below. Sketches in a) and b) are modified from Ring et al. (2001).

explaining continental rifting, breakup and subsequent tectonic phases controlling the evolution of ICMs. A key aspect of ICMs is their tendency to experience enhanced periods of subsidence during continental breakup (Jeannot et al., 2016; Alves and Cunha, 2018; Beniest et al.,

2017; Quirk and Rüpke, 2018). This enhanced subsidence can be explained by a two-stage plate breakup system that divides continental margins in two types: Types I and II (Huismans and Beaumont, 2011) (Fig. 5). According to these authors, Type I margins experience crustal-

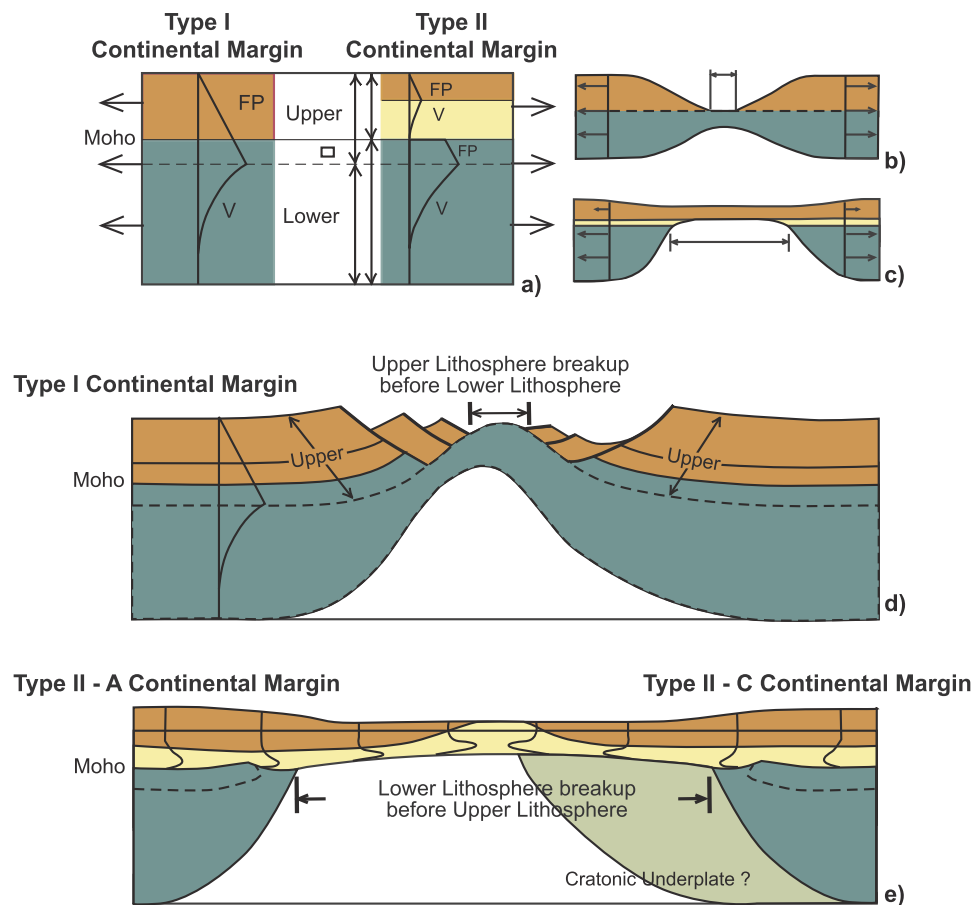


Fig. 5. Contrasting depth-dependent extension of type I and type II margins cf. [Huisman and Beaumont \(2011\)](#). a) Sketch summarising the lithospheric properties of the two types of margins. FP, frictional–plastic; V, viscous; pale yellow, low-viscosity crust. b) and c) Conceptual laminate representation of crustal necking styles highlighting the early breakup of crust and mantle lithosphere. Adding isostasy to b) and c) leads to d) Type I margins and e) Type II-A and type II-C, with asthenospheric (left) and cratonic (right) underplating. The region of the embedded cratonic lithosphere is shown to the right of panel e). Also shown are the strong FP crust (orange), low-viscosity crust (pale yellow), mantle lithosphere (green) and cratonic underplate (light green). (For interpretation of the references to colour in this figure legend, the reader is referred to the Web version of this article.)

necking breakup before mantle breakup is finally achieved. Type II margins, which are relatively wider and show a thinner upper lithosphere when compared with Type I, record mantle-breakup at first before the crust is ruptured in a second regional event (Fig. 5). [Huisman and Beaumont \(2011\)](#) classification complements that separating volcanic and non-volcanic passive margins as distinct, unrelated types ([White et al., 2003](#)). A good account of this dual classification is given by [Geoffroy et al. \(2015\)](#) who consider non-volcanic passive margins to record no significant mantle melting in their upper crustal section immediately before and throughout lithosphere extension (see also [Whitmarsh et al., 2001](#), [Minshull, 2009](#); [Davis and Lavier, 2017](#)). However, sub-crustal mantle can, later in the rifting process, be exhumed and serpentinised in association with extreme crustal stretching and thinning ([Lavier and Manatschal, 2006](#); [Reston and McDermott, 2011](#)) (Fig. 5). Lithosphere necking is accommodated by an early system of upward-concave conjugate detachment faults dipping oceanwards ([Lavier and Manatschal, 2006](#)). A translithospheric detachment developing seawards exhumed the upper lithospheric mantle through a rolling-hinge deformation of the footwall in a second stage before continental breakup is fully established ([Reston and McDermott, 2011](#)) (Fig. 5).

Volcanic passive margins relate to continental breakup in Large Igneous Provinces (LIPs) ([Geoffroy et al., 2015](#)). Here, significant lithosphere extension is not necessarily a pre-requisite for initial mantle

melting and consecutive syn-magmatic breakup ([Sengor and Burke, 1978](#); [Courtilot et al., 1999](#)). Early melt produces volcanic traps that cover large areas, and crustal dilatation occurs through dyking in the upper crust and magma underplating at the Moho ([Geoffroy et al., 2015](#)). Lithosphere extension leading to breakup is coeval with the focusing of mantle melting.

Regardless of the type of margin, and the processes forming it, continental breakup is now recognised as an event prolonged in time and associated with a distinctive stratigraphic (or volcano-sedimentary) *breakup sequence* ([Soares et al., 2012](#); [Alves and Cunha, 2018](#); [Quirk and Rüpke, 2018](#)). The deposition of *breakup sequences* relates to the two-step breakup of continental margins considered in [Huisman and Beaumont \(2011\)](#) and reflects a margin-propagating breakup event that is prolonged in time. It is associated with discernible unconformity-bounded stratigraphic sequences of regional extent, showing distinct depositional architectures to older (syn-rift) strata and younger (drift) units. According to [Soares et al. \(2012, 2014\)](#), the *breakup sequence* marks the period spanning from the onset of continental breakup per se to the establishment of thermal relaxation as the main process controlling subsidence in a specific segment of a newly-formed continental margin. This is true regardless of the type of continental margin (Type I or II) defined in [Huisman and Beaumont \(2011\)](#), the relative timings(s) of continental breakup ([Beranek, 2017](#); [Monteleone et al., 2019](#)), or the relative importance of magmatism to the breakup process.

On the continental slope of west Iberia, Soares et al. (2012) analysed the sedimentological and palaeontological character of the breakup sequence (Fig. 6). Based on information gathered from DSDP Site 398 (Leg 49B) and ODP Site 641 (Leg 103), Soares et al. (2012) identified a sharp boundary between rhythmic successions of turbidites and slump deposits at the end of the syn-rift interval (Fig. 6). The unit immediately above syn-rift strata, at the base of the breakup sequence, marks the end of mass-wasting and slumping and the beginning of the deposition of organic-rich 'black shales' with abundant plant debris, kaolinite and interstratified clays derived from the continent, in a setting marked by high sedimentation rates (Shipboard Scientific Party, 1979; Taugourdeau-Lantz et al., 1982) (Fig. 6). The end of 'black shale' deposition is marked at DSDP Site 398 by an abrupt change in sedimentation, the deposition of barren red-brown shales, and the development of a probable unconformity ranging from mid-Cenomanian to Santonian-Campanian (Sigal, 1979). Note in Fig. 6 the relative scarcity of carbonate material in the *breakup sequence*, and the appearance of palinomorphs, sporomorphs and other continental-derived material only during the deposition of a late Aptian-Cenomanian sequence associated with continental breakup.

3.2. Strata deposited during continental breakup

Enhanced tectonic subsidence during continental breakup is associated with the deposition of mass-wasting and footwall degradation complexes in marine to continental environments (Alves and Cupkovic, 2018; Alves and Gamboa, 2020). On seismic, borehole and outcrop data from non-volcanic margins, continental breakup is associated with the deposition of stratigraphic successions representing a phase of forced marine regression (Fig. 7). They form a well-defined offlapping sequence on seismic data, particularly when associated with sand fairways that channelled siliciclastic material from the continent (Figs. 7 and 8). On volcanic continental margins, this same event is marked by the deposition of a seismic package with seaward-dipping reflectors (SDRs) comprising mixed volcano-sedimentary sequences (Skogseid et al., 2000; Franke et al., 2010; Norcliffe et al., 2018) (Fig. 9). Vertically stacked breakup sequences can occur on the margins of propagating rift-breakup systems and reflect successive continental breakup events (Alves and Cunha, 2018).

The latter fact is important as successive breakup sequences will record the full history of subsidence and uplift in distinct parts of ICMs, in time, as continental breakup develops. In addition, the development of such sequences is also the first evidence of a fully developed ICM, recording the conditions in which these margins were initially formed, e.g. continental vs. marine conditions, volcanic vs. non-volcanic settings or under subsidence vs. uplift tectonic forces. Relative magnitudes of crustal stretching, mantle exhumation and footwall erosion during the continental breakup event are materialised as differing *breakup sequences* (Alves and Cunha, 2018).

In NW Iberia, the breakup sequence records widespread subsidence after the complete separation of mantle lithosphere was achieved, and minor or no heave is observed between crustal tilt-blocks after this stage (Alves and Cunha, 2018) (Figs. 7 and 8). Conversely, hyper-extended tilt-blocks in parts of Newfoundland (Flemish Cap, Orphan Knoll) filled by wedge-shaped breakup sequences hint at some degree of crustal stretching in distinct sub-basins during the breakup event. Off-shore Namibia and Argentina, the breakup sequence coincides with SDRs, with their top marking the end of the continental breakup event (Norcliffe et al., 2018) (Fig. 9). In NW Iberia, the same onset of the drift phase is marked by the widespread deposition of contourites (Wilson et al., 2001; Soares et al., 2014), prior to a widespread (drift) condensed interval that spans the Santonian to the Maastrichtian (Groupe Galice, 1979; Wilson et al., 2001). In Newfoundland, the deposition of successive sandstone-rich breakup sequences is followed by the deposition of the drift Banquereau Group, essentially a mud-rich unit (Sinclair, 1995).

4. Regional configuration(s) of developed intraplate continental margins

This section gives an account of the regional structures and configurations of ICMs, for the greatest part based on seismic data from several parts of the world (Fig. 1). These structures are key diagnostic features for ancient ICMs. Whenever necessary, comments on the hydrocarbon potential of specific basin types will be included in the following sub-sections.

4.1. Shelf-slope-rise configuration (NW Australia, West Iberia)

Shelf-slope-rise configurations comprise mature intraplate continental margins with a seaward thickening wedge of shelf deposits on top of continental crust, which is thinner seaward (Busby and Azor, 2012). In these configurations, the so-called *transitional crust* (both quasicontinental and quasioceanic) underlies the seaward transition from thick shelf deposits to thin slope deposits, merging into thick turbiditic rise and abyssal plain deposits on oceanic crust (Busby and Azor, 2012).

Shelf-slope-rise configurations are typical of fully rifted ICMs that are not sediment-starved, and are instead dominated by carbonate sedimentation such as those from equatorial regions around the world. They were defined by Busby and Azor (2012) as mature rifted ICMs with a shelf edge near the boundary between continental and oceanic crust. Hence, ICMs recording important tectonic uplift and fault reactivation may present more abrupt slope geometries with the development of a broad region of sediment bypass towards oceanic crust (Reeve et al., 2015). A key aspect of shelf-slope-rise configurations is that rapid (and abundant) sediment influx onto continental slopes favours source rock maturation at syn-rift level (and in older units) by increasing basin temperatures. Indirectly, it may lead to overpressure intervals in siliclastic intervals that are able to preserve part of their original porosity. This means that the common compaction trends can be delayed by the presence of trapped fluids below rapidly depositing overburden strata (e.g. Wilkinson and Haszeldine, 2011).

Two ICMs are used as examples of this margin configuration: NW Australia and West Iberia. Fig. 10 shows a relatively uniform distribution of strata in NW Australia, with post-rift units showing greater thickness when compared with the faulted syn-rift successions below. A similar configuration occurs in West Iberia, but here the thicker post-rift strata does not reach more than 2.0 s (~2200 m) above syn-rift depocentres (Figs. 7 and 8). This latter character is evidence for a broad period of post-rift subsidence after continental breakup, with footwall blocks and basin-bounding horsts being coincident with zones where TWT thickness approaches zero (Alves and Cunha, 2018).

Backstripping results for the NW Australia margin reveal a gentle syn-rift subsidence, which is accelerated during continental breakup (Mid Jurassic), and a drift evolution dominated by gentle subsidence and later tectonic uplift (Fig. 11a–c). As recorded by other exploration wells drilled on the continental shelf of NW Australia (Belde et al., 2017), water depths were relatively shallow during the syn-rift stage, and the margin was moderately deepened after continental breakup. A consequence of this moderate deepening was the development of a setting dominated by large amounts of sediment influx onto the continental slope of this ICM.

Offshore West Iberia, a similar setting is recorded with gentle subsidence dominating the post-breakup evolution of this ICM. However, no significant tectonic uplift is recorded on the subsidence plots in Fig. 11d–f. Tectonic uplift was markedly concentrated, after continental breakup, on the shelf and onshore parts of West Iberia (Alves and Cunha, 2018). A first pulse of Early Jurassic subsidence is well defined, and occurs together with an increase in palaeowater depths. However, this pulse is relatively moderate in its magnitude and precedes a second episode of enhanced subsidence in the Early Cretaceous, accompanying continental breakup. This same pulse was followed by prolonged,

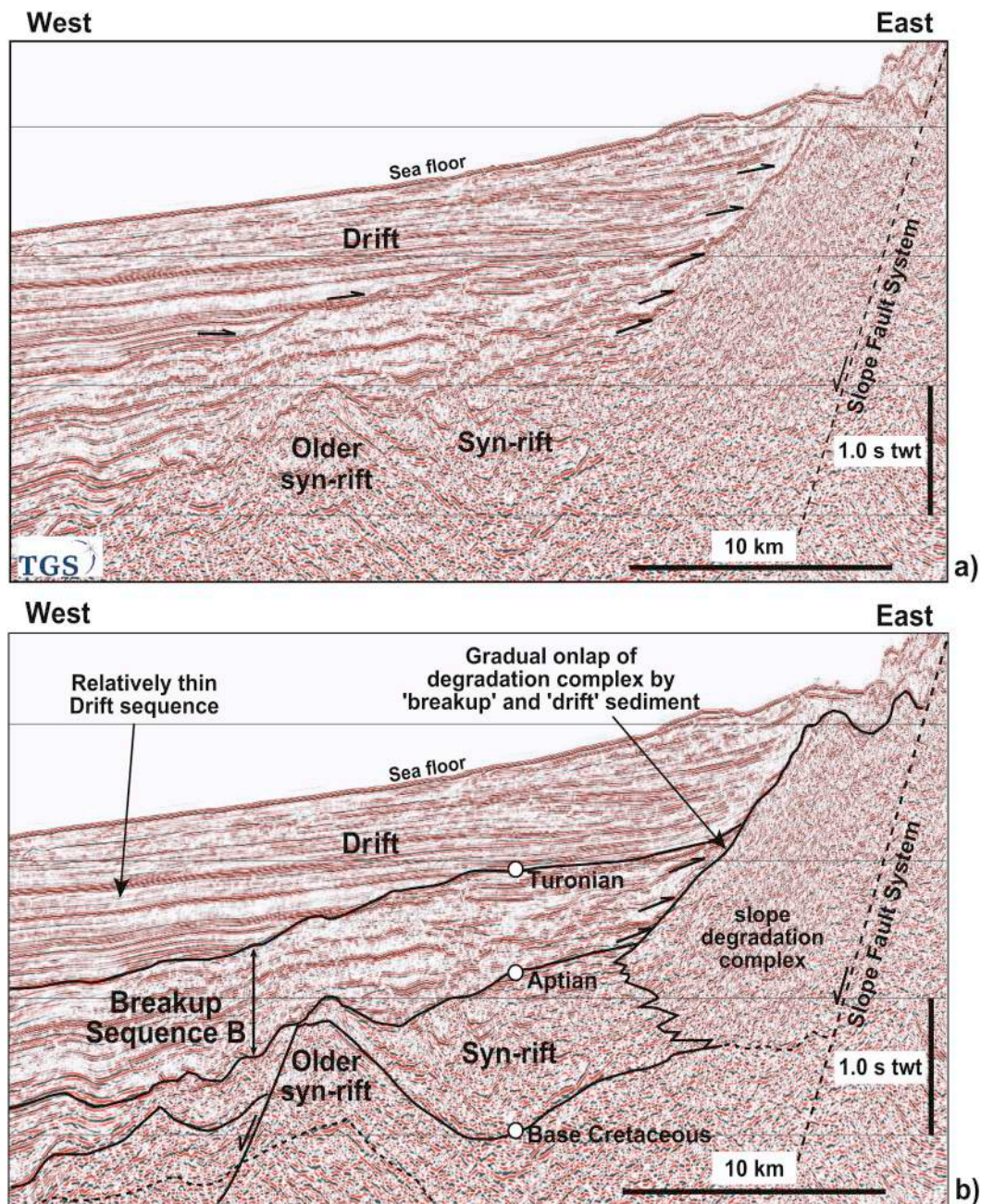


Fig. 7. Example of a shelf-slope-rise configuration in ICMs. a) Uninterpreted and b) interpreted seismic profile from NW Iberia revealing the presence of a breakup sequence (Breakup Sequence B) west of a well-developed slope degradation complex. The profile is located in the central part of West Iberia, west of Peniche. The time-depth of key seismic markers used in the subsidence models is shown in the figure.

typical post-rift tectonic quiescence after the Early Cretaceous (Fig. 11e and f).

Implications for the maturation of hydrocarbon prospects are evident from the computed burial histories. In NW Australia a terraced continental slope forms a continuum between shelf and the abyssal plain, with fault-bounded terraces comprising main depocentres (Fig. 10). Most of these fault-bounded terraces are limited by rift-related faults reactivated due to subduction in the Timor Trough, and relate to regional uplift episodes on the continental shelf (Rosleff-Soerensen et al., 2012, 2014). In addition, a key event in NW Australia was the onset of a sediment-rich post-rift thermal sag – a phenomenon resulting in widespread deposition on the North West Shelf. In NW Australia, organic-rich marine sediments were deposited at this time in a series of long-lived sedimentary basins (Stephenson and Cadman,

1993; Rosleff-Soerensen et al., 2012). Later, margin parallel half-grabens were blanketed by passive-margin sediments above the Middle Jurassic structural relief (Langhi and Borel, 2005; Rosleff-Soerensen et al., 2012). The onset of subduction on the Timor Trough, offshore Australia, promoted the updip migration of hydrocarbons towards the south, into Australian waters.

There is evidence in both Australia and West Iberia that the breakup sequence marks the start of the continental embankment stage insofar as revealing blanketing of the whole margin by continent-derived material (Soares et al., 2012; Reeve et al., 2015). In West Iberia, the most significant event occurring after continental breakup is the development of a prograding slope system and associated degradation complexes (Figs. 7 and 8). In NW Australia, a similar configuration is observed on regional seismic data by the deposition of a shaley, postrift

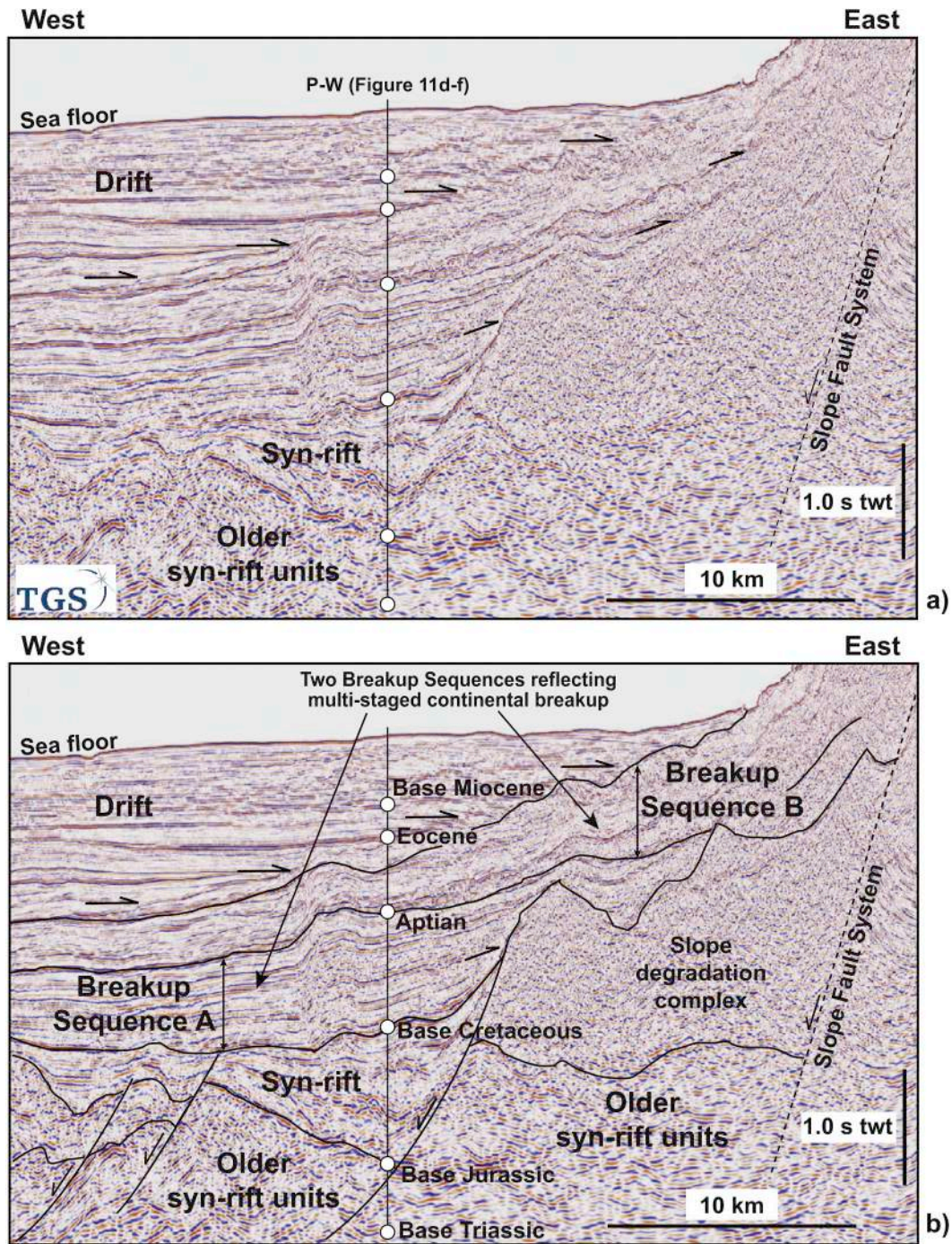


Fig. 8. Example of a shelf-slope-rise configuration in ICMs. a) Uninterpreted and b) interpreted seismic profile across SW Iberia revealing the presence the two Breakup Sequences A and B, and the time-depth of key seismic markers used in our subsidence models. The profile is located SW of Lisbon. PW refers to the pseudo-well described in Fig. 11.

sequence that gradually changes into a carbonate ramp in the Paleogene (Fig. 10).

West Iberia shows important reactivation and uplift during the Cenozoic, but only on the continental shelf and onshore basins. Interpreted 2D profiles reveal the generation of a tripartite margin, with a shallow inner proximal margin giving rise (oceanward) to a steep slope (outer proximal margin) and a distal abyssal realm. Sediment influx from the continental shelf and hinterland areas resulted in a pronounced progradational event dominated by mass-flow deposits. On the inner proximal margin postrift strata are relatively thin and limited

deposition occurred after the Late Jurassic. The outer proximal margin shows relatively thick (> 2.0 s twt) postrift units, but erosion is marked on what is a bypass continental slope. The distal margin coincides with the Iberia Abyssal Plain and presents the thickest post-rift succession of the three zones. Nevertheless, the area was relatively starved of sediment after the Early Cretaceous, with much impact on the maturation rates of hydrocarbons at depth. In this aspect the more proximal, marine setting of Australia was capable of accumulating enough sediment to blanket hydrocarbon source rocks at a reasonable depth, under temperatures able for oil and gas generation.

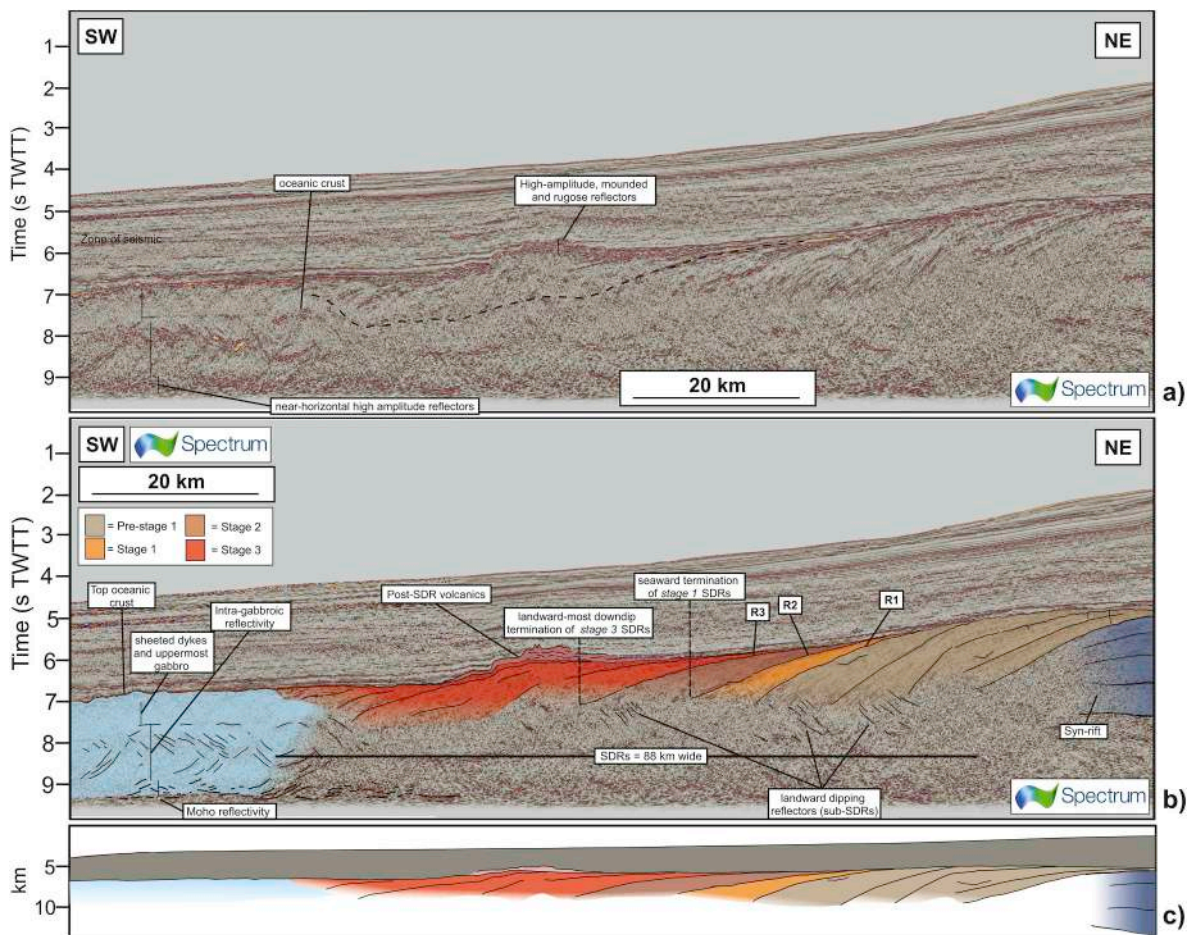


Fig. 9. Example of Laterally Confined Volcanic Successions (LCVS) in magma-rich ICMs. These types of LCVSs document rift-jumps during the formation of magma-rich ICMs, as in the case of offshore Namibia exemplified in the figure. Figure modified from [Norcliffe et al. \(2018\)](#).

4.2. Transform configuration (Ceará and Pará-Maranhão Basins, Equatorial Brazil)

Transform margins are ICMs that originate along transform plate boundaries ([Busby and Azor, 2012](#)). Intraplate continental margins that originate along transform boundaries rather than rift boundaries have narrower sediment prisms and transitional crust. Tens of millions of years may pass between the time of initiation of transform motion, which is coincident with the rift-to-drift transition on other margin configurations, and the time of intraplate sedimentation that follows the movement of the spreading ridge along the transform boundary ([Busby and Azor, 2012](#)).

Characteristic features of transform configurations include their very steep continental slopes and broad continental rises, which can be interrupted by volcanic ridges and reactivated basement highs ([Davison et al., 2015](#)). Examples of transform configurations in ICMs are known offshore Equatorial Brazil, in SW Iberia and in parts of the Gulf of Aden into Oman ([Fig. 1](#)).

Two ICMs are used as examples of this margin configuration; the deep-water Ceará Basin, and more proximal parts of the Pará-Maranhão Basin (PAMA), both in Equatorial Brazil. The Ceará and the PAMA basins are located in between major fault zones that accommodated the opening of the Equatorial Atlantic region (see [Azevêdo, 1991](#); [Nemčok et al., 2012](#)). They also experienced relatively later continental rifting and breakup when compared with the Central and Austral Segments of Brazil. The two events may have also been diachronous when comparing the PAMA and the Ceará basins, which are some 500 km distant from each other ([Fig. 1](#)). After the late Albian, Equatorial Brazil

recorded continental drift and far-field tectonic reactivation, the latter of which resulted in moderate inversion during specific tectonic events related to the Andean Orogeny ([Lima, 2003](#)). The PAMA Basin is therefore limited by Fracture Zones and local structural highs that are roughly coincident with the boundaries of modern sedimentary basins ([Nemčok et al., 2012](#)). A similar setting is recorded by the Ceará Basin ([Fig. 1](#)).

The example shown in [Fig. 12](#) is thus marked by a family of Paleocene-early Eocene listric faults associated with a phase of gravitational collapse at the shelf-edge and slope of the Ilha de Santana Platform, PAMA Basin. The acoustic basement below these listric faults coincides with latest Cretaceous-early Paleogene strata ([Fig. 12](#)). Underneath the listric faults there are structural lineaments associated with an older structural fabric, namely NW-SE ridges and faults on the footwall of the listric fault complex. [Fig. 12](#) shows some of this latest Cretaceous-early Paleogene structural fabric. Further North, on the continental slope, the Paleocene-Eocene gravitational system imaged on the shelf is detached on top of late Cretaceous strata, which is highly compartmentalised by Mesozoic faults. In the Ceará Basin, gravitational collapse is not as prominent as in PAMA, but evidence still exists of the effect of transform faults in the basin compartmentalisation and faulting ([Fig. 13](#)). Here, E-W transform faults in ocean crust propagate into continental crust to generate important transtension, transpression and associated faulting on the continental slope ([Almeida et al., 2019](#)) ([Fig. 13](#)).

Petroleum systems in the PAMA and Ceará Basins are thus controlled by northwest-trending normal faults with a marked listric geometry, developed towards the modern shelf-break ([Figs. 12 and 13](#)).

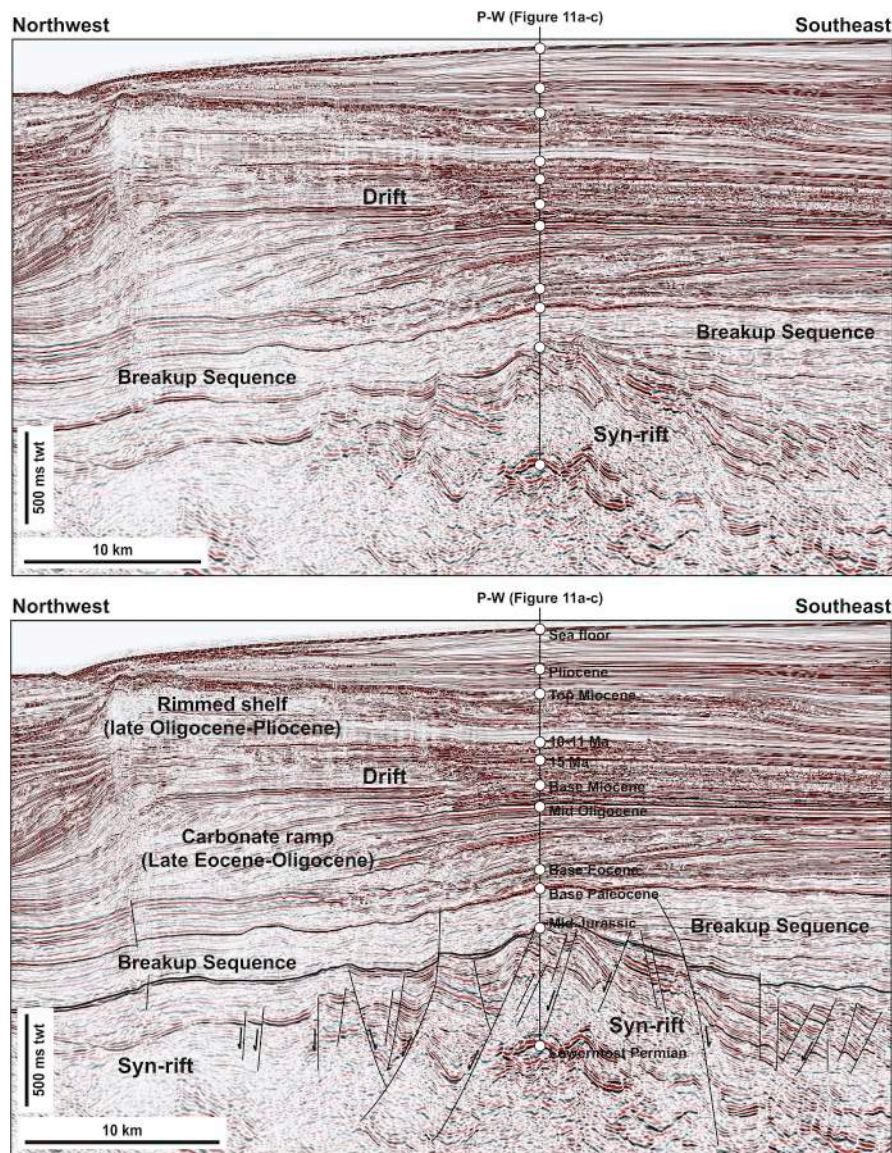


Fig. 10. Example of a shelf-slope-rise configuration in ICMs. a) Uninterpreted and b) interpreted seismic profile across the central part of the Browse Basin depicting the geometry of syn-rift structures at depth, the presence of a breakup sequence, and a thick carbonate-rich drift succession above. A Paleogene carbonate ramp gave rise to a rimmed carbonate shelf after the middle Oligocene. PW refers to the pseudo-well described in Fig. 11.

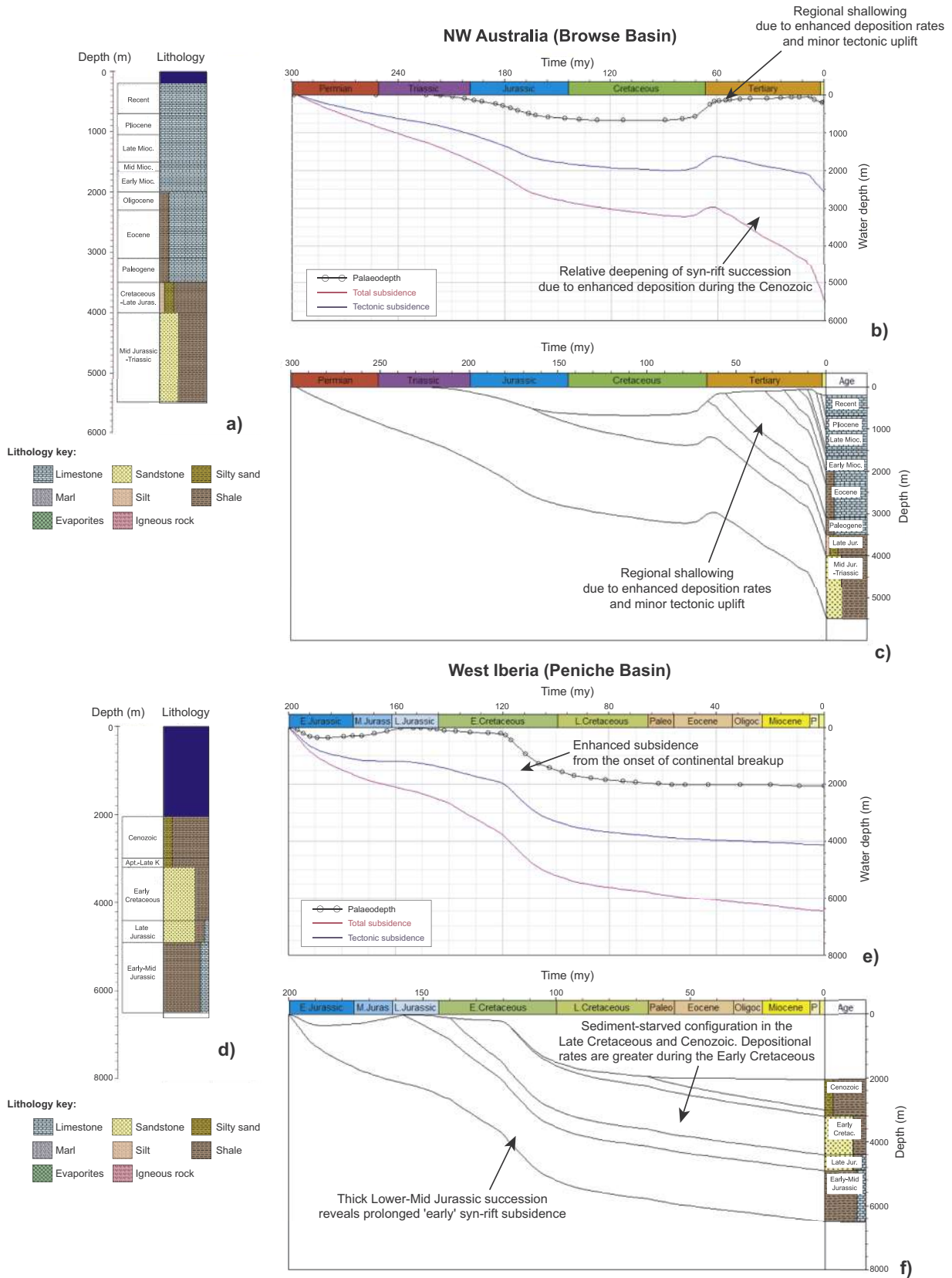
Such a character makes them preferential fluid migration paths from the continental slope to shallower structural traps near the shelf edge, where depressions and linear features resembling aligned karstic caves are ubiquitous at Upper Eocene-Oligocene level. In essence, the observed linear features follow the trend of shelf-margin faults. Depressions are more randomly distributed, but the largest occur above shelf-margin and listric faults at depth.

The tectonic subsidence inferred from 1-D backstripping in the Ceará Basin reveals a gentle acceleration of subsidence during continental breakup (latest Early Cretaceous), accompanying the even gentler syn-rift and drift phases of subsidence (Fig. 13). As recorded in exploration wells drilled on the continental shelf (Almeida et al., 2019), water depths were relatively shallow during the syn-rift stage, and the margin was significantly deepened after continental breakup. A second, abrupt deepening event is recorded after the Oligocene, and led to the development of a sediment-starved setting in the distal parts of the Ceará Basin. Between the two stages of subsidence (latest Early Cretaceous and Oligocene), the margin experienced a relatively quiescent

period in which the Ceará Basin was relatively shallow. This quiescence may be associated with thermal uplift associated with magmatism on the distal margin, an area marked by the emplacement of large volcanic seamounds (Jovane et al., 2016).

Backstripping results for the PAMA show a marked deepening after continental breakup, but with a broad continental shelf evolving as a shallow carbonate platform during the post-rift history of this ICM (Fig. 14). The onset of Early Cretaceous breakup is marked by enhanced subsidence, which is further enhanced the Miocene. Of relevance to the PAMA is the generation of large-scale gravitational complexes on the continental slope in association with this second stage of tectonic subsidence, as recorded on the shelf by the accumulation of Eocene and younger strata above the basal detachment of such complexes (Fig. 14). The near 2 km of tectonic uplift recorded in Fig. 14 is probably a result of the Andean compressional phases, and localised wrench tectonics along major transform faults, causing local uplift.

Comparative tectonic subsidence curves: Shelf-slope-rise configuration



(caption on next page)

Fig. 11. Pseudo-well models and calculated burial history and tectonic subsidence curves for shelf-slope-rise ICM configurations in NW Australia and West Iberia (Peniche Basin). See Figs. 8 and 10 for location of the PWs along the seismic lines. The two regions show a distinct drift evolution, but a common enhancement of tectonic sediment when continental breakup ensued. Sediment-starved conditions also prevailed in West Iberia during the Late Cretaceous as continental breakup was achieved and vast abyssal areas became the recipients of sediment from a small hinterland mass (Iberia microplate). a) Pseudo-well lithostratigraphy for NW Australia. b) Assumed palaeowater depths and calculated tectonic and total subsidence for the NW Australia pseudo-well. c) Calculated burial history in NW Australia relative to time. d) Lithologies considered in the subsidence modelling for West Iberia. e) Assumed palaeowater depths and calculated tectonic and total subsidence for West Iberia. f) Calculated depths of key stratigraphic units in West Iberia relative to time.

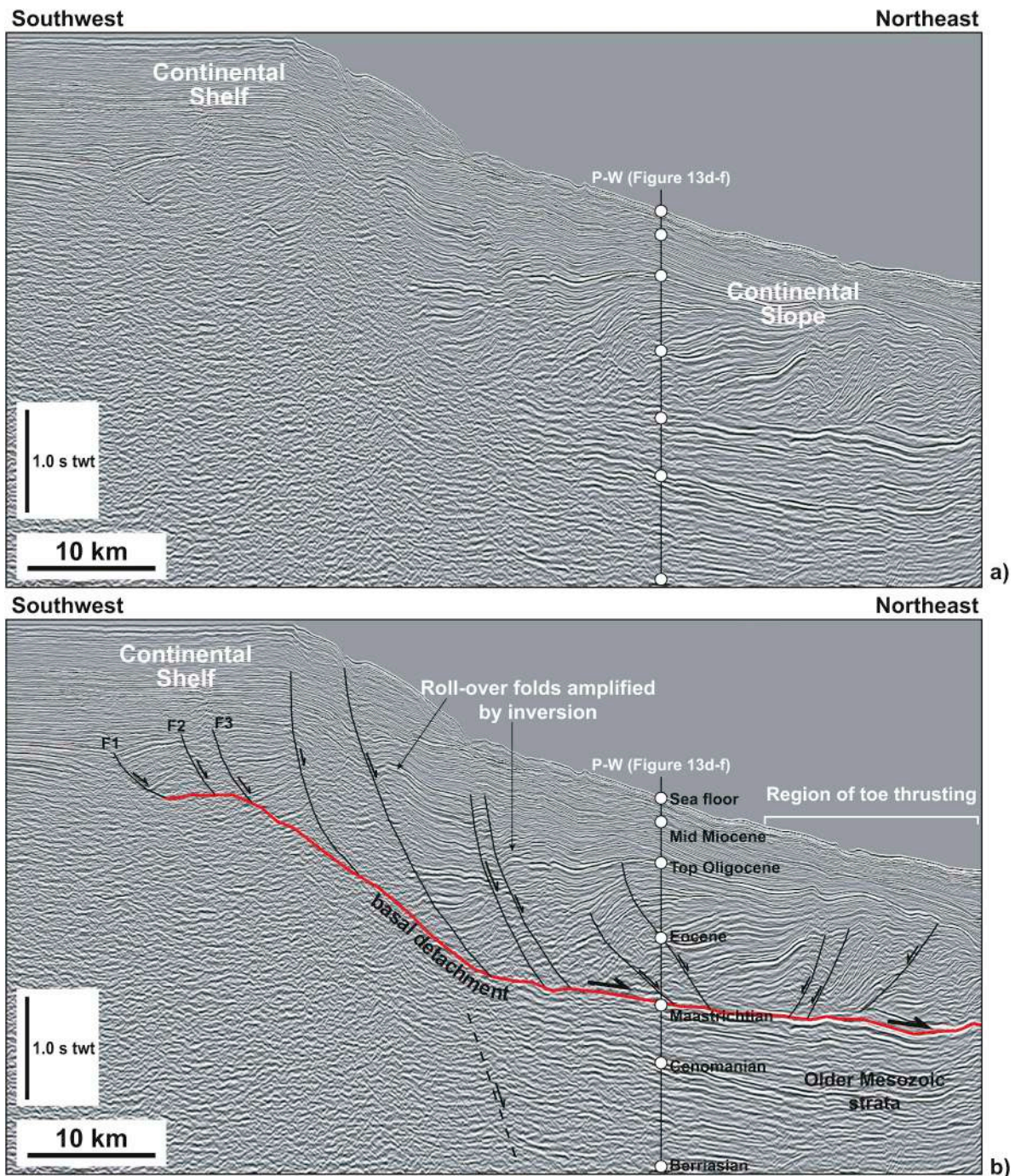


Fig. 12. Example of a transform configuration in ICMs. a) Uninterpreted and b) interpreted seismic profile across Equatorial Brazil (PAMA Basin) highlighting the development of large gravitational complex on the continental slope. Extensional faults on the shelf edge change into a localised fold-and-thrust belt on the continental slope and rise, likely detached on a soft, shalley succession. Borehole data suggests a late Cretaceous-early Paleogene age for the strata below the basal detachment (Azevedo, 1991). PW refers to the pseudo-well described in Fig. 13.

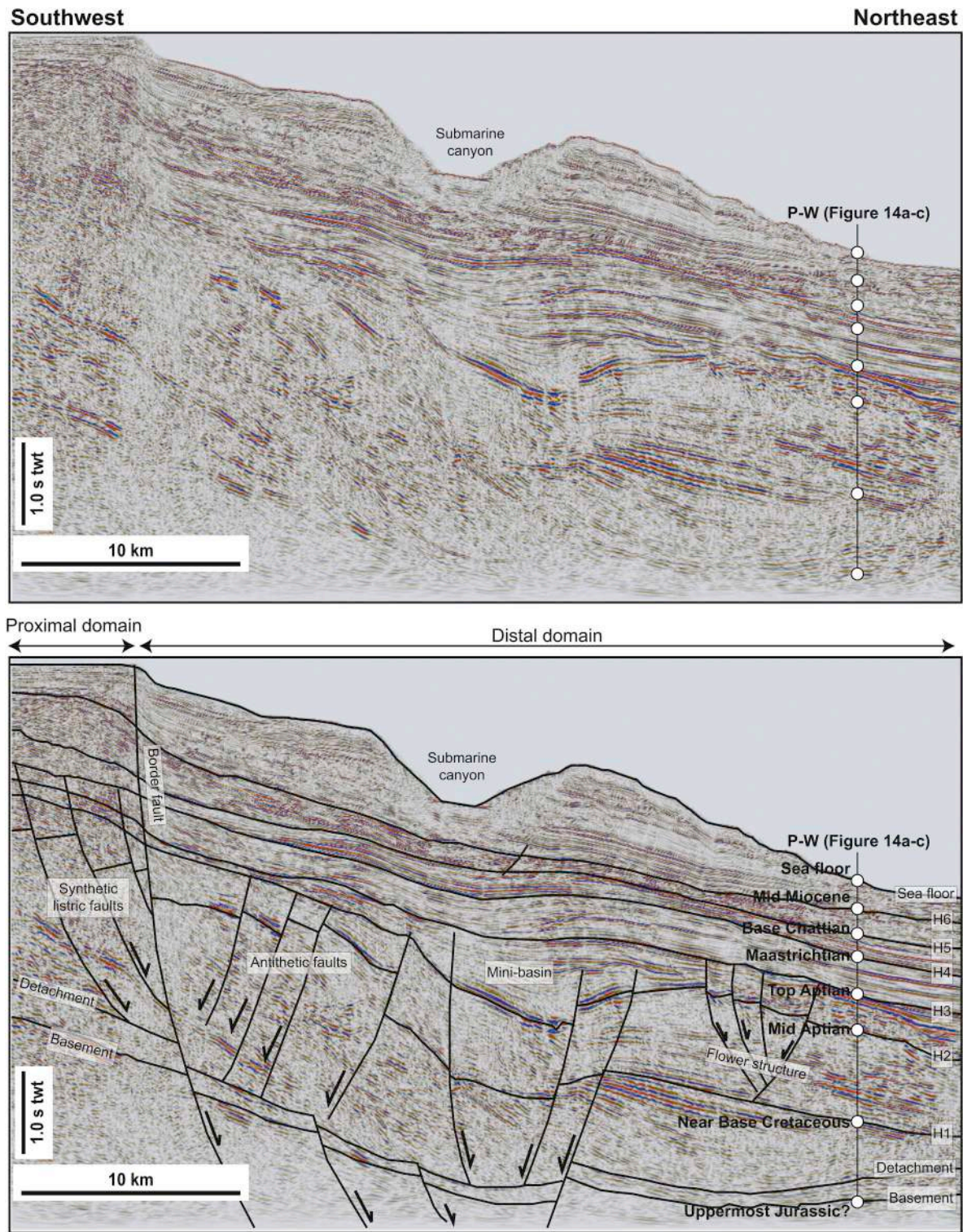


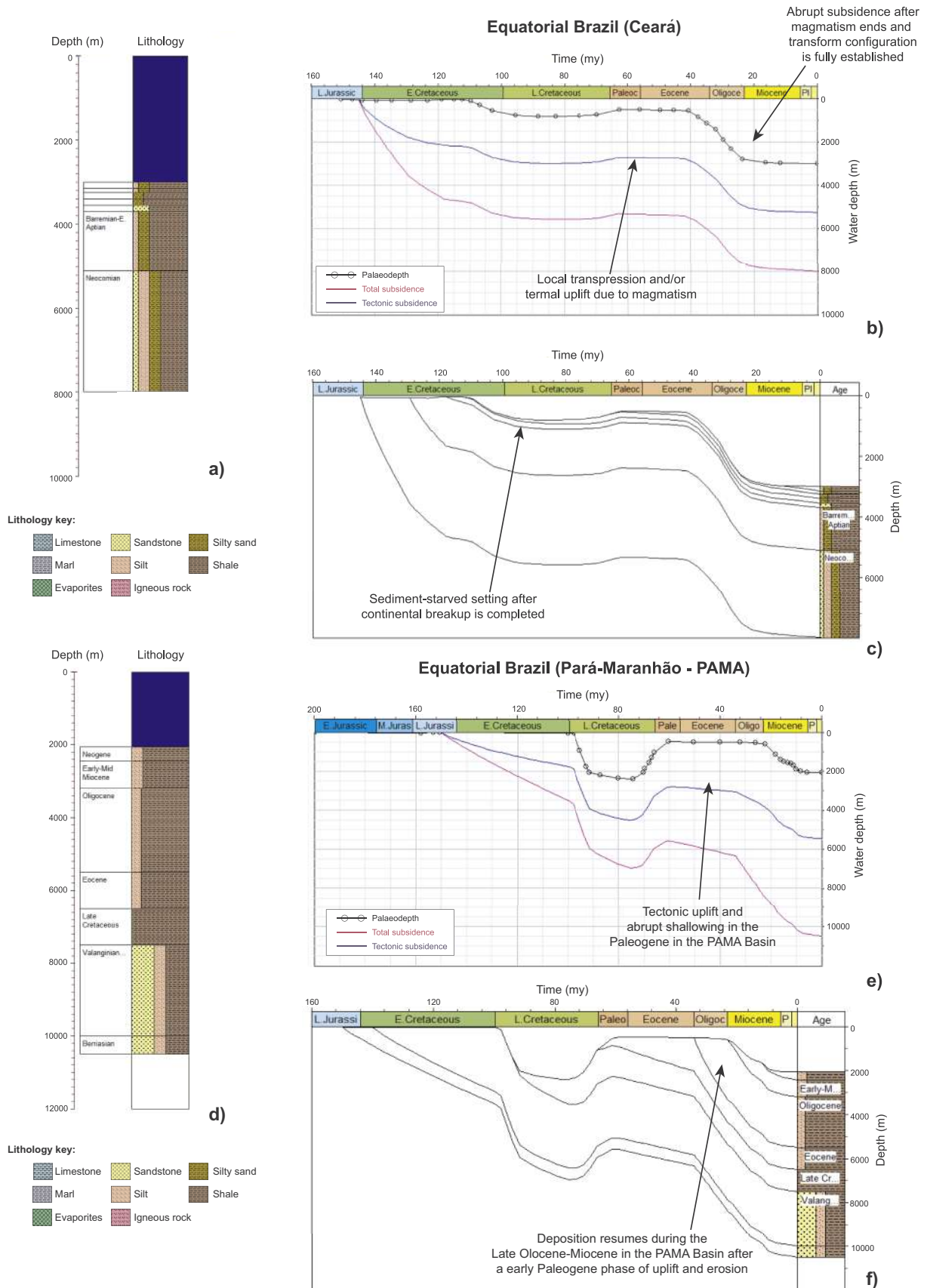
Fig. 13. Example of a transform configuration in ICMS. a) Uninterpreted and b) interpreted seismic profile across the Ceará Basin (Mundaú sub-basin) revealing important reactivation of a slope border fault and localised flower structures. The geometry of normal faults in this basin hints at important strike-slip reactivation in the Ceará Basin. The slope is narrow, dominated by sediment bypass, and steep. Seismic profile was modified from Almeida et al. (2019). PW refers to the pseudo-well described in Fig. 14.

4.3. Continental embankment (Liwuan Sub-Basin in China; Espírito Santo Basin, SE Brazil)

Continental embankment occurs in ICMS that record high sediment influx during their post-rift stage. The resulting continental embankment configuration comprises ICMS with a shelf edge above oceanic crust

(Busby and Azor, 2012), although such a configuration is often observed in an incomplete form on continental margins due to sediment bypass and erosion on the continental slope. As a result of the high sediment influx, prograding sedimentary units in these ICMS are dominated by important mass-wasting and channel incision. When present, evaporite successions are commonly remobilised to produce

Comparative tectonic subsidence curves: Transform configuration



(caption on next page)

Fig. 14. Pseudo-well (PW) models and calculated burial history and tectonic subsidence curves for transform ICM configurations in Equatorial Brazil. See Figs. 12 and 13 for location of the PWs along the seismic lines. The two regions show a stepped subsidence curves, and an acceleration of subsidence in the Oligocene-Miocene. Sediment-starved conditions were not achieved on the shelf, as organic productivity is very large and carbonate sediment was accumulated both on the shelf and slope. In addition, regular by-pass of rivers onto the slope and rise led to enhanced sedimentation in deeper parts of the two basins. a) Pseudo-well lithostratigraphy for Ceará. b) Assumed palaeowater depths and calculated tectonic and total subsidence for Ceará. c) Calculated burial history in the Ceará Basin relative to time. d) Pseudo-well lithostratigraphy considered in the subsidence modelling for the PAMA Basin. e) Assumed palaeowater depths and calculated tectonic and total subsidence for PAMA. f) Calculated depths of key stratigraphic units in the PAMA Basin relative to time.

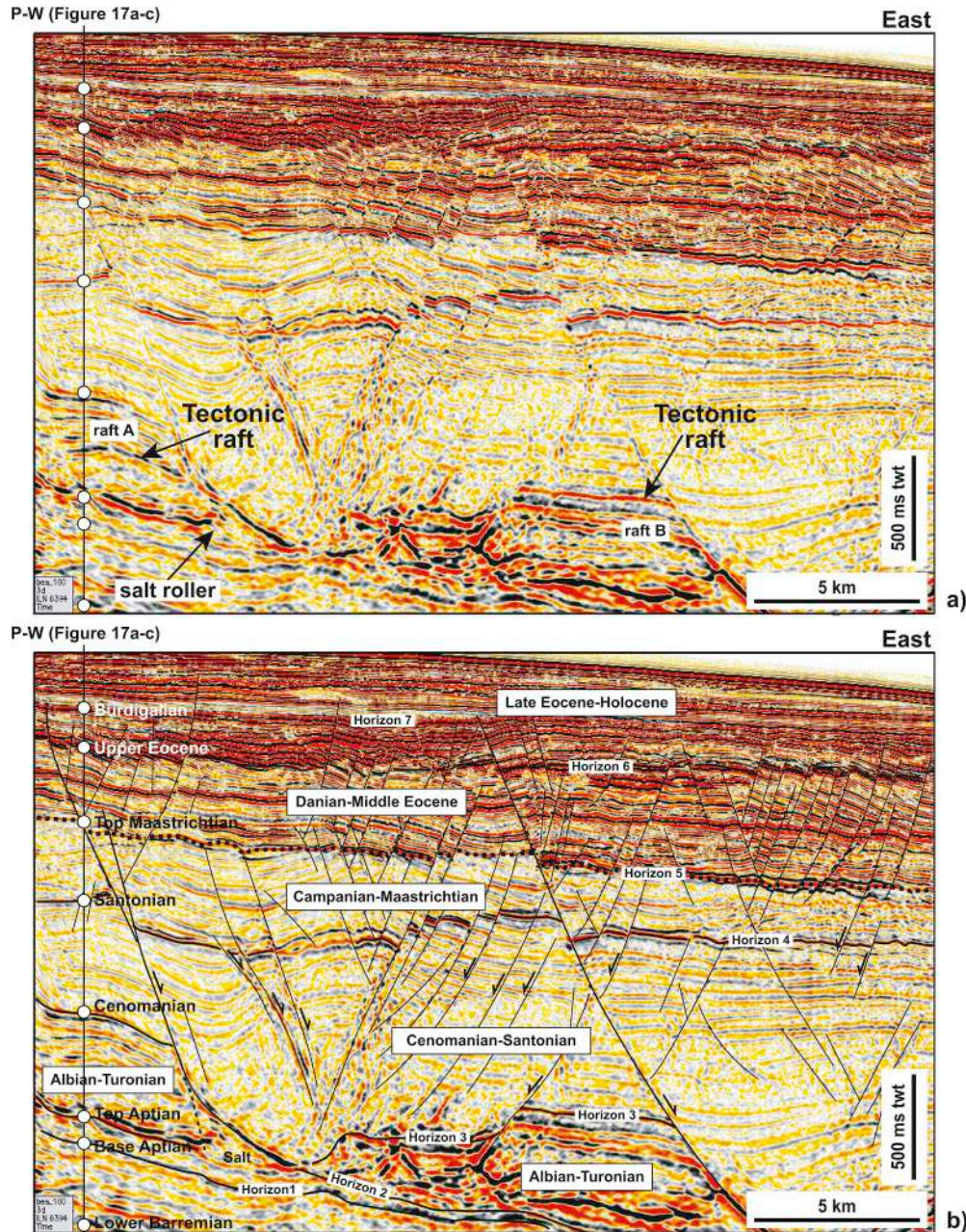


Fig. 15. Example of the continental embankment configuration in ICMs, with an example from the Espírito Santo Basin, SE Brazil. a) Uninterpreted and b) interpreted seismic profile depicting thick post-rift sediments affected by gravitational gliding and associated raft tectonics. Large roller faults, and associated keystone faults, offset a thick succession of Cretaceous and Cenozoic strata fed by a large hinterland area (SE Brazil). Figure modified from Alves (2012). PW refers to the pseudo-well described in Fig. 17.

large salt diapirs, salt domes and anticlinal structures, as in the case of the Niger and Mississippi Deltas (Busby and Azor, 2012). On the other part of the spectrum is the northern South China Sea and the vast region dominated by the Pearl River and its adjacent Pearl River Basin (Zhao et al., 2015; Sun et al., 2017; Sun et al., 2019).

Two ICM's are used as examples of this margin configuration, the

Espírito Santo Basin in SE Brazil, and the Liwuan Sub-basin in the South China Sea (Figs. 15 and 16). These two examples are located on the mid continental slope of both margins, with the continental shelf coinciding with large rivers (sediment sources) where large volumes of sediment have accumulated. Subsidence models for the Espírito Santo Basin highlight the near constant, but gentle subsidence of the continental

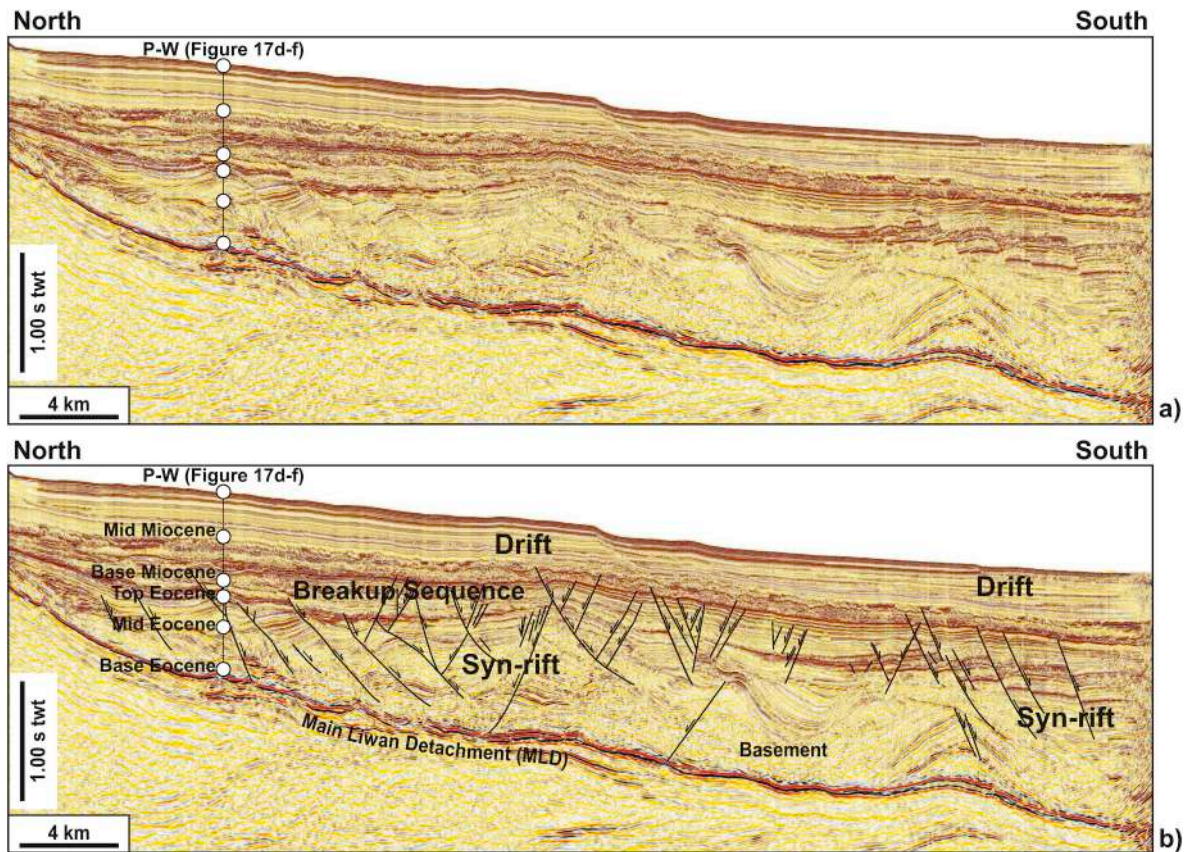


Fig. 16. a) Uninterpreted and b) interpreted seismic profile depicting a series of highly-rotated tilt blocks over a basal detachment – the Main Liwan Detachment (MDL) – in the Liwan Basin of the northern South China Sea. The figure also reveals a series of faults tipping out inside a breakup sequence associated with the opening of the South China Sea. Figure modified from Lei et al. (2019). PW refers to the pseudo-well described in Fig. 17.

slope in this area (Fig. 17a–c). The continental slope was also subject to important salt tectonics and records an apparent shallowing event during the Albian (latest Early Cretaceous), at a time of important halokinesis and formation of a shallow carbonate shelf over Aptian salt. Soon after, the computed tectonic subsidence curves reveal moderate subsidence, likely in association with salt withdrawal from below the post-Aptian successions. The tectonic subsidence curves derived in the Liwan Basin (South China Sea) reveal a short break-up event during the Oligocene that led to a moderate rate of subsidence from the Mid Miocene to the present day, with no major tectonic uplift stage (Fig. 17e and f). The Middle Miocene marks the full establishment of oceanic crust in the South China Sea, with a post-rift setting dominating the region after this time (Zhao et al., 2016). In the South China Sea, the Oligocene continental breakup event was accompanied by widespread magmatism in response to tectonic readjustments associated with the migration of the loci of continental breakup from the NE to the SW, along the northern and Vietnamese margins of the South China Sea (Sibuet et al., 2016; Zhao et al., 2016).

Fig. 15 shows a seismic profile from the Espírito Santo Basin, where depositional systems reflect the incision of channels and intense halokinesis. Developed salt diapirs and salt walls bounded the preferential pathways for transport and deposition of channelised and mass-wasting deposits, some sourced from the continental shelf and upper slope. Such a character indicates that turbidite and mass-transport deposition tend to occur at the same time and are complementary during the continental embankment stage. In the Espírito Santo Basin, Upper Cenozoic slope strata comprising channel-fill deposits alternate with submarine fan deposits and blocky mass-transport deposits part of the upper Urcutuca Formation. Conglomerates and sands relate to submarine canyon deposits (Alves, 2010; Gamboa et al., 2010). Massive marls, siltstones/sandstones and massive mudstones reflect lower-slope

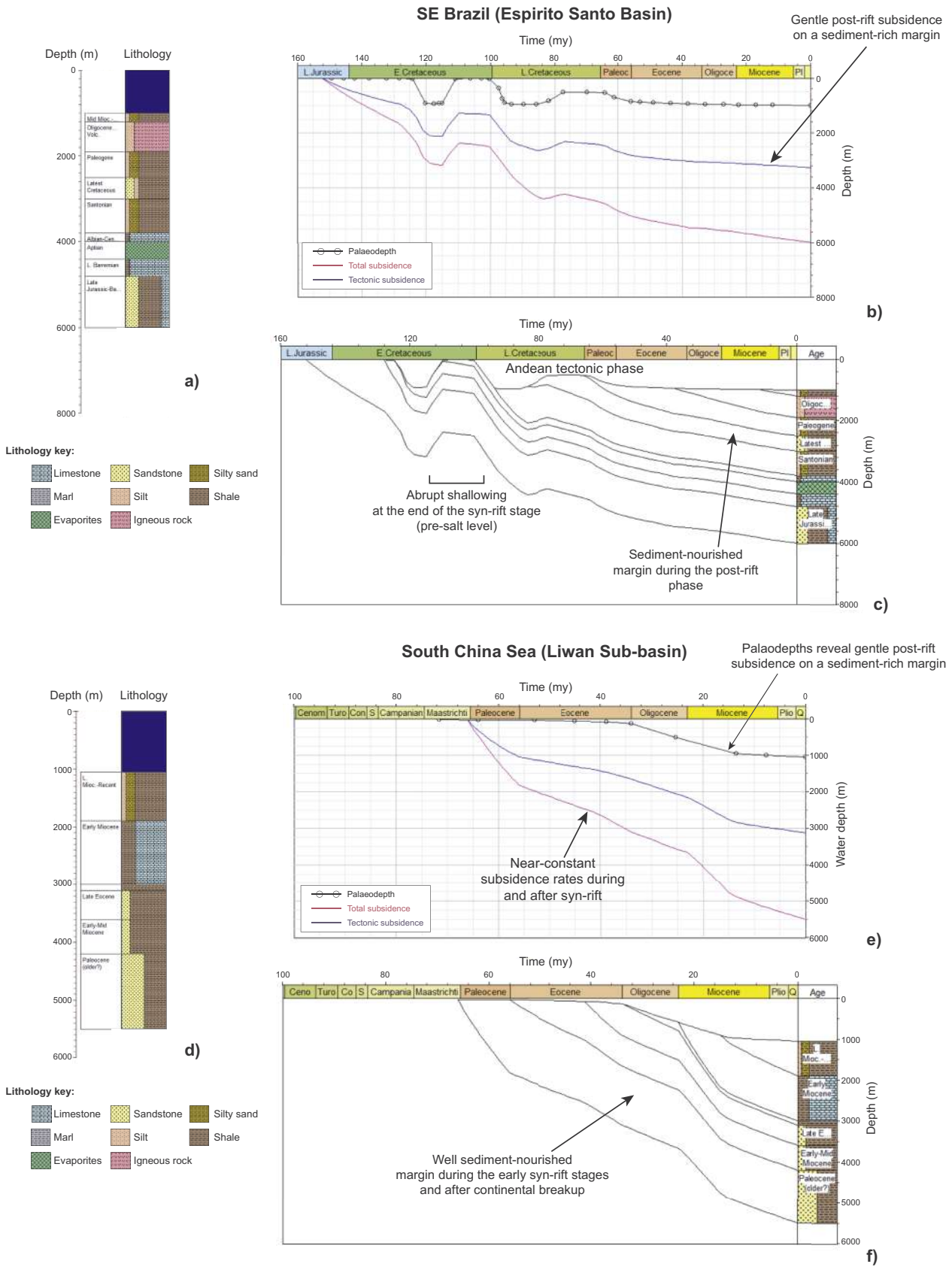
turbidites and distal hemipelagic fall-out.

In the Espírito Santo Basin, the rejuvenation of hinterland sediment sources was expressed by the deposition of coarse-grained gully- and channel-fill units, occurring together with marked sediment progradation (Alves et al., 2009). We interpret these channel-fill intervals as reflecting combined tectonic uplift and relative sea-level fall, which promoted the erosion of hinterland sediment sources through a vast area. Most of these channel-fill deposits show an affinity with MTDs that were vertically stacked in discrete cycles. Some channels seem not to incise the ‘background’ slope strata and are emplaced in slope depressions above and around slide blocks. In this case, overbank deposits show continuity towards the axis of channel-fill strata, pinching-out gradually away from the same channel axes (see Ward et al., 2018a, 2018b).

In the Liwan Sub-basin, 3D seismic data at the locus of continental breakup reveal the presence of multiple crustal blocks above a basal crustal detachment, named the Main Liwan Detachment (MLD) by Lei et al. (2019) (Fig. 16). Consequently, accommodation space during the deposition of syn-rift strata was controlled by normal faults comprising at this stage high-angle structures that precluded an abrupt phase of crustal extension ~12 Ma later. Lei et al. (2019) have also shown syn-rift strata to be composed of sandstones and gravel, interpreting this character as relating to the predominance of local sources of sediment during this initial syn-rift stage. In a second stage, hyperextension above the MLD added a total heave of ~30 km to the basin, with highly-rotated basement blocks adding important accommodation space for sediment sourced from multiple areas. Consequently, strata deposited at this time are relatively thin, accompanying the excess accommodation space created by hyperextension and the local uplift of large swaths of the distal margin.

In terms of its lithology, the syn-rift interval (Wenchang Formation)

Comparative tectonic subsidence curves: Continental Embankment configuration



(caption on next page)

Fig. 17. Pseudo-well (PW) models and calculated burial history and tectonic subsidence curves for continental embankment ICM configurations in SE Brazil and South China Sea (Liwan Sub-basin). See Figs. 15 and 16 for location of the PWs along the seismic lines. The two regions show marked subsidence and sediment accumulation (embankment) since their syn-rift stages. A brief shallowing phase in SE Brazil is associated with salt deposition and halokinesis. Both basins are well fed by sediment and record late tectonism, either in the form of halokinesis (SE Brazil) or regional tectonic reactivation and uplift (South China Sea). a) Pseudo-well lithostratigraphy for the Espírito Santo Basin, SE Brazil. b) Calculated palaeodepths, tectonic and total subsidence for the Espírito Santo Basin. c) Calculated burial history in the Espírito Santo relative to time. d) Pseudo-well lithostratigraphy for the South China Sea. e) Assumed palaeowater depths and calculated tectonic and total subsidence for the Liwan Sub-basin, South China Sea. f) Calculated depths of key stratigraphic units in the Liwan Sub-basin relative to time.

drilled by an exploration well south of China (LW116) recovered two different sandstone lithofacies: 1) moderately sorted, fine-grained sandstones in the upper lithofacies, and 2) grey, fine-grained to pebbly sandstones with sub-angular and semi-rounded quartz grains in the lower lithofacies (Lei et al., 2019). Pebbly intervals in the sandstones are poorly sorted, comprising clasts that are 7–12 mm in diameter, the largest reaching ~20 mm (see also Alves and Cupkovic, 2018).

4.4. Halokinetic basins (Lula Field, SE Brazil; Barents Sea, Northern Norway)

Some of the most important hydrocarbon discoveries of the past decade, e.g. the pre-salt fields of Santos-Campos-Espírito Santo basins, in SE Brazil occur in halokinetic basins (Fig. 1). Busby and Azor (2012) defined *halokinetic basins* as those formed due to the deformation of salt, chiefly in areas of continental embankment and in deformed forelands. Subsidence mechanisms creating salt-withdrawal, or *minibasins* in such a margin configuration, were considered by Hudec and Jackson (2007) as being akin to smaller scale models of crustal basins.

Two examples from the Lula Field (SE Brazil) and the Samson Dome (Barents Sea) are used in this section (Figs. 18–20). Tectonic subsidence curves derived for the Lula Field reveal moderate subsidence during the Late Cretaceous, when salt was mobile and significantly shortened on the SE Brazilian margin. An acceleration in subsidence occurred after the Cretaceous, a time also characterised by sediment-starved conditions around the Lula Field (Fig. 21a–c). An alternative way of explaining such a phase of virtually no Late Cretaceous subsidence relates to salt movement and deformation associated with ocean ridge-push (Alves et al., 2017). In fact, the significant erosion recorded by the Aptian Salt at its top hints at subaerial exposure of the larger salt ridges at this stage (Fig. 18). After the Paleocene, water depth increased significantly with regional (basement-driven) tectonic subsidence prevailing over gravitational deformation and halokinesis of salt structures in this region.

On the Samson Dome, Barents Sea, Late Carboniferous-Permian carbonate reefs and mounds are blanketed by a succession of Triassic, Jurassic and Cretaceous strata with distinct thicknesses (Mattos et al., 2016). Evidence for Cretaceous tectonic uplift and shortening of the Samson dome is observed in seismic data (Fig. 20) and throughout the western part of the Barents Sea (Indrevær et al., 2016). Subsidence curves record this deformation in the form of abrupt pulses of subsidence and uplift (Fig. 21d–f). In the particular case of the Samson Dome, its Mesozoic evolution shows important subsidence from the mid Triassic until the Early Cretaceous. Early Cretaceous uplift was due to the propagation of continental rifting towards the region to the west of the Svalbard Archipelago and Loppa High, where continental break-up finally occurred in the Paleogene (Ritzmann and Jokat, 2003; Polteau et al., 2019). Tectonic subsidence resumed after the Early Cretaceous at similar rates to those of the Late Triassic and Mid Jurassic (Fig. 21f). Tectonic uplift occurred again in two distinct Late Cenozoic stages in response to far-field crustal deformation (Indrevær et al., 2016).

A key aspect of halokinetic basins is that they systematically show a tendency to deform with time as salt is buried or remobilised on subsiding continental slopes. The resulting tectonic shortening is therefore capable of depressing the overburden strata above the salt creating salt welds, until they form a spillage point for oil accumulated in sub-salt units. In the Barents Sea, this effect is best documented by the pinched-

out to fully withdrawn evaporite units that occur on the flanks of the Samson dome, controlling the thickness and distribution of Carboniferous-Early Permian carbonate build-ups and mounds (Fig. 22).

In the Lula Field, seismic data reveal three zones when characterising their deformation styles (Figs. 18, 19 and 23). The central zone (Zone 2) shows tight folds in supra-salt strata, with local duplex structures and eroded salt anticlines (Figs. 18 and 19). Significant erosion is observed on top of salt structures in this region, particularly above pre-salt highs (Figs. 18 and 19). Zone 3, presenting the thickest salt accumulations around the Lula Field, is composed of structurally complex salt minibasins and anticlines, some of which are active at present (Figs. 18 and 19). Thrusts and salt withdrawal basins predominate in Zone 3 (Figs. 19 and 23).

Petroleum systems in this area will develop depending on three major parameters, assuming the presence of source rock around the Lula Field: a) the thermal history of syn-rift source intervals, b) the development of wide thrusts and salt welds in the salt, allowing for the escape of hydrocarbons (including its volatile components) to supra-salt units; c) the generation of structural traps and deep reservoirs below a salt succession that reaches > 3000 m in thickness in some locations (Figs. 18 and 19).

In halokinetic basins, subsidence (and associated extension of post-salt overburden units) is promoted by (1) density contrasts, (2) diapir shortening, (3) extensional diapir fall, (4) decay of salt topography, (5) sedimentary topographic loading, and (6) sub-salt deformation, including fault-controlled subsidence and uplift (Hudec and Jackson, 2007). Significantly, halokinetic basins tend to show post- or supra-salt structural styles (faulting, folding, and overburden degradation; Reeve et al., 2015) that are distinct from pre- or sub-salt strata (Alves et al., 2017). In supra-salt units, extensional faulting is chiefly concentrated on the crests and flanks of salt structures (Rowan et al., 1999; Tao and Alves, 2016), but important exceptions are observed whenever extensional detachments lead to the formation of tectonic rafts and associated listric (master) faults (e.g. Ruby et al., 2002; Mauduit et al., 1997). In this latter case, sub- and supra-salt units are connected through evolving listric fault systems and welds (Alves and Elliott, 2014; Piedade and Alves, 2017). In sub-salt units, continuing extensional collapse and thermal subsidence during (and after) continental break-up imposes important controls on the growth of salt structures (Dooley et al., 2007; Alves et al., 2017). Tectonic reactivation of sub-salt units can, therefore, induce important controls on the location and growth of salt structures, their deformation, and on resulting supra-salt structures.

5. Common geological features of ICMs

Some communality is observed between all types of ICMs, as explained in detail in the following sub-sections.

5.1. Extensional geometries

Stratigraphic successions on ICMs are characterised by an initial phase of crustal extension that generates strata with a ‘syn-rift’ geometry. In fact, approximately 50% of the total sediment volume of ICMs (but ranging from less than 10%–80%) are deposited in fault-bounded basins generated during crustal stretching (Busby and Azor, 2012). Sediment-starved parts of ICMs record the thinner syn-rift strata,

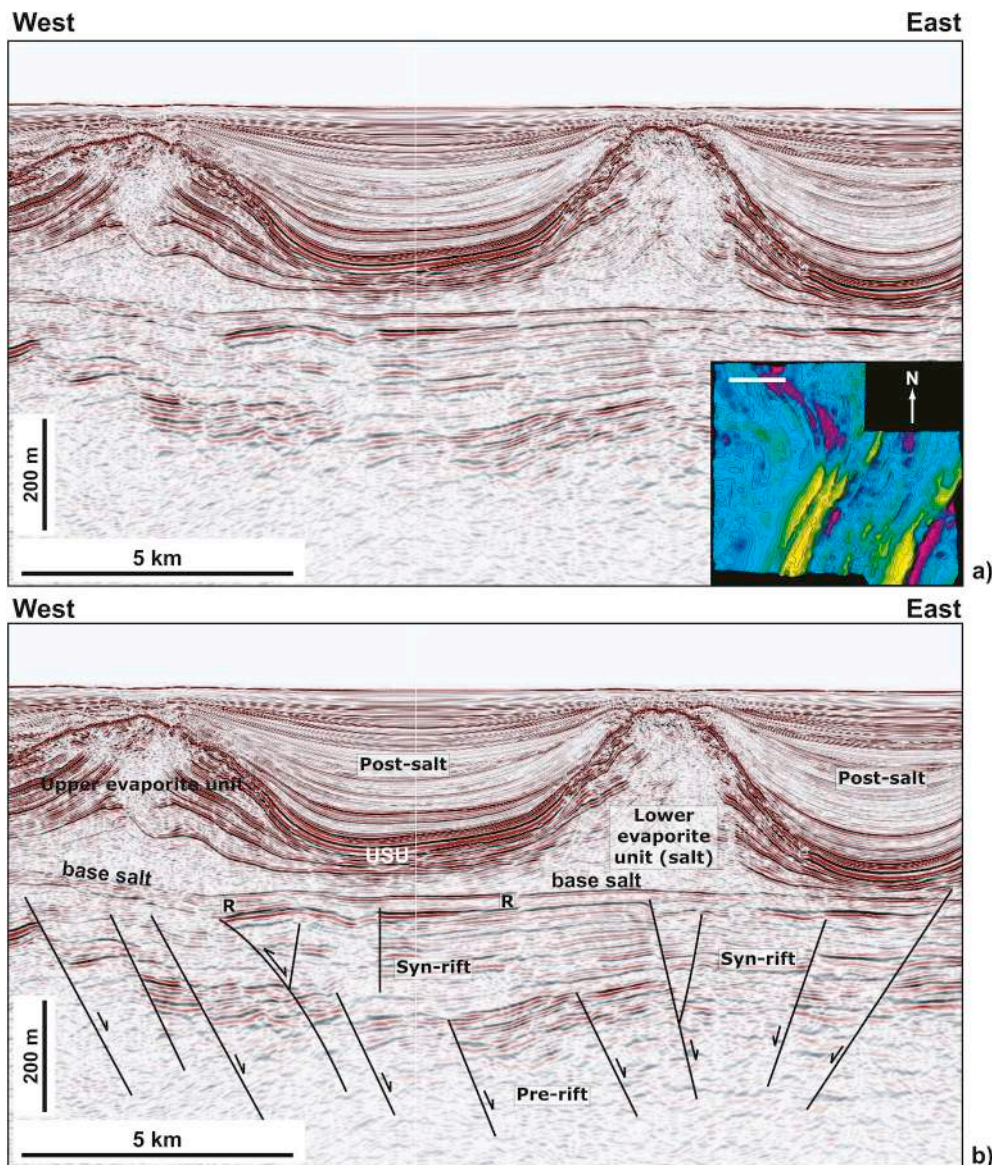


Fig. 18. Example of a halokinetic configuration in ICMs. a) Uninterpreted profile and b) interpreted profile highlighting the generation of large salt pillows and associated salt withdrawal basins in the Santos Basin, SE Brazil. See inset and Fig. 23 for location of the seismic profile.

particularly in shoulder areas of rift axes on proximal or most distal parts of these latter axes. Alves et al. (2009) and Alves and Cunha (2018) have shown that the thicker parts of these axes coincide with continental-slope areas at present, on most continental margins.

Syn-rift successions are better imaged when extensional (tilt) blocks were rotated and stretched by low-angle faults during the final extensional episode(s) leading to continental breakup (Fig. 24). This character makes ICMs geometry markedly distinct from aulacogens and abandoned rift axes that did not develop into fully rifted margins.

The classical definition of a rift axis, or graben, includes the generation of a 'steer-head' geometry with uplifted shoulder areas providing sediment to principal depocentres (White and McKenzie, 1988). Such a geometry is clear in aulacogens as the North Sea, where most concepts in syn-rift stratigraphy have been defined, with the generation of a 'Central Graben' separated by structural highs to the east (e.g. Jaeren High, Troedland Platform) and by the UK landmass to the west.

In contrast with aulacogens, extensional basins on ICMs are often asymmetric in response to enhanced crustal stretching preceding continental breakup and record important exhumation and erosion of footwall blocks formed adjacently to them (Manatschal and Bernoulli,

1998). This asymmetry is, both on seismic and conceptual models, a result of a late stage of extension leading to final continental breakup (Huisman and Beaumont, 2011). Figs. 16 and 24 show examples of rotated tilt blocks in South China and West Iberia. In these three regions, syn-rift strata are highly asymmetric and rotated tilt-blocks were stretched in the direction of crustal stretching that led to continental breakup. Mathematical and subsidence models indicate that crustal stretching (and associated tectonic subsidence) accompanied continental breakup, inducing an important time-dependent collapse of deep-water basins as a last-stage of continental stretching precludes full continental breakup (Alves and Cunha, 2018; Monteleone et al., 2019).

5.2. Degradation complexes during syn-rift tectonics

Degradation complexes are ubiquitous in syn-rift basins around the world and have been identified on geophysical data from several ICMs (Alves and Cunha, 2018; Alves and Gamboa, 2019; Ribes et al., 2019). One of the best examples at outcrop is located in Crete, South Aegean Sea, where exhumed Miocene-Pliocene rift basins are located. These rift basins are bounded by a series of N10 to N70 faults that sourced

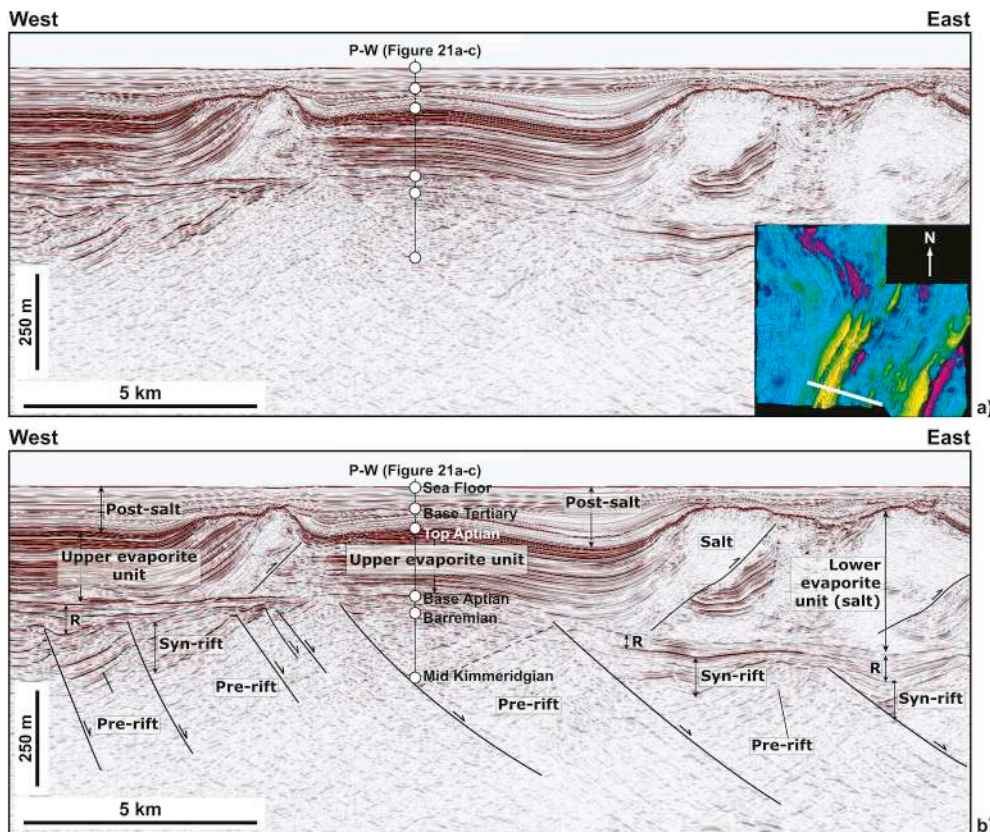


Fig. 19. Example of a halokinetic configuration in ICMS. a) Uninterpreted profile and b) interpreted profile highlighting the generation of a series of normal faults bordering a series of half-grabens to the east and west of a basement high. Note the significant erosion over this high and the putative salt weld between the upper evaporite unit and the structural high *per se*. Main thrusts at salt level are highlighted together with the largest normal faults crossing pre-salt strata. PW refers to the pseudo-well described in Fig. 21.

sediment to the rift basins during syn-rift extension (Postma and Drinia, 1993; Alves and Cupkovic, 2018) (Fig. 25). In these basins, distal marine facies (Fa A to C; Postma and Drinia, 1993) give way to mass-wasting deposits near tectonic faults, some of which show large scale megabreccia blocks and boulder-conglomerate units with variable thickness (Fig. 26).

Fan deltas (Fa1; Postma and Drinia, 1993) reflect the most proximal deposits in the extensional basins of Crete. They comprise autochthonous megabreccia fans and rotated slabs that are, at outcrop, tens to hundreds of metres thick (Fig. 26a). Fan deltas are stacked vertically on top of rotated hanging-wall blocks (Fig. 26a). Fan deltas were sourced from basement units of distinct nature and lithologies to include polymictic breccias and conglomerates derived from a supra-detachment unit (Tripolitza Unit) that was eroded on top of the pre-detachment metamorphic basement. Dispersed clasts of higher-grade metamorphic rocks include marbles and ophiolites sourced from rocks below the Cretan detachment (i.e., Lower Sequence) (Fig. 4). In summary, coarse-grained material in these facies associations was deposited in slope environments where seafloor instability was common and tectonic oversteepening prevailed (Alves and Cupkovic, 2018).

Degradation complexes on ICMS often interfinger with mass-transport deposits towards basin depocentres. On Crete, mass-transport deposits (Fa2–4 and A–C in Postma and Drinia, 1993) are observed on the lower part of fault-bounded slopes together with large 5–100 m-wide blocks (Fig. 26a and b). They also occur in the lower parts of fan deltas as the most distal facies in Fa 2–4 (Fig. 26c). In contrast, background hemipelagites and distal submarine fan deposits are particularly observed in the largest depocentres of SE Crete, and in coastal outcrops. They are mostly consolidated silty sands and clays that can be interrupted by channel-fill deposits. Burrows were considered common in Fa 2–4 and include *Skolithos*, *Chondrites* and *Thalassinoides* spp. (Postma and Drinia, 1993). Intervals with sand and silt in Fa 2–4 were affected by wave action and likely triggered by stream floods and hyperpycnal flows during periods of extreme water discharge.

Alves and Cunha (2018) and Ribes et al. (2019) posed the question if sedimentary breccias at rifted margins always belong to the “syn-tectonic” phase. In Crete, gully and channel-fill deposits, as well as breccias, are ubiquitous at coastal outcrops and in several locations around exhumed basement units (Fig. 26). As suggested by the authors above, breccia generation has exceeded on Crete the usual time activity for normal faulting – they are essentially associated with the degradation of a Miocene-Pliocene syn-rift topography that may, or may not, be active at present along Crete. Quaternary uplift has renewed the fault-related topography and re-energised sediment sources to produce localised coarse-grained deposits. Grain size varies from well sorted coarse-to medium-sands, to polymictic gravel and conglomerate channel-fill deposits.

5.3. Syn-to post-rift magmatism

Syn-to post-rift magmatism is highly variable and induce important variability in the thermal and subsidence histories of ICMS (Autin et al., 2010; Armitage and Collier, 2017). Magma-poor and magma-rich basins were firstly presented as two defined types of continental margins in the geological record (White et al., 2003). Data has shown, however, that magma-poor margins can record important magmatism during syn-rift and continental breakup in the form of local intrusions and (post-rift) volcanism. In fact, the terms magma-poor and magma-rich continental margins have recently been given importance as two end-members of what is a wide spectrum of geometries and magmatic evolutions (Franke et al., 2010; Franke, 2013).

Magmatic episodes are capable of affecting ICMS in dramatic ways (e.g. Keir, 2014). For example, in SW Africa, flood tholeiites of the Paraná-Etendeka system were accumulated during continental rifting and breakup. Transverse lineaments to the SW Africa comprise alkaline and alkaline-carbonatitic complexes; sodic and potassic suites (Trumbull et al., 2007; Comin-Chiaromonte et al., 2011). Offshore Equatorial Brazil, large volcanic seamounts were suggestively formed

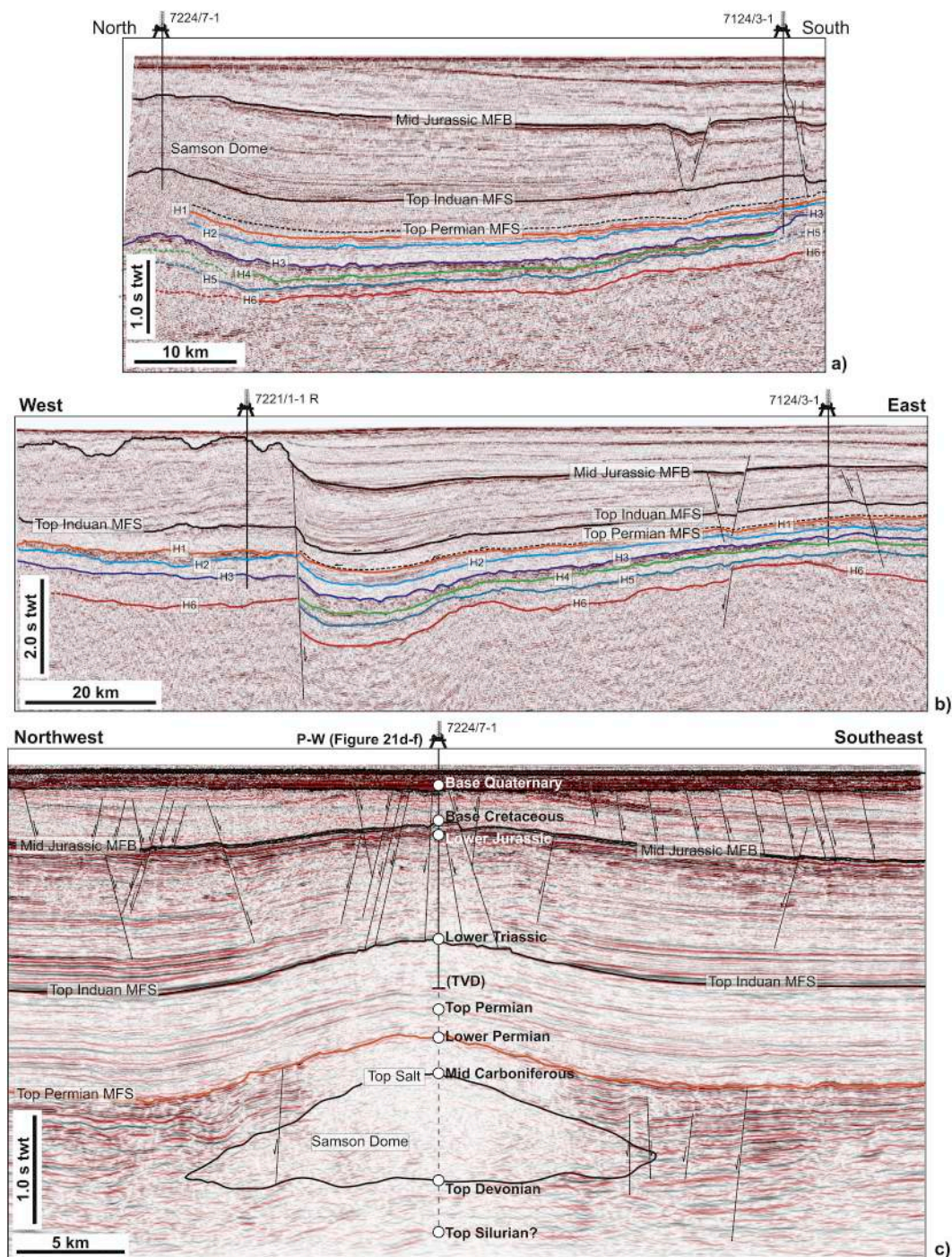


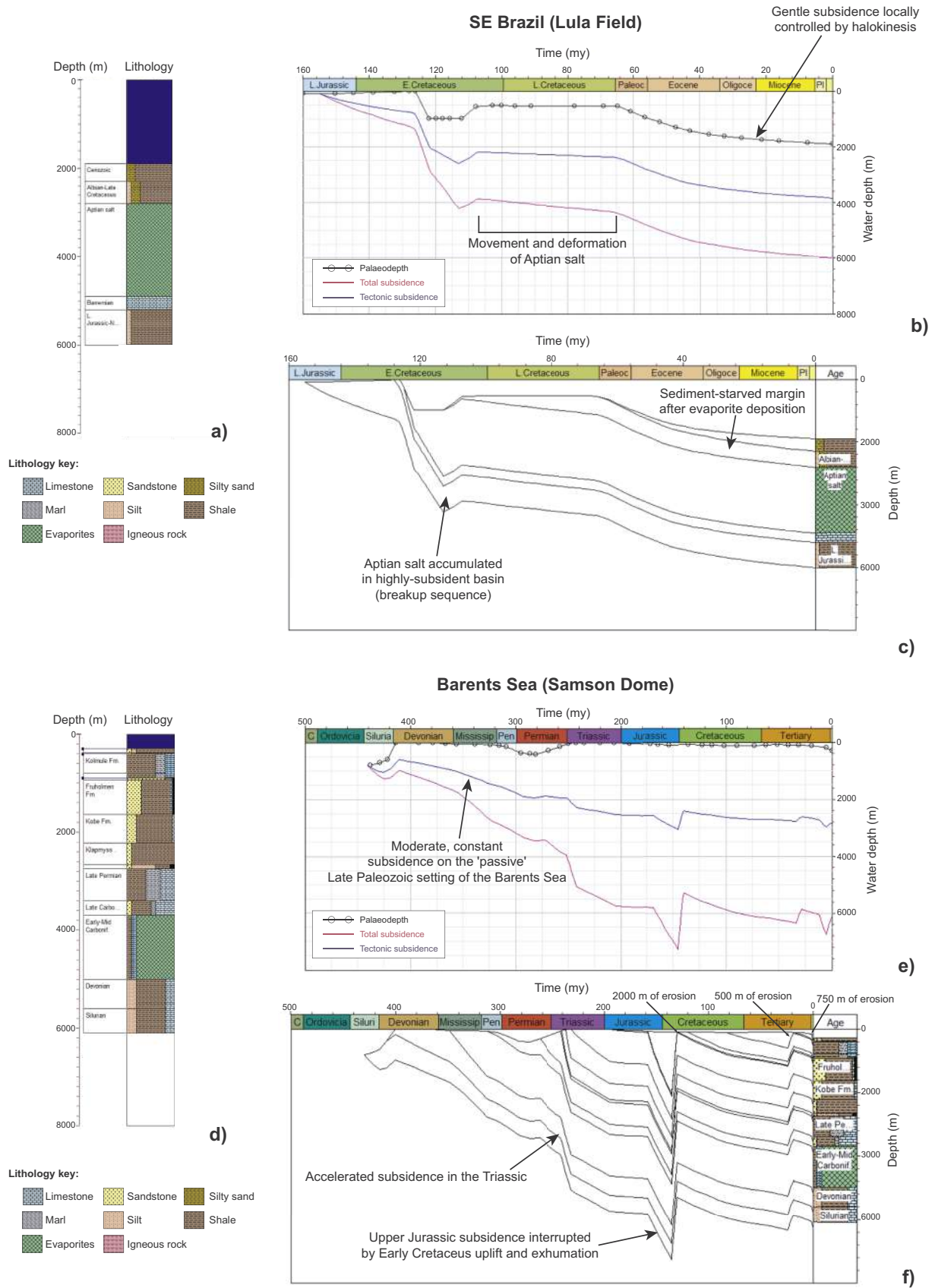
Fig. 20. Northwest-Southeast 2D seismic profile crossing the Samson Dome, Barents Sea, highlighting the main structures in the study area and key seismic stratigraphic intervals. b) Composite 2D seismic profile crossing the region south of the Samson Dome and Loppa High illustrating the main seismic-stratigraphic boundaries interpreted in the Barents Sea by Alves (2016). c) Interpreted section showing the interpreted seismic units, horizons and some of the faults observed around the Samson Dome, together with an interpretation of the Carboniferous salt in this same area. The Samson Dome comprises an anticline with units of relatively constant thickness, with the exception of Late Cretaceous strata. These strata are truncated over the crest of the Samson Dome. The location of well 7224/7-1 is also indicated in this section. Figures a) and b) are taken from Alves (2016). Figure c) is modified from Mattos et al. (2016). PW refers to the pseudo-well described in Fig. 21.

during diachronous continental breakup (Wilson, 1992; Davison, 2007; Davison et al., 2015) and are associated with important magmatism in the Tertiary, well after continental breakup was achieved.

Newfoundland-Iberia constitutes an example of magma-poor ICMS in the literature, but magmatism is still ubiquitous in these two regions. DSPD and ODP data have drilled a series of dikes and sills offshore Newfoundland and Galicia (Tucholke and Sibuet, 2007). Onshore

Portugal (West Iberia) are recognised four magmatic events during early rifting (CAMP-related basalts offshore SW Iberia into NW Africa), associated Late Jurassic-Early Cretaceous syn-rift (Miranda et al., 2009; Neres et al., 2018), and during later post-rift plate readjustments (Campanian-Maastrichtian) (Neres et al., 2013; Pereira et al., 2017; Merle et al., 2018) (Fig. 27).

Comparative tectonic subsidence curves: Halokinetic Basins configuration



(caption on next page)

Fig. 21. Backstripped subsidence curves for halokinetic basins on ICMs off SE Brazil (Santos Basin) and Barents Sea (Finnmark Platform). See Figs. 19 and 20c for location of the PWs along the seismic lines. The two regions show gradual sedimentation interrupted by short-lived, but abrupt, episodes of uplift and basin inversion. These latter episodes are facilitated by the presence of salt at depth, which is reactivated and deformed during post-rift tectonic events. a) Pseudo-well lithostratigraphy for the Lula Field, SE Brazil. b) Assumed palaeowater depths and calculated tectonic and total subsidence for the Lula Field, SE Brazil. c) Calculated depths of key stratigraphic units in the Lula Field relative to time. d) Pseudo-well lithostratigraphy for the Samson Dome area, Barents Sea. e) Assumed palaeowater depths and calculated tectonic and total subsidence for the Samson Dome, Barents Sea. f) Calculated depths of key stratigraphic units around the Samson Dome relative to time.

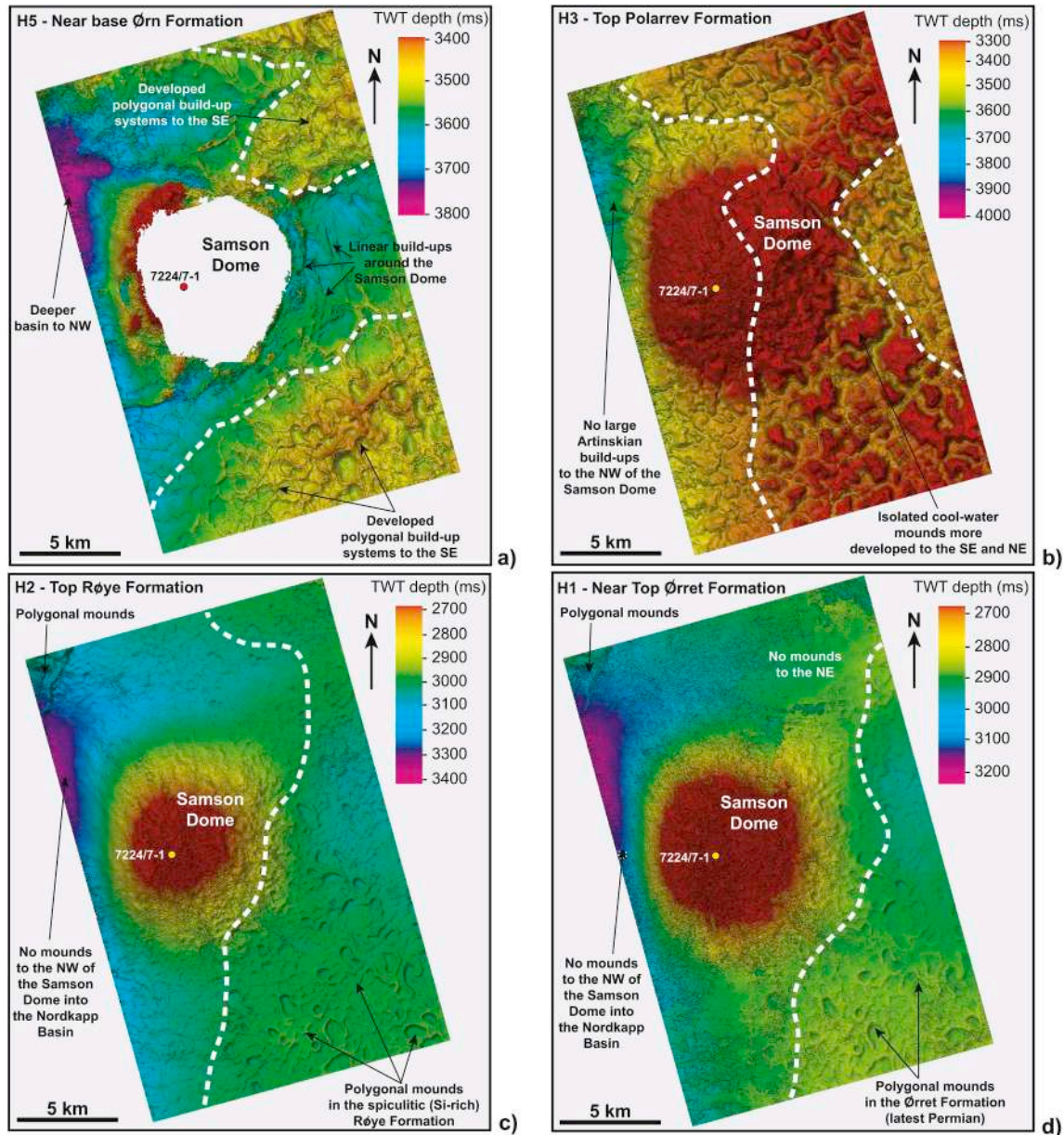


Fig. 22. TWT structure maps highlighting the geometry of carbonate build-ups around the Samson Dome during the late Paleozoic, and the influence of this same dome in the distribution of carbonate mounds and polygonal buildups. a) Shows sets of developed polygonal build-ups at the base of the Ørn Formation, Late Carboniferous, but only occupying the NE and S portions of the map. b) Highlights the distribution and geometry of isolated spiculitic mounds from the Polarrev Formation (Early Permian). At this time, these mounds were controlled by the growth of a N-S salt ridge over which they reached maximum thickness, width and overall development. c) Records the return of polygonal mounds in the Late Permian, within the Røye Formation, in a region to the east of the Samson Dome. This latter high does not show polygonal features and was likely sheltering the eastern part of the study area. d) Reveals polygonal mounds approximately 50 ms below the Permian-Triassic boundary (Top Permian – Horizon 1), but only restricted to the SE flank of the map. The polygonal features were soon drowned above the Ørret Formation. The maps have a 30× vertical exaggeration and were modified from Alves (2016).

5.4. Overprinting of younger crustal stretching on older pre- and syn-rift fabric(s)

Using the example of West Iberia-Newfoundland once again, seismic

and borehole data indicate that syn-rift extension records a concentration of tectonic subsidence in continental-slope basins (Alves et al., 2009). Inboard from these continental slope basins (i.e. in the Lusitanian and Porto Basins), tectonic subsidence was particularly

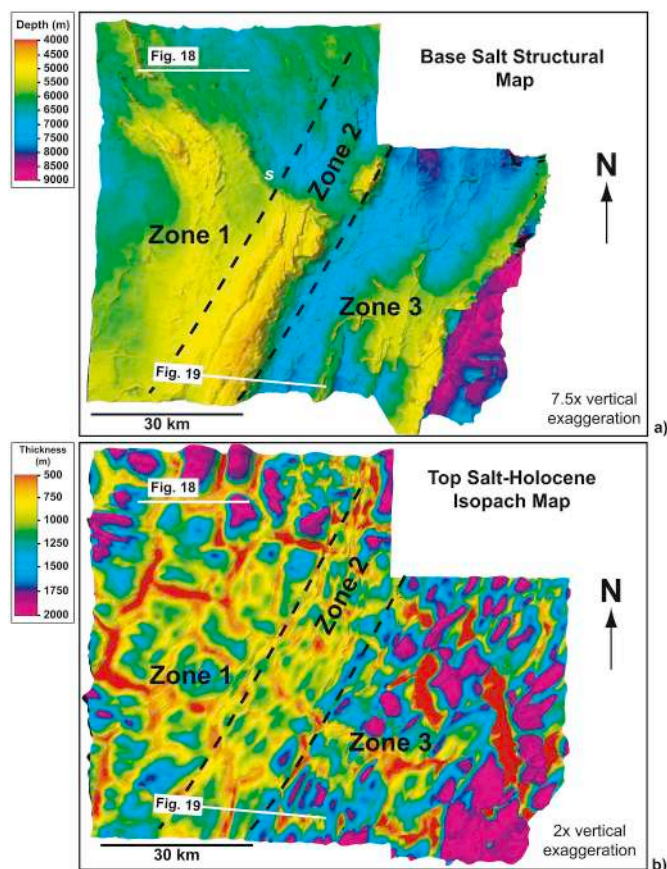


Fig. 23. a) Depth map of the base salt surface around the Lula Field showing the relative position of the three main salt deformation zones in relation to the underlying the pre-salt structure. b) Isopach map of the Top Salt-Holocene interval highlighting the three main zones considered in Alves et al. (2017). Note the development of multiple salt withdrawal basins in Zones 1 and 3 during this time span. Many of these salt withdrawal basins are accompanied by thrust faults and significant deformation of the upper evaporite layer, as exemplified in Fig. 19.

active during the Triassic-Mid Jurassic interval (Cunha, 2008). Also in the deeper parts of West Iberia, the tectonic subsidence recorded during the first Jurassic rift episodes was later enhanced during continental breakup (Alves and Cunha, 2018). The ages of the largest subsidence pulses in West Iberia coincide with similar episodes in the Jeanne d'Arc Basin (Baur et al., 2010), and Lusitanian Basin (Stapel et al., 1996), but had a much larger magnitude in deep-offshore basins when compared with proximal rift basins.

Alves et al. (2009) postulated on the reasons why syn-rift strata is markedly thicker on the outer proximal margin of West Iberia when compared with the more proximal Lusitanian and Porto basins on the continental shelf (Fig. 24). According to the authors, a first reason may relate to greater rates of crustal stretching and tectonic subsidence occurring on the outer proximal margin during the extensional episodes that led to continental breakup. This partly justifies the tectonic subsidence curves modelled for West Iberia and Newfoundland by Alves and Cunha (2018). However, such an explanation seems to contradict the relatively smaller rates of subsidence recorded in the Jeanne d'Arc Basin, ranging from 40 to 120 m/Ma, when compared with the Lusitanian Basin, a character that nevertheless resulted in the accumulation of substantially thicker syn-rift successions in Canada. A way to justify the discrepancy in subsidence between West Iberia and Canada is by postulating a longer period of Late Jurassic-Early Cretaceous basement subsidence offshore Canada (Hiscott et al., 1990; Leinfelder and Wilson, 1998), as the Lusitanian Basin was likely not in an equivalent position

on the continental margin to the Jeanne d'Arc Basin when of the final rifting episodes leading to continental breakup.

A second possibility invoked by Alves et al. (2009) was that the more distal rift basins record longer (but not necessarily greater) episodes of crustal stretching and subsidence when compared to the most proximal margins. Syn-rift strata filling continental slope basins would result from a rather prolonged extensional episode spanning from the early rifting stage until continental breakup (Fig. 24). For this postulate to be confirmed, syn-rift deposits older than the late Oxfordian must occur on the continental slope basins of West Iberia, into the distal margin. However, such an assumption contradicts the DSDP/ODP data from the distal margins, and it does not corroborate the seismic reflection and well data along West Iberia margin. Here, a clear stratigraphic boundary separates pre-rift strata from syn-rift units on the outer proximal margin, i.e. dividing units deposited during the early rifting stage from strata accumulated in the advanced rifting stage (e.g., Groupe Galice, 1979; Pinheiro et al., 1996) (Fig. 24). An alternative explanation includes a closer similarity between the continental slope basins of West Iberia and the Canadian Grand Banks. Offshore Canada, discrete extensional episodes occurred diachronously in distinct segments of the Newfoundland margin, adding up to the final values of tectonic subsidence recorded in adjacent sedimentary basins (Sinclair, 1995; Hiscott et al., 1990).

Tectonic subsidence curves for West Iberia and Newfoundland reveal marked subsidence during the final Late Jurassic-Early Cretaceous syn-rift episode that preceded continental breakup. This same episode coincides with a shift in the locus of extension towards the outer proximal margin and precedes a further period of abrupt tectonic subsidence during the continental breakup process per se (Alves and Cunha, 2018). In this setting, Late Jurassic-Early Cretaceous extension was able to re-activate and re-use early syn-rift faults, overprinting the older syn-rift structure of the margin. Tectonic subsidence in distal parts of West Iberia and Newfoundland thus results from the superposition of discrete extensional episodes, particularly those related to Late Jurassic-Early Cretaceous rifting and the continental breakup event per se. Basin-bounding faults on the outer proximal margin, including prominent Slope Fault Systems, were generated prior to the Late Jurassic accounting for 1) the thickness variations observed in Triassic-Middle Jurassic strata along west Iberia and 2) variations in the distribution of Triassic-Hettangian salt across the North Atlantic (Fig. 24). Such a scenario implies that the final episodes of extension leading to continental breakup were accompanied by significant early-rift subsidence and extensional faulting in continental-slope basins (Fig. 24).

6. Discussion

6.1. Effect of variable subsidence and magmatic histories on ICMs' hydrocarbon potential

All wells and pseudo-wells modelled in this work show distinct subsidence histories for the ICM configurations considered. These distinct evolutions for ICM types have a key impact on their petroleum potential. Tectonic subsidence is one of the key parameters controlling the burial history of sedimentary basins, and thus the maturity of potential source rock intervals leading to oil and gas generation and expulsion (Magoon and Beaumont, 1999). Tectonic uplift, conversely, has the main effect of withdrawing source rocks from the oil and gas windows, at the same time exhuming reservoir and seal units. However, the balance between subsidence and uplift is a fine one in sedimentary basins, as very moderate tectonic reactivation is often needed to promote the efficient expulsion of hydrocarbons from the source rock, and its eventual migration to conventional reservoirs.

In the four (4) margin configurations considered in this work, the often hydrocarbon-rich halokinetic configuration comprises multiple periods of regional tectonic reactivation and uplift. One key aspect in these areas is that tectonic reactivation, a key promoter of fluid

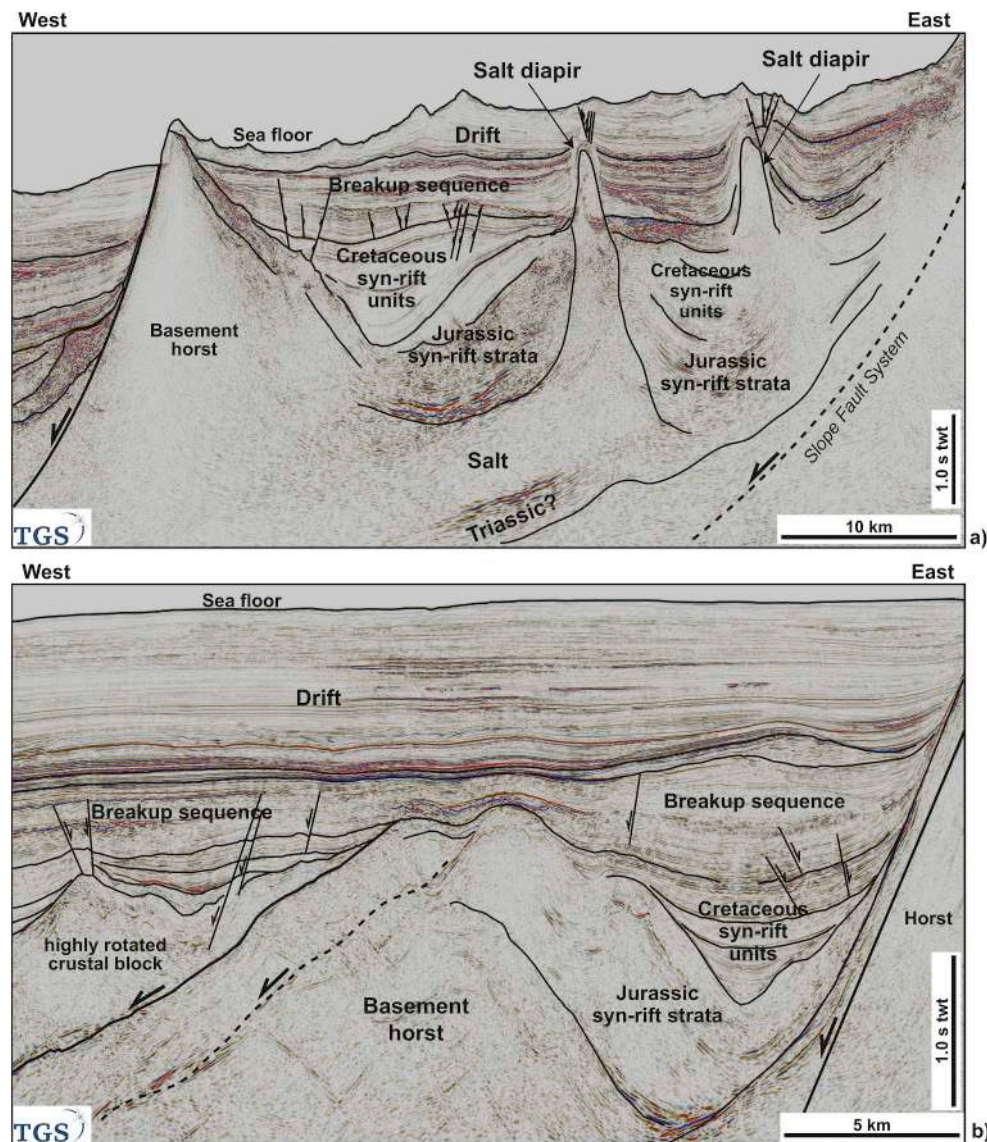


Fig. 24. Example of thick syn-rift successions in West Iberia, hinting at the presence of well-developed early Mesozoic successions in deep-offshore basins. A) Shows salt diapirs and underlying units reaching a thickness of more than 5 s TWT. Here, salt and overlying tilted syn-rift strata reveal a seismic character akin to the Lusitanian Basin. b) Upper Jurassic-Upper Cretaceous syn-rift successions on the distal margin of NW Iberia revealing a relative absence of salt, thick syn-rift strata that are putatively younger than in a), and thick breakup and drift successions.

migration in this margin configuration, is not of enough magnitude to compromise thick salt as a major seal unit (Alves et al., 2017), or affects deeply-buried salt (at particular times) to allow the migration of hydrocarbon sourced deep in sedimentary basins to shallower reservoirs (Piedade and Alves, 2017). With most halokinetic configurations occurring in areas of significant continental embankment (Busby and Azor, 2012), the significant influx of sediment onto continental slopes has the dual effect of burying any source rocks and promote halokinesis to favour the migration of hydrocarbons to salt-related traps and reservoirs (Peel, 2014). A final effect of salt is to cool-down sedimentary basins in relative terms, thus allowing deeply buried source intervals to remain in the oil and gas window.

In contrast to the latter setting, pseudo-wells in West Iberia show ‘typical’ syn-rift subsidence with no tectonic reactivation or significant sediment influx into continental-slope basins (Fig. 11). Importantly, great part of the late syn-rift history of the margin during the Late Jurassic and Early Cretaceous records a relative shallowing, erosion and potential subaerial exposure of large parts of its basins (Alves and Cunha, 2018). The end of the Early Cretaceous is characterized by an

acceleration of the subsidence, but this occurs during the onset of continental breakup some 25 Ma after the initiation of the last (Late Jurassic) pulse of continental rifting. Hence, on the continental shelf and over syn-rift horsts in the deeper continental slope, it is not uncommon to record Early-Mid Jurassic strata below Cretaceous (and younger) units, reflecting the exhumation of large parts of West Iberia (Fig. 24).

A prolonged and marked phase of continental embankment is therefore a positive characteristic of hydrocarbon-rich basins, contributing to the maturation of source intervals and formation of reservoir and seal units above these latter. In the example from the South China Sea and NW Australia provided in this paper, the main difference between the two regions is the relative importance of post-rift magmatism. In the South China Sea, volcanic mounds occur above “acoustically dim” zones and are developed close to the upper tips of faults, which extend downwards into older Cenozoic strata. Gentle folds developed above volcanic mounds result from differential compaction (Zhao et al., 2016). In this same area, volcanic mounds are developed between two distinct seismic markers; they are dated as ~18 Ma and

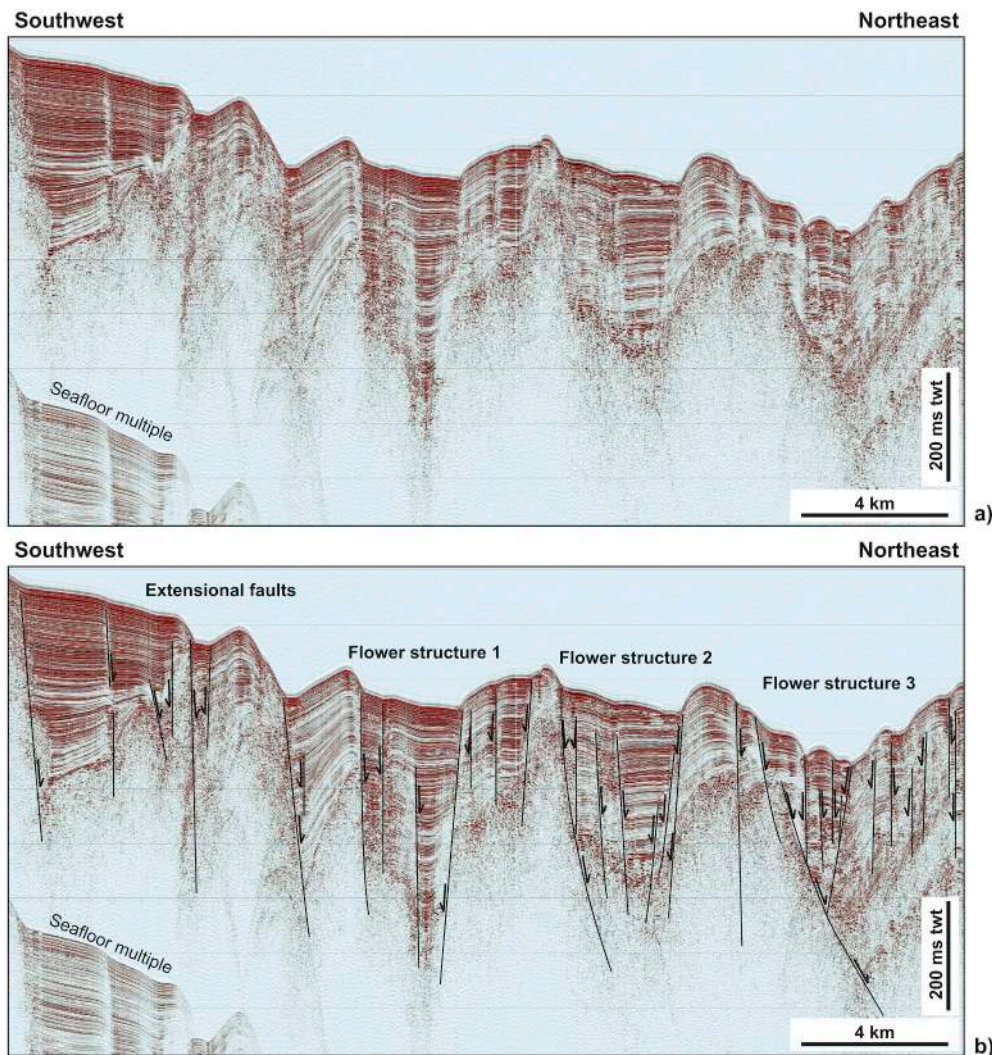


Fig. 25. Example of the transtensional structural style recorded offshore Crete, in tectonically active basins. The figure shows the progressive change from an extension-dominated regime to the SW, to a transtensional regime to the NE. Note the thin sediment cover above Flower Structure 3, which should be the most active of the three flower structures observed at present.

~23.8 Ma, corresponding to a phase of latest Oligocene-early Miocene magmatism (Zhao et al., 2016).

Zhao et al. (2016) have documented the lithology of such mounds using core data from two industry wells. The first well (BY2) sampled vertically stacked lava flows, mostly basalt lavas and tuffs that alternate with carbonate sediments and terrestrial clastics. Intervals of acidic volcanic rocks, including dacites and rhyolites, were also encountered. The principal minerals of the altered volcanic rock are plagioclase, pyroxene and altered ferromagnesian minerals (Zhao et al., 2016). Basalt collected in sidewall cores have been widely replaced by siderite, chert and Fe-dolomite. Fe-dolomite fills some of the observed fractures.

Well BY7-1 documented by Zhao et al. (2016) drilled through a 420 m-thick succession of basaltic lavas and tuffs, alternating with thin-bedded limestones and sandstones. Eleven limestone intervals were found in well BY7-1 to be intercalated with basaltic lava and ash. These limestone intervals comprise encrusting algae, benthic foraminifera, bryozoans, sponge spicules and scleractinian corals with an essentially micrite matrix. The thickness of these limestone intervals ranges from 0.75 m to 9.0 m, indicating shallow marine depositional environments. Extrusive rocks and sediments are intercalated in well BY7-1 to suggest important hiatuses in volcanic activity. Sidewall cores collected altered amygdaloidal basalt lavas and tuffs with lava and basaltic glass fragments (Zhao et al., 2016). The primary minerals of what is a partially

altered basalt are plagioclase, pyroxene, opaque minerals and olivine. Zeolite is an important cement in the rock and is accompanied by calcite in fractures.

Heat flow on ICMs is markedly variable and depends on a multitude of local and regional factors. On a regional scale, the history and geometries of crustal and mantle stretching are paramount controls on basement heat-flow distributions (McKenzie, 1978; White et al., 2003; Scheck-Wenderoth and Maystrenko, 2008). Together with sedimentation it determines the heat flow distribution within the basin through time, and thus source rock maturity, through a series of processes that can be parameterized and modelled within a given degree of uncertainty (e.g. Souche et al., 2017). Overprinting the more predictable effects of stretching and sediment blanketing of ICMs prior to continental breakup are parameters (or processes) notoriously hard to quantify such as the character of the rifted continental crust and mantle and the nature of transitional basement - suggestively distinct from basement units outcropping on the continents (Artemieva and Mooney, 2001; Scheck-Wenderoth and Maystrenko, 2013). The ages and lithological character of stretched basement rocks can be variable, imposing conduits for heat in the deeper crust, and deep-rooted faults can act as very efficient heat conduits to the surface.

On ICMs, the effect of salt on heat flow distribution is also significant (e.g., Serié et al., 2017; Canova et al., 2018). Thick salt

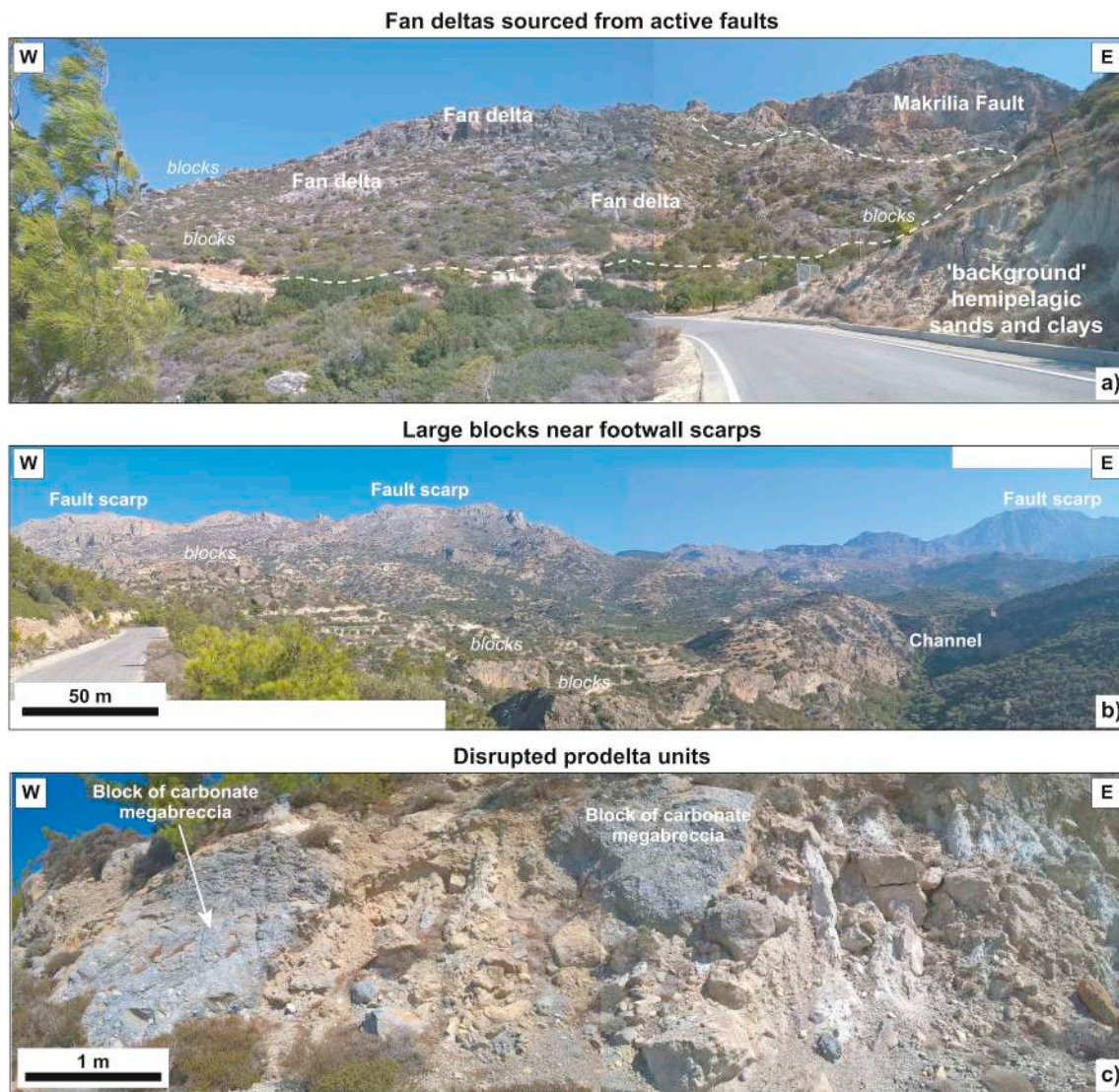


Fig. 26. Photographic examples of degradation complexes sourced from active faults in SE Crete. a) Megabreccia fan deltas sourced from the Makrilia Fault, north of Ierapetra. Note their interfingering with ‘background’ slope sands and clays next to the road cut in the photo. b) Large blocks and cobble/breccia-conglomerate channels sourced from fault scarps to the east of Ierapetra. These facies are accumulated within and above shallow-marine sands, which become more distal to the south, i.e. towards the present-day coastline of SE Crete. c) Example of disrupted prodelta units around the Makrilia Fault. These units are highly chaotic and include both disrupted fan-delta blocks (megabreccias) and very coarse chaotic intervals that were transported *en masse* (mass-transport deposits) close to an active fault.

intervals with high thermal conductivity are capable of concentrating and funnelling heat towards the surface, thus contributing to the regional ‘cooling’ of sedimentary basins (Weijermars et al., 1993; Canova et al., 2018). This is a phenomenon particularly known in regions such as SE Brazil and Gulf of Mexico, where deeply buried sub-salt units are markedly colder than expected for the depth in which they occur, with Late Jurassic source rocks in the oil window at burial depths > 10 km (Hudec and Jackson, 2007; Davison and Cunha, 2017).

Another factor causing variability in heat-flow patterns of ICMs is magmatism affecting a sedimentary basin late in its evolution, for example in association with tectonic plate readjustments, strike-slip tectonics, or movement of mantle hotspots (Omosanya et al., 2018). In these cases, abrupt increases in regional heat flow may occur, particularly when magmatism is widespread and associated with the underplating of magma in regions of ICMs. An example of the impact of late magmatism is recorded offshore Namibia, where underplating and the intrusion of the Cape Cross and Messum igneous bodies are (and were in the past) capable of re-heating the crust prior to ~90 Ma (Fernández et al., 2010; Comin-Chiaramonti et al., 2011).

Climate and oceanographic changes through time are also capable

of imposing variations to local heat-flow patterns. Wygrala (1989) has tracked changes in water temperature with time, throughout the Phanerozoic, and proposed a table relating palaeo-water temperatures with latitude. These data are often used to model the surface temperature contribution to basin heat flows in basin maturation models (Ritter et al., 2004). Hence, colder waters are capable of lowering the background temperature of sedimentary basins, with the opposite effect occurring in regions with warmer waters. In the Earth’s history, water temperature gradients have varied with latitude, and in time, following major oceanographic and climatic changes (Wygrala, 1989). Nevertheless, oceanographic effects are difficult to constraint back in time, and on ICMs, relative increases in water depth largely overprint the effect of latitude changes, especially below 1–2 km in water depth.

A final control on heat-flow distribution on ICMs relates to post-rift tectonic events and associated crustal deformation. (Sibson, 1982; Kutas and Rusanov, 2004; Khutorski and Polyak, 2017). Tectonic uplift, associated with basin/margin inversion, for example, can result in two main competing effects for the margin heat flow and source rock maturity. On the one hand, the uplifted basin may be partially eroded, exposing and cooling the underlying formations and eventually halting

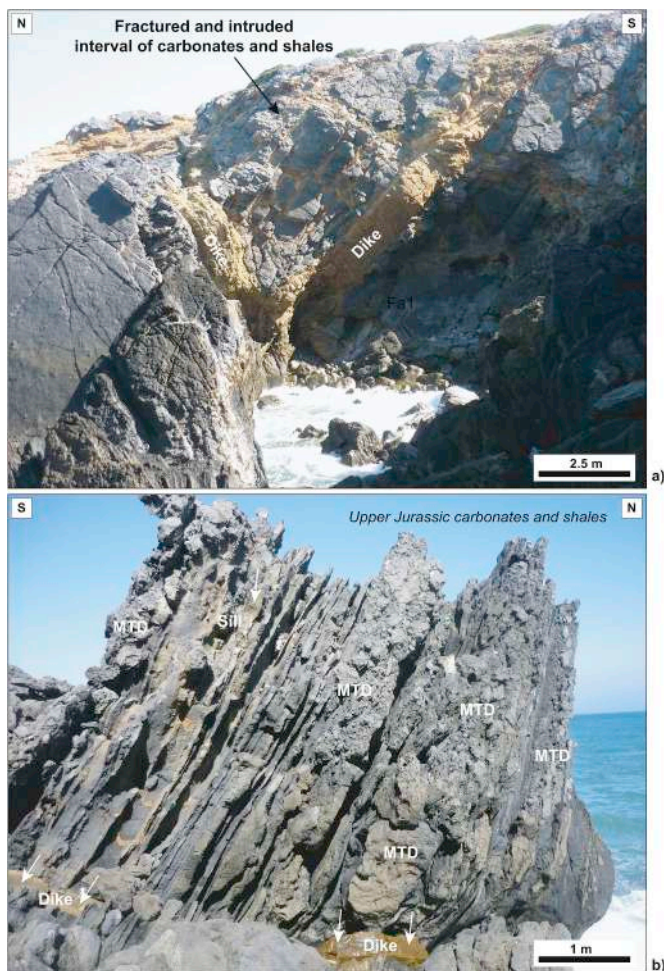


Fig. 27. Examples of magmatic intrusions in Upper Jurassic strata in West Iberia, west of Lisbon. a) Series of dikes intruding and fracturing Upper Jurassic carbonates and shales. The dikes do not follow the local bedding planes and dilated the host rock in a dramatic way, forcing fractures and faults to open. b) Example of smaller-scale sills and mass-transport deposits in the same area as a). Here, sills follow the finer-grained intervals and putatively dilated the bedding planes of a cyclic succession of hemipelagites and mass-transport deposits. These latter mass-transport deposits (MTDs in the figure) denote tectonic instability of a carbonate ramp dipping to the E-SE at the end of the Jurassic syn-rift period in the Lusitanian Basin.

hydrocarbon generation. On the other hand, the thickening of the radiogenic crust may lead to locally higher geothermal gradients. If a subduction zone develops, then the thickening of the lithosphere would likely counteract the crustal thickening effect and result in very low geothermal gradients (e.g. the Adriatic-Ionian Sea; Jiménez-Munt et al., 2003).

6.2. Are there 'typical' tectono-sedimentary evolutions on ICMs?

A key aspect in this review is the recognition of typical tectono-sedimentary evolutions in all ICMs. Continental breakup and associated subsidence maximum record widespread mass-wasting and footwall degradation, precluding the gradual establishment of 'drift' conditions. Previously considered in the literature as a 'rift-to-drift', or transitional stage, this work demonstrates that ICMs are developed when: 1) tectonic and thermal subsidence lead to the widespread flooding continental margins, and b) exhumation and uplift occurs in proximal areas of the newly formed ICMs. The way thermal and subsidence histories vary across the different types of ICMs is a major theme for discussion.

On multiple ICMs, the continental breakup per se records the

deposition of turbidite successions and debrites to form a well-defined offlapping sequence (Alves and Cunha, 2018). These are obvious on seismic data when associated with sand fairways on the continental shelf and slope into the deepest parts of ICMs (Figs. 7 and 8). In all the ICM types considered in this paper, mass-wasting strata is associated with maxima in subsidence rates recorded on the pseudo-wells and exploration wells, being gradually draped by thick intervals of low-amplitude seismic reflections (Figs. 7 and 8). These *breakup sequences* have distinct development, and reflect distinct depositional facies, on different ICMs (Alves and Cunha, 2018).

Recent geophysical and lithological data have recognised intervals above syn-rift units that represent transitional strata documenting the cessation of rifting on continental margins. These *breakup sequences* are documented in places as varied as the Black Sea (Monteleone et al., 2019), SE Asia (Zhao et al., 2016; Lei et al., 2019), South Atlantic (Beglinger et al., 2012b; Mohriak and Leroy, 2012; Davison et al., 2015), Gulf of Mexico (Pindell et al., 2014), or Australia (Hall et al., 2013; Holford et al., 2014). In all these regions, continental breakup (i.e. the establishment of ICMs as completely rifted margins) is marked by the accumulation of regressive-transgressive (R-T) depositional cycles of distinct nature, but always reflecting an abrupt phase of tectonic subsidence on the newly formed margin. These R-T cycles have distinct characters but always reflect marked shallowing and sediment bypass on ICMs before an abrupt phase of subsidence and accommodation-space creation takes over (Figs. 28 and 29).

6.2.1. Carbonate-evaporite sequences

R-T cycles in South America start by the deposition of shallow-water (or microbial) carbonates and calcarenites, followed by a thick succession of evaporites (Davison, 2007). This is a pattern recognised in West Africa, South America and Gulf of Mexico in the form of 'transitional' units that represent the end of the development of syn-rift depocentres (Davison, 2007; Beglinger et al., 2012b; Mohriak and Leroy, 2012; Pindell et al., 2014; Zhao et al., 2016). Evaporite sequences, however, are often thick on these margins – to a total of more than 2000 m in thickness – and hint at very marked subsidence during this same 'transitional' stage (Fig. 29).

6.2.2. Sandstone-shale sequences

Particularly on the Equatorial Margins of Brazil and Africa, continental/shallow marine strata at the start of *breakup sequences* are followed by the accumulation of deep-marine units (Roberts and Bally, 2012). In the case of the Iberia and Newfoundland conjugate, regressive sandstones and conglomerates in proximal areas of the two margins give rise to shales (including black shales) and mass-transport deposits in deeper continental-slope depocentres (Alves and Cunha, 2018). Similar depositional patterns are recorded on margins as distinct as East Greenland, NW Morocco Argentina and South China Sea (Fig. 29).

6.2.3. Sandstone-carbonate sequences

Sandstone-carbonate sequences are scarcer in the geological record, but still recorded on proximal parts of continental margins such as Equatorial Brazil (Nemčok et al., 2012). In essence, sandstone-carbonate sequences represent the rejuvenation of sediment-source areas at the start of the continental breakup process, with subsequent stages keeping the ICMs at a relatively shallow depth. Palaeogeographic changes such as movement of a basin towards equatorial regions due to plate tectonics, may also have a role in controlling the deposition of these types of *breakup sequences* (Fig. 29).

6.3. Gulf of California as a late Cenozoic example of continental breakup

The Gulf of California (Fig. 30) is an archetype of continental rupture through transtensional rifting. It forms a narrow sea that lies between the Baja California Peninsula and the western margin of mainland Mexico, consisting of several short spreading segments separated

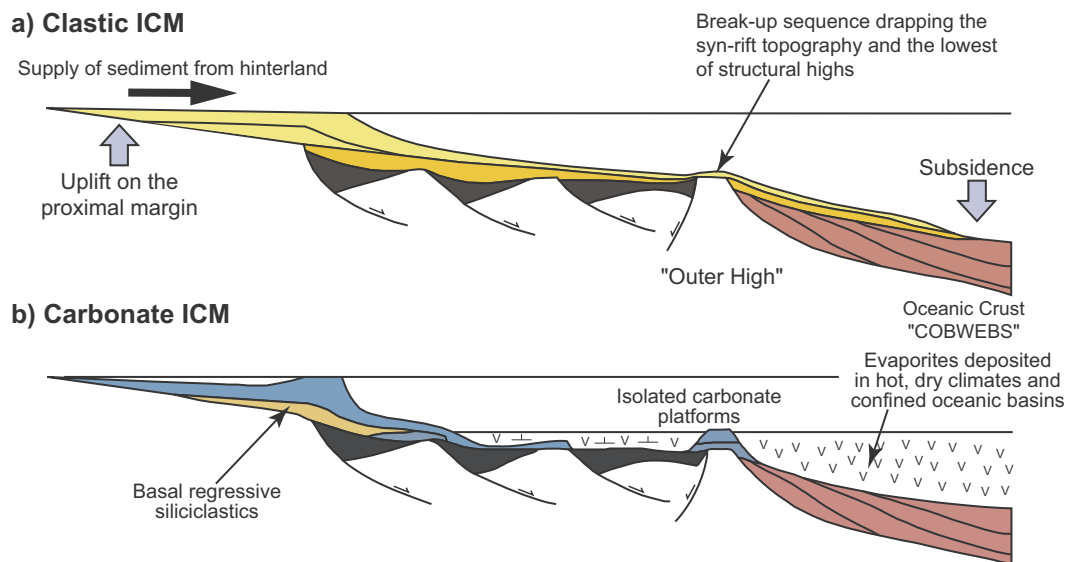


Fig. 28. Examples of breakup-related deposition on a siliciclastic and mixed carbonate evaporite margin. a) Represents the final deposition of a breakup sequence when oceanic crust is finally formed, and enhanced tectonic subsidence prevails (see Alves and Cunha, 2018). b) Depicts a hypothetical ICM with shallow-marine carbonates in proximal parts, and evaporites deposited where confined oceanic basins are finally developed more distally on ICMs.

by transform faults that together represent the northern extent of the East Pacific Rise plate boundary. The Gulf of California ruptured much more rapidly than is typical of continental rifts (Fig. 30), with seafloor spreading commencing only 6–10 m.y. after the formation of the oblique-convergent plate boundary at 12.5 Ma. Rapid rupture was promoted by two factors:

- (1) The transtensional rift follows the axis of a subduction-related extensional arc that was centred over the future site of the Gulf of California from c. 24–12.5 Ma (Comondú arc, Fig. 30). East-west extension accompanied the arc magmatism at most localities along the length of the Gulf of California (cf. Busby et al., in press). The transtensional rift thus exploited thermally weakened continental crust that was already partially thinned. Subduction ended when the East Pacific Rise was partially overridden by North America, and the remnants of the convergent Farallon plate broke into microplates (GM and MM, Fig. 30). These microplates and the Baja California Peninsula were transferred to the Pacific plate when the plate boundary jumped eastward into the thermally weakened, extensional arc axis, and east-west intra-arc extension was replaced by northwest-southeast extension at the trailing edge of the Pacific plate.
- (2) Pull-apart basins are the most efficient tectonic setting for localising rapid thinning of the crust (Christie-Blick and Biddle, 1985; Pitman and Andrews, 1985; Nilsen and Sylvester, 1995; Allen and Allen, 2013; Xie and Heller, 2009). In the Gulf of California, this has produced several short spreading segments separated by transform faults (Fig. 30).

We focus here on the earliest ruptured segment of the Gulf of California transtensional rift, the Guaymas-Santa Rosalía segment in the centre of the Gulf (Fig. 30), because that is the segment with the most offshore and onshore combined data. The Guaymas rift is a magmatically-robust rift that achieved continental breakup 3–4 m.y. before transtensional pull-apart basins to the north and south ruptured the continental crust (Lizarralde et al., 2007). It has about 8 km of igneous product, compared to mid-ocean ridge production (6 km) or basins in the rest of the Gulf of California. (Lizarralde et al., 2007). The Guaymas basin has been the focus of a DSDP expedition, as well as wide-angle and multi-channel seismic surveys (Curry and Moore, 1982; Lizarralde et al., 2007; Miller and Lizarralde, 2013) The IODP expedition on

September 16 to November 16, 2019, focused on Late Pleistocene organic sediments intruded by magmatic sills that lie up to 40 km off axis, across the width of the basin (Teske et al., 2018). Tectonic reconstructions show that the 2 km thick evaporite body imaged by multichannel seismic in the Guaymas basin was fringed by thinner (up to ca. 70 m thick) gypsum deposits exposed onshore in the Santa Rosalía basin (Fig. 31; Miller and Lizarralde, 2013). However, the evaporite and underlying crustal rocks in the Guaymas basin have not been sampled or dated. The Santa Rosalía area (Fig. 31) offers the opportunity to do this.

In the Santa Rosalía area, subduction-related volcanic rocks pass conformably upward into rift transitional volcanic rocks (Fig. 31). Clastic sedimentary rocks are absent from the early rift stage, because explosive and effusive volcanism flooded the basin (Busby et al., in press). Like other parts of the Gulf of California, the onset of rifting at Santa Rosalía is marked by the deposits of large-volume silicic ignimbrite eruptions. These are overlain by rift transitional lavas, which were ponded in grabens. The rift transitional volcanic rocks were then rotated eastward, presumably toward a north-south fault that now lies below sea level to the east. This is consistent with the fact that the shape of the east Guaymas evaporite indicates that the basin it formed in was bounded by N-S normal faults that were active before seafloor spreading and transform faulting began (Miller and Lizarralde, 2013). Tectonic reconstructions show that the 2 km thick evaporite body imaged by multichannel seismic in the Guaymas basin was fringed by thinner (up to ca. 70 m thick) gypsum deposits exposed onshore in the Santa Rosalía basin (Fig. 1; Miller and Lizarralde, 2013). However, the evaporite and underlying crustal rocks in the Guaymas basin have not been sampled or dated. The Santa Rosalía area offers the opportunity to do this.

The breakup sequence of the Santa Rosalía basin (Boleo Formation, Fig. 31) consists of a basal marine carbonate, overlain by evaporites. This in turn is overlain by a series of clastic fan delta progradational sequences sourced locally by erosion of andesitic volcanic rocks. Cu-Co-Zn ore beds occur at the base of each cycle and are inferred to have formed from brine pools in a marginal marine environment, analogous to the Red Sea (Conly et al., 2006, 2011). High-magnesian andesite intrusions in the Santa Rosalía area are approximately the same age as the Boleo Formation, and may have provided the heat engine and fluids for Boleo mineralization; alternatively, or in addition, the onset of seafloor spreading at ca. 6 Ma in the Guaymas basin could have

Lithological character of *breakup sequences* on rifted margins

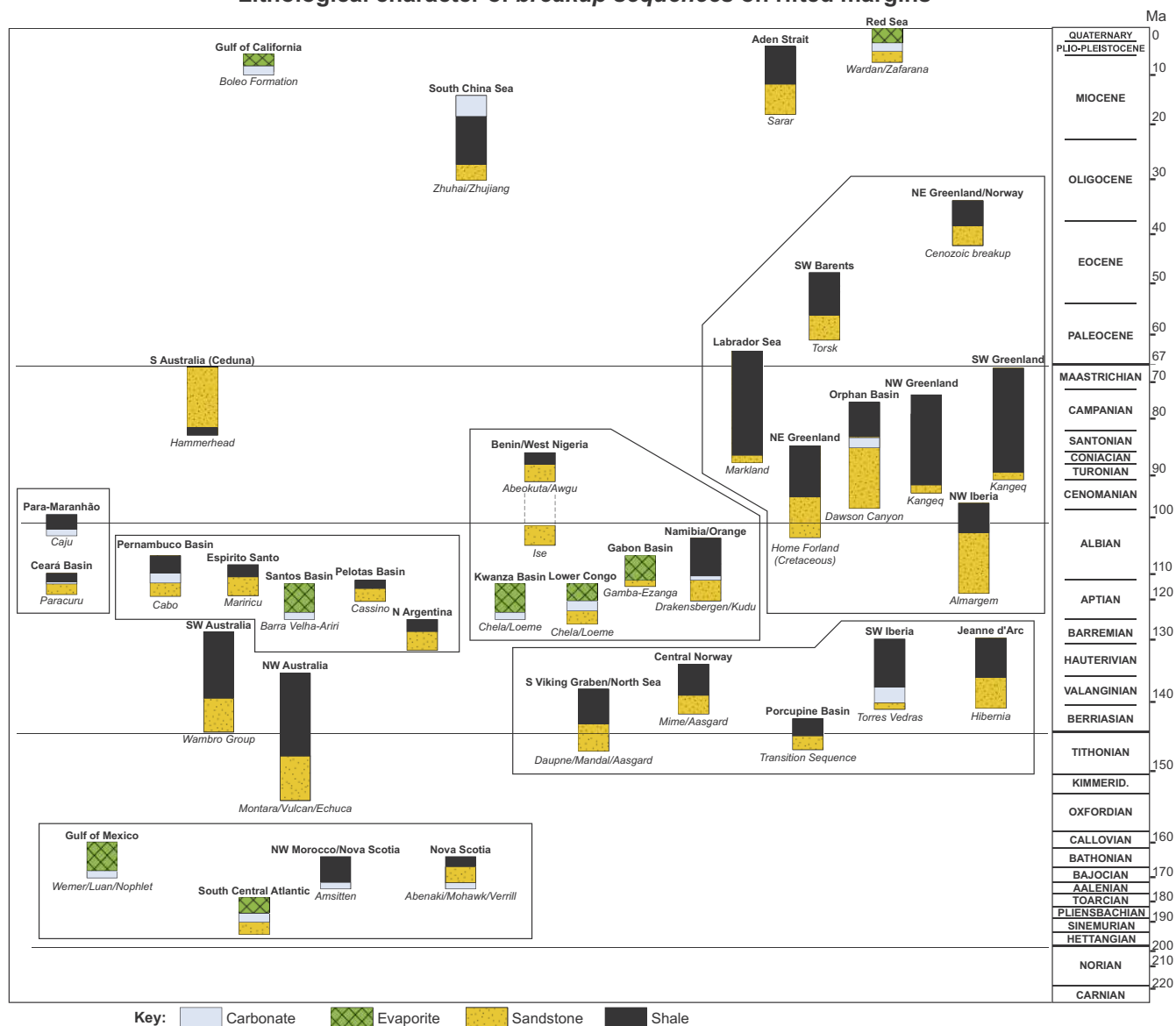


Fig. 29. Expected lithologies of regressive–transgressive depositional cycles in breakup sequences around the world, as classified in Alves and Cunha (2018). These breakup sequences comprise three (3) main classes: a) sandstone–shale, b) carbonate–evaporite and c) sandstone–carbonate. Minor amounts of carbonate may occur in sandstone–shale breakup sequences. Geographic names (in bold) are shown together with the names of the stratigraphic formations representing breakup sequences (in italic). Stratigraphic information used for in this panel was taken from Klitgord and Schouten (1986), Horsthemke et al. (1990), Moore (1992), Chalmers and Pulvertaft (1993), Keeley and Light (1993), Light et al. (1993), Clark et al. (2014), Baker (1995), Sinclair (1995), Whitman et al. (1999), Chalmers and Pulvertaft (2001), Gabrielsen et al. (2001), Bradshaw et al. (2003), Kyrkjebø et al. (2004), Bird et al. (2005), Bosworth et al. (2005), Heine and Muller (2005), Brownfield and Charpentier (2006), Pedersen et al. (2006), Bueno et al. (2007), Condé et al. (2007), Córdoba et al. (2007), França et al. (2007), Moreira et al. (2007), Soares et al. (2007), Alves et al. (2009), Schettino and Turco (2009), Espurt et al. (2009), Zachariah et al. (2009), Beglinger et al. (2012a), Beglinger et al. (2012b), Mello et al. (2012), Soares et al. (2012), Kaki et al. (2013), Tamannai et al. (2013), Tari and Jabour (2013), Cazier et al. (2014), Schmidt (2014), Pindell et al. (2014), Brownfield (2016), Nova Scotia Department of Energy (2016), d’Almeida et al. (2016), Geissler et al. (2016), Howarth and Alves (2016), Ndiaye et al. (2016), Zhao et al. (2016), Biari et al. (2017), Gouiza et al. (2017) and Parsons et al. (2017) and Busby et al. (in press).

provided the brines (Busby et al., in review).

The seismic structure beneath Baja California shows a distinct low-velocity (i.e. hot) zone crossing the Baja California Peninsula (Di Luccio et al., 2014), at the latitude of the Santa Rosalía-Guaymas rift. This lies above the boundary between the Guadalupe and Magdalena slab remnants (Fig. 31), and the slab appears to bow out toward the palaeo-trench at this locality, suggesting that there is a long slab window there. The high-magnesian andesites in the Santa Rosalía area are further inboard from the trench than any others found so far in Baja California, perhaps due to the presence of a large slab tear in this area. Perhaps this also contributed to anomalous high magma production at the Guaymas

spreading centre, and its early rifting relative to other basins in the Gulf of California.

In summary, the Gulf of California offers a view of a young “Intraplate Continental Margin”, where plate reconstructions are very well constrained. It formed at a tectonically active margin, where continental crust was weakened and thinned in an extensional arc setting immediately prior to the onset of continental rifting. Transtensional rifting promoted rapid rupture, in less than 6 my in the case of the Santa Rosalía-Guaymas rift. The Santa Rosalía-Guaymas rift was magmatically robust, from the subduction to rift transitional stages, also with post-subduction slab window magmatism, and throughout its

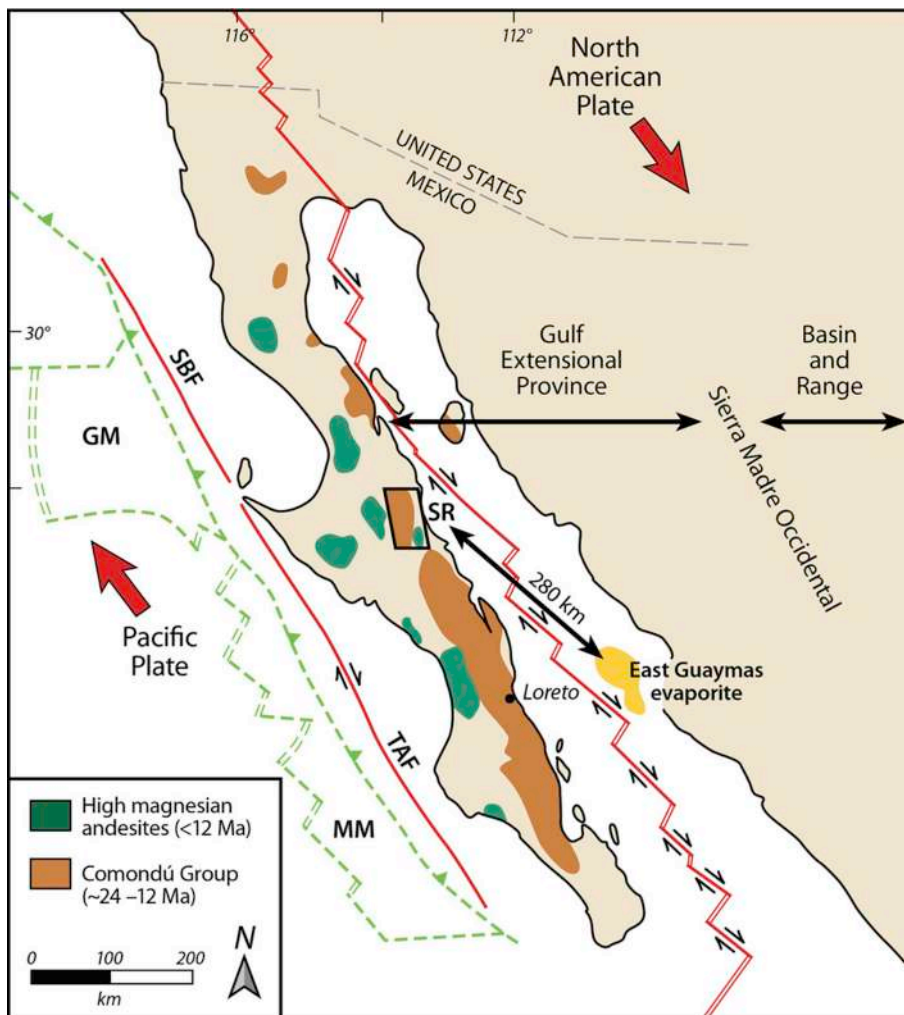


Fig. 30. Simplified map of the Baja California Peninsula, and sea floor structures in the Gulf of California and Pacific margins to the east and west, respectively (modified from Busby et al., in review). Red single line indicates active fault, and red double line indicates active spreading centre; green dashed lines indicate inactive spreading centres, transforms and trench. Large red arrows indicate present-day motion between Pacific plate and North American plate, and oceanic spreading centres are present along the entire length of the rift (Schmitt et al., 2013). From ~24 to 12 Ma, a subduction-related extensional arc occupied the future axis of the Gulf of California rift (Comondú Group); this was formed by subduction of the Farrallon plate, which was segmented into microplates (Guadalupe Microplate, GM, and Magdalena Microplate, MM) as the mid-ocean ridge approached the subduction zone. These microplates, and the entire Baja California Peninsula, were transferred to the Pacific plate at ~12 Ma, when the plate boundary jumped eastward into the arc axis, and transtensional rifting began to separate the Baja California Peninsula from mainland Mexico. Rift volcanism has occurred along the length of the Gulf of California for the past 12 m.y. (much of it now below sea level, not shown). This was accompanied by eruption of high-magnesian andesite volcanism across the width of the central Baja California Peninsula, corresponding to a relict slab geophysically imaged under that region and attributed to slab breakup. This case study focuses on the best-studied and earliest-ruptured breakup sequence, the Guaymas basin (below sea level) and its onland margin, the Santa Rosalía basin (SR).

seafloor spreading history, to the Late Pleistocene.

7. Conclusions

This work has provided a review of ICMs and their common characteristic. A key result stressed in this paper is that common features are observed on ICMs throughout the world. These diagnostic features include:

- The presence of a slope fault system, previously named hinge zone by Falvey, 1974, separating the deeper regions of ICMs from continental shelf basins. Developed continental-slope basins are formed oceanwards from slope fault systems and are often accompanied by important gravitational processes, fault- or salt-controlled, reflecting important post-rift degradation of newly-formed tectonic slopes.
- Crustal extension leading to continental breakup is responsible for important subsidence on ICMs which, nonetheless, do not become tectonically 'passive' in their entirety at this stage. ICMs record important vertical movements during and after continental break-up is achieved.
- The latest extensional episodes leading to continental breakup overprint early extensional phases (and geometries). Key structures are nevertheless capable of inducing subsidence in discrete basins throughout the whole of the rift and post-rift stages of ICMs. In this paper we postulate that these regional normal faults accommodate the bulk of extension and tectonic reactivation on ICMs well after continental breakup is achieved.
- Depositional facies in deep-water margins display great variability in their lithological composition and spatial distribution. This characteristic of strata imaged on seismic data, and outcropping in SE Crete, results from intense tectonic activity. A complex pattern of relatively uplifted and subsiding blocks is produced in such extensional settings.
- Outcrop analogues for syn-rift (Crete) and continental breakup (California) evolutionary stages of ICMs corroborate the predominance of degradation complexes and breakup sequences, respectively. In Crete, fault-scarp degradation is controlled by the footwall uplift histories, relative base level, and basement lithology, all factors leading to distinct 'regoliths' in various parts of Crete. In the Gulf of California, a carbonate-evaporite breakup sequence was formed at the end of the Cenozoic in association with local magmatism and late tectonic uplift of the margins of a new ocean.

Acknowledgements

Part of this work was developed with the support of the Royal Society and industrial partners such as Petrobras, Total and Husky Energy. The Geological and Mining Institute (IGME) in Greece is acknowledged for the fieldwork permission awarded to T. Alves. The COST Action ES1301: FLOWS - Impact of Fluid circulation in old oceanic Lithosphere on the seismicity of transform-type plate boundaries: new solutions for early seismic monitoring of major European Seismogenic zones in acknowledged for a meeting and field trip in 2016. C. Busby's contribution was supported by NSF-REU-151120 (to

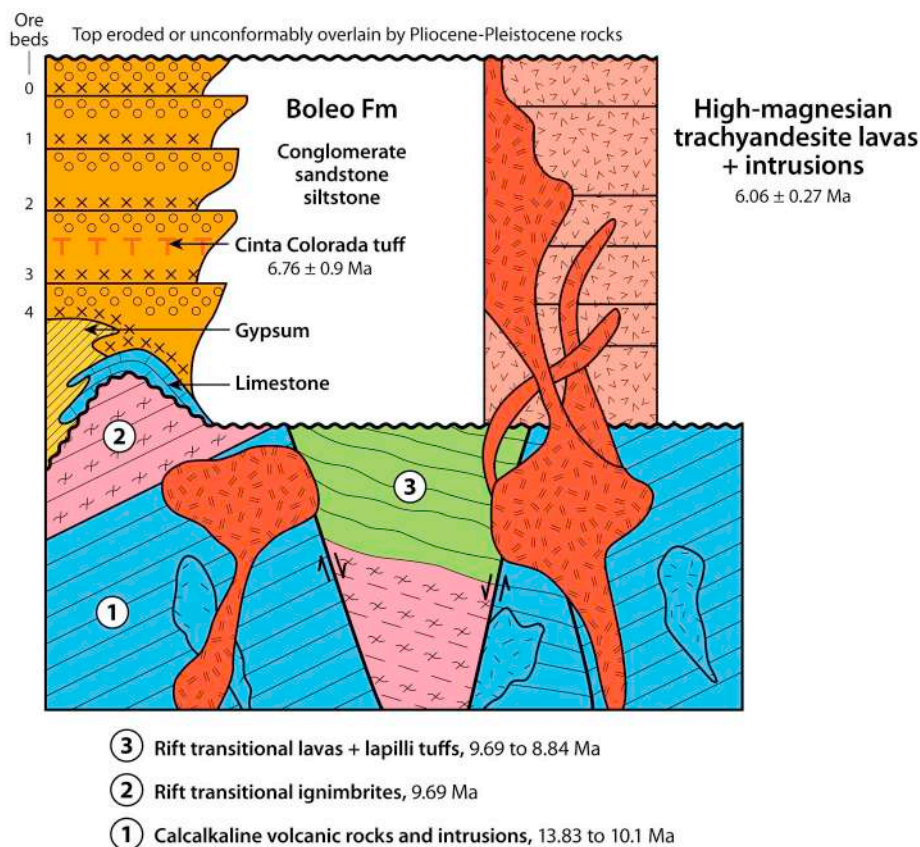


Fig. 31. Schematic representation of stratigraphic, structural, intrusive and geochronological relations on the Baja California margin of the Guaymas rift basin (Fig. 31), modified from Busby et al. (in press). Subduction-related calcalkaline volcanic rocks (1) pass upward into rift transitional ignimbrites and lavas (2, 3) with no time gap. These were faulted and eroded prior to the deposition of Boleo Formation sedimentary rocks in a pull-apart basin, representing the onshore equivalent of the Guaymas rift basin. High-magnesian magmatism occurred at the same time as Boleo sedimentation and was also coeval with the onset of sea floor spreading in the Guaymas basin, estimated at ~6 Ma by Lizarralde et al. (2007).

Busby and Niemi) and a 2017–2018 UC Mexus-Conacyt Collaborative Research Grant (to Busby and López Martínez). We thank O. Heidbach (Potsdam) for providing us with an editable version of Fig. 3. R. Huismans is acknowledged for the provision of Fig. 5 in this work. J. Norcliffe is acknowledged by providing Fig. 9 from offshore Namibia. S. Krastel and the crew of Poseidon-Cruise P336 are thanked for acquiring and providing Fig. 25. Finally, we thank JMPG's editor-in-chief M. Zecchin and two anonymous reviewers for their constructive comments.

Appendix A. Supplementary data

Supplementary data to this article can be found online at <https://doi.org/10.1016/j.marpetgeo.2020.104341>.

References

- Allen, P.A., Allen, J.R., 2013. *Basin Analysis: Principles and Application to Petroleum Play Assessment*, third ed. Wiley-Blackwell, pp. 632.
- Almeida, N.M., Alves, T.M., Nepomuceno Filho, F., Freire, G.S.S., Souza, A.C.B., Normando, M.N., Oliveira, K.M.L., Barbosa, T.H.S., 2019. Tectono-sedimentary evolution and petroleum systems of Mundaú Sub-basin: a new deep-water exploration frontier in Equatorial Brazil. AAPG (Am. Assoc. Pet. Geol.) Bull. <https://doi.org/10.1306/07151917381>.
- Alves, T.M., 2010. 3D Seismic examples of differential compaction in mass-transport deposits and their effect on post-failure strata. Mar. Geol. 271, 212–224. <https://doi.org/10.1016/j.margeo.2010.02.014>.
- Alves, T.M., 2012. Scale-relationships and geometry of normal faults reactivated during gravitational gliding of Albian rafts (Espírito Santo Basin, SE Brazil). Earth Planet Sci. Lett. 331–332, 80–96. <https://doi.org/10.1016/j.epsl.2012.03.014>.
- Alves, T.M., 2016. Polygonal mounds in the Barents Sea reveal sustained organic productivity towards the P–T boundary. Terra. Nova 28, 50–59. <https://doi.org/10.1111/ter.12190>.
- Alves, T.M., Cunha, T.A., 2018. A phase of transient subsidence, sediment bypass and deposition of regressive–transgressive cycles during the breakup of Iberia and Newfoundland. Earth Planet Sci. Lett. 484, 168–183. <https://doi.org/10.1016/j.epsl.2017.11.054>.
- Alves, T.M., Gamboa, D., 2019. Mass-Transport Deposits as Markers of Local Tectonism in

Extensional Basins. In: Ogata, K., Festa, A., Pini, G.-A. (Eds.), *Submarine Landslides: Subaqueous Mass Transport Deposits from Outcrops to Seismic Profiles*. Geophysical Monograph Series. American Geophysical Union, pp. 71–90. <https://doi.org/10.1002/9781119500513.ch5>.

- Alves, T.M., Cupkovic, T., 2018. Footwall degradation styles and associated sedimentary facies distribution in SE Crete: insights into tilt-block extensional basins on continental margins. Sediment. Geol. 367, 1–19. <https://doi.org/10.1016/j.sedgeo.2018.02.001>.
- Alves, T.M., Elliott, C., 2014. Fluid flow during early compartmentalisation of rafts: a North Sea analogue for divergent continental margins. Tectonophysics 634, 91–96. <https://doi.org/10.1016/j.tecto.2014.07.015>.
- Alves, T.M., Fetter, M., Lima, C., Cartwright, J.A., Cosgrove, J., Gangá, A., Queiroz, C.L., Strugale, M., 2017. An incomplete correlation between pre-salt topography, top reservoir erosion, and salt deformation in deep-water Santos Basin (SE Brazil). Mar. Petrol. Geol. 79, 300–320. <https://doi.org/10.1016/j.marpetgeo.2016.10.015>.
- Alves, T., Gamboa, D., 2020. Mass-transport deposits as markers of local tectonism in extensional basins. In: Ogata, K. (Ed.), *Submarine Landslides: Subaqueous Mass Transport Deposits from Outcrops to Seismic Profiles*. American Geophysical Union - Wiley Publishers, pp. 71–90. <https://doi.org/10.1002/9781119500513.ch5>.
- Alves, T.M., Manuppella, G., Gawthorpe, R., Hunt, D.H., Monteiro, J.H., 2003. The depositional evolution of diapir- and fault-bounded rift basins: examples from the Lusitanian Basin of West Iberia. Sediment. Geol. 162, 273–303. [https://doi.org/10.1016/S0037-0738\(03\)00155-6](https://doi.org/10.1016/S0037-0738(03)00155-6).
- Alves, T.M., Moita, C., Cunha, T., Ullnaess, M., Myklebust, R., Monteiro, J.H., Manuppella, G., 2009. Diachronous evolution of Late Jurassic–Cretaceous continental rifting in the northeast Atlantic (west Iberian margin). Tectonics 28. <https://doi.org/10.1029/2008TC002337>.
- Andreasen, A.D., Japsen, P., Watts, A.B., Nielsen, T., Jokat, W., Thybo, H., Dahl-Jensen, T., 2016. Miocene uplift of the NE Greenland margin linked to plate tectonics: seismic evidence from the Greenland Fracture Zone, NE Atlantic. Tectonics 35, 257–282. <https://doi.org/10.1002/2015TC004079>.
- Armitage, J.J., Collier, J.S., 2017. The thermal structure of volcanic passive margins. The thermal structure of volcanic passive margins. Petrol. Geosci. 24. <https://doi.org/10.1144/petgeo2016-101>.
- Artemieva, I.M., Mooney, W.D., 2001. Thermal thickness and evolution of Precambrian lithosphere: a global study. J. Geophys. Res.: Solid Earth 106, 16387–16414. <https://doi.org/10.1029/2000JB900439>.
- Autin, J., Leroy, S., Beslier, M.-O., D'Acromont, E., Razin, Ph., Ribodetti, A., Bellahsen, N., Robin, C., Al Toubi, K., 2010. Continental break-up history of a deep magma-poor margin based on seismic reflection data (northeastern Gulf of Aden margin, offshore Oman). Geophys. J. Int. 180, 501–519. <https://doi.org/10.1111/j.1365-246X.2009.04424.x>.
- Azevêdo, R.P., 1991. *Tectonic Evolution of Brazilian Equatorial Continental Margins Basins*. PhD Thesis. Department of Geology, Royal School of Mines, Imperial College

- of Science, Technology and Medicine, University of London, London, pp. 455.
- Baker Jr., E.T., 1995. Stratigraphic nomenclature and geologic sections of the Gulf coastal plain of Texas. USGS Open File Rep. 94 (461), 34.
- Baur, F., Littke, R., Wielens, H., Lampe, C., Fuchs, T., 2010. Basin modeling meets rift analysis – a numerical modeling study from the Jeanne d'Arc basin, offshore Newfoundland, Canada. *Mar. Petrol. Geol.* 27, 585–599. <https://doi.org/10.1016/j.marpetgeo.2009.06.003>.
- Bayona, G., Montes, C., Cardona, A., Jaramillo, C., Ojeda, G., Valencia, V., Ayala-Calvo, C., 2011. Intraplate subsidence and basin filling adjacent to an oceanic arc-continent collision: a case from the southern Caribbean-South America plate margin. *Basin Res.* 23, 403–422. <https://doi.org/10.1111/j.1365-2117.2010.00495.x>.
- Beglinger, S.E., Corver, M.P., Doust, H., Cloething, S., Thurmond, A.K., 2012a. A new approach of relating petroleum system and play development to basin evolution: an application to the conjugate margin Gabon coastal and Almada-Camamu basins. *AAPG (Am. Assoc. Pet. Geol.) Bull.* 96, 953–982. <https://doi.org/10.1306/10271111040>.
- Beglinger, S.E., Doust, H., Cloething, S., 2012b. Relating petroleum system and play development to basin evolution: west African South Atlantic basins. *Mar. Petrol. Geol.* 30, 1–25. <https://doi.org/10.1016/j.marpetgeo.2011.08.008>.
- Belde, J., Back, S., Bourget, J., Reuning, L., 2017. Oligocene and Miocene carbonate platform development in the Browse Basin, Australian northwest shelf. *J. Sediment. Res.* 87, 795–816. <https://doi.org/10.2110/jsr.2017.44>.
- Beniast, A., Koptev, A., Burov, E., 2017. Numerical models for continental break-up: implications for the south atlantic. *Earth Planet Sci. Lett.* 461, 176–189. <https://doi.org/10.1016/j.epsl.2016.12.034>.
- Beranek, L.P., 2017. A magma-poor rift model for the Cordilleran margin of western North America. *Geology* 45, 1115–1118. <https://doi.org/10.1130/G39265.1>.
- Biari, Y., Klingelhoefer, F., Sahabi, M., Funk, T., Benabdellouahed, M., Schnabel, M., Reichert, C., Gutscher, M.-A., Bronner, A., Austin, J.A., 2017. Opening of the central Atlantic Ocean: implications for geometric rifting and asymmetric initial seafloor spreading after continental breakup. *Tectonics* 36, 1129–1150. <https://doi.org/10.1002/2017TC004596>.
- Bird, D.E., Burke, K., Hall, S.A., Casey, J.F., 2005. Gulf of Mexico tectonic history: hotspot tracks, crustal boundaries, and early salt distribution. *AAPG (Am. Assoc. Pet. Geol.) Bull.* 89, 311–328. <https://doi.org/10.1306/10280404026>.
- Bonini, M., 2012. Mud volcanoes: indicators of stress orientation and tectonic controls. *Earth Sci. Rev.* 115, 121–152. <https://doi.org/10.1016/j.earscirev.2012.09.002>.
- Bosworth, W., Huchon, Ph., McClay, K., 2005. The Red Sea and Gulf of aden basins. *J. Afr. Earth Sci.* 43, 334–378. <https://doi.org/10.1016/j.earscirev.2012.09.002>.
- Bradshaw, B.E., et al., 2003. A revised structural framework for frontier basins on the southern and southwestern Australian continental margin. *Geosci. Australia* iv, 44 2003/03, Canberra.
- Brown, A.R., 2011. sixth ed. Interpretation of Three-Dimensional Seismic Data, vol. 42. American Association of Petroleum Geologists, Memoirs, pp. 646. <https://doi.org/10.1306/M4271346>.
- Brownfield, M.E., 2016. Assessment of undiscovered oil and gas resources of the west African coastal Province, West Africa. In: *Geologic Assessment of Undiscovered Hydrocarbon Resources of Sub-saharan Africa, Digital Data Series 69–GG, vol. 3*. pp. 12.
- Brownfield, M.E., Charpentier, R.R., 2006. Geology and Total Petroleum Systems of the West-Central Coastal Province (7203), West Africa. *U.S. Geological Survey Bulletin* 2207-B, pp. 52.
- Bueno, G.V., Zacharias, A.A., Oreiro, S.G., Cupertino, J.A., Falkenheim, F.U.H., Neto, M.A.M., 2007. Bacia de Pelotas. *Buletim de Geociências da Petrobras* 15, 551–559.
- Busby, C., Azor, A.A., 2012. *Tectonics of Sedimentary Basins: Recent Advances*. Blackwell Publishing Ltd., pp. 633.
- Busby, C.J., Graettinger, A., Lopez Martinez, M., Medynski, S., Andrews, C., Bowman, E., Gutierrez, E.P., Lodes, E., Ojeda, J., and Rice, J., in press. Volcanic record of the arc-to-rift transition onshore of the Guaymas basin in the Santa Rosalia area, Gulf of California, Baja California: Geosphere, 91 ms pp.
- Canova, D.P., Fisher, M.P., Jayne, R.S., Pollyea, R.M., 2018. Advective heat transport and the salt chimney effect: a numerical analysis. *Geofluids* 18. <https://doi.org/10.1155/2018/2378710>. 2018, Article ID 2378710.
- Cavazza, W., Albino, I., Zattin, M., Galoyan, G., Imamverdiyev, N., Melkonyan, R., 2015. Thermo-chronometric evidence for Miocene tectonic reactivation of the Sevan–Akera suture zone (Lesser Caucasus): a far-field tectonic effect of the Arabia–Eurasia collision? In: In: Sosson, M., Stephenson, R.A., Adamia, S.A. (Eds.), *Tectonic Evolution of the Eastern Black Sea and Caucasus*, vol. 428. Geological Society, London, Special Publications, pp. 187–198. <https://doi.org/10.1144/SP428.4>.
- Cazier, E.C., Bargas, C., Buambua, L., Cardoso, S., Ferreira, H., Inman, K., Lopes, A., Nicholson, T., Olson, Ch., Saller, A., Shinol, J., 2014. Petroleum geology of Cameia field, deepwater pre-salt Kwanza basin, Angola, West Africa. In: *AAPG International Conference and Exhibition, Istanbul, Turkey, September 14–17*, pp. 11.
- Chalmers, J.A., Pulvertaft, T.C.R., 2001. Development of the continental margins of the Labrador Sea: a review. *Wilson, R.C.L., Whitmarsh, R.B., Taylor, B., Frotzheim, N. (Eds.), Geol. Soc. Spec. Publ.* 187, 79–107. <https://doi.org/10.1144/GSL.SP.2001.187.01.05>.
- Christie-Blick, N., Biddle, K.T., 1985. Deformation and basin formation along strike-slip faults. *Soc. Econ. Paleontol. Mineral. Spec. Publ.* 37, 1–34. <https://doi.org/10.2110/pec.85.37.0001>.
- Condé, V.C., Lana, C.C., Neto, O.C.P., Roesner, E.H., Neto, J.M.M., Dutra, D.C., 2007. Bacia do Ceará Buletim Geociências da Petrobras 15, 347–355.
- Comin-Chiaromonti, de Min, A., Girardi, V.A.V., Ruberti, E., 2011. Post-Paleozoic magmatism in Angola and Namibia: a review. In: In: Beccaluva, L., Bianchini, G., Wilson, M. (Eds.), *Volcanism and Evolution of the African Lithosphere*, vol. 478 Geological Society of America. <https://doi.org/10.1130/SPE478>.
- Conly, A.G., Beaudoin, G., Scott, S.D., 2006. Isotopic constraints on fluid evolution and precipitation mechanisms for the Boléo Cu-Co-Zn deposit, Mexico. *Miner. Deposita* 41, 127–151. <https://doi.org/10.1007/s00126-005-0045-3>.
- Conly, A.G., Scott, S.D., Bellon, H., 2011. Metalliferous manganese oxide mineralization associated with the Boléo Cu-Co-Zn district. *Econ. Geol.* 106, 1173–1196. <https://doi.org/10.2113/econgeo.106.7.1173>.
- Córdoba, V.C., Sá, E.F.J., Sousa, D.C., Antunes, A.F., 2007. Bacia de Pernambuco-Paraíba. *Bacia do Ceará Buletim Geociências da Petrobras* 15, 391–403.
- Corti, G., Agostini, A., Keir, D., Van Wijk, J., Bastow, I.D., Ranalli, G., 2015. Magma-induced axial subsidence during final-stage rifting: implications for the development of seaward-dipping reflectors. *Geosphere* 11, 563–571. <https://doi.org/10.1130/GES01076.1>.
- Courtillot, V., Jaupart, C., Manighetti, I., Tapponnier, P., Besse, J., 1999. On causal links between flood basalts and continental breakup. *Earth Planet Sci. Lett.* 166, 177–195. [https://doi.org/10.1016/S0012-821X\(98\)00282-9](https://doi.org/10.1016/S0012-821X(98)00282-9).
- Craddock, J.P., Malone, D.H., Porter, R., Compton, J., Luczaj, J., Konstantinou, A., Day, J.E., Johnston, S.T., 2017. Paleozoic reactivation structures in the Appalachian-Ouachita-Marathon foreland: far-field deformation across Pangea. *Earth Sci. Rev.* 169, 1–34. <https://doi.org/10.1016/j.earscirev.2017.04.002>.
- Clark, S.A., Glorstad-Clark, E., Faleide, J.I., Hartz, E., Fjeldskaar, W., 2014. Southwest Barents Sea rift basin evolution: comparing results from backstripping and time-forward modelling. *Basin Res.* 26, 550–566. <https://doi.org/10.1111/bre.12039>.
- Cunha, T., 2008. *Gravity Anomalies, Flexure and the Thermo-Mechanical Evolution of the West Iberia Margin and its Conjugate of Newfoundland*. Unpublished PhD Thesis, Oxford, pp. 383.
- Chalmers, J.A., Pulvertaft, T.C.R., 1993. The southern West Greenland continental shelf – was petroleum exploration abandoned prematurely? In: *Vorren, T.O. (Ed.), Special Publication, Norwegian Petroleum Society v. 2*, pp. 55–66. <https://doi.org/10.1016/B978-0-444-88943-0.50008-3>.
- Curry, J.R., Moore, D.G., Shipboard Scientific Party, 1982. *Guaymas Basin: Sites 477, 478 and 481: Initial Reports of the Deep-Sea Drilling Project*, vol. 64. pp. 211–415. <https://doi.org/10.2973/dsdp.proc.64.104.1982>.
- d'Almeida, G.A.F., Kaki, C., Adeoye, J.A., 2016. *Benin and western Nigeria offshore basins: a stratigraphic nomenclature comparison*. *Int. J. Geosci.* 7, 177–188.
- Davis, J.K., Lavier, L.L., 2017. Influences on the development of volcanic and magma-poor morphologies during passive continental rifting. *Geosphere* 13, 1524–1540. <https://doi.org/10.1130/GES01538.1>.
- Davidson, I., Cunha, T.A., 2017. Allochthonous salt sheet growth: thermal implications for source rock maturation in the deepwater Burgos Basin and Perdido Fold Belt, Mexico. *Interpretation* 5, 1F–T141. <https://doi.org/10.1016/INT-2016-0035.1>.
- Davidson, I., Faulstich, T., Greenhalgh, J., Beirne, E.O., Steele, I., 2015. Transpressional structures and hydrocarbon potential along the Romanche Fracture Zone: a review. In: *Nemčok, M., Rybár, S., Sinha, S.T., Hermeston, S.A., Ledvenyiova, L. (Eds.), Transform Margins: Development, Controls and Petroleum Systems*, vol. 431. Geological Society, London, Special Publications, pp. 235–248. <https://doi.org/10.1144/SP431.2>.
- Davidson, I., 2007. Geology and Tectonics of the South Atlantic Brazilian Salt Basins, vol. 272. Geological Society, London, Special Publications, pp. 345–359. <https://doi.org/10.1144/GSL.SP.2007.272.01.18>.
- Demercian, S., Szatmari, P., Cobbold, P.R., 1993. Style and pattern of salt diapirs due to thin-skinned gravitational gliding. Campos and Santos basins, offshore Brazil. *Tectonophysics* 228, 393–433. [https://doi.org/10.1016/0040-1951\(93\)90351-J](https://doi.org/10.1016/0040-1951(93)90351-J).
- Demuth, A., Tjälund, N., Ottemöller, L., 2019. Earthquake source parameters in Norway determined with empirical Green's functions. *J. Seismol.* 23, 715–724. <https://doi.org/10.1007/s10950-019-09831-4>.
- Dias, F.L., Assumpção, M., Bianchi, M.B., Barros, L.V., Carvalho, J.M., 2018. The intraplate Maranhão earthquake of 2017 January 3, northern Brazil: evidence for uniform regional stresses along the Brazilian equatorial margin. *Geophys. J. Int.* 213, 387–396. <https://doi.org/10.1093/gji/ggx560>.
- Dietz, R., 1961. Continent and ocean basin evolution by spreading of the sea floor. *Nature* 190, 854–857. <https://doi.org/10.1038/190854a0>.
- Di Luccio, F., Persaud, P., Clayton, R.W., 2014. Seismic structure beneath the Gulf of California: a contribution from group velocity measurements. *Geophys. J. Int.* 199 (3), 1861–1877. <https://doi.org/10.1093/gji/ggu338>.
- Dooley, T.P., Jackson, M.P.A., Hudec, M.R., 2007. Initiation and growth of salt-based thrust belts on passive margins: results from physical models. *Basin Res.* 19, 165–177. <https://doi.org/10.1111/j.1365-2117.2007.00317.x>.
- Ebinger, C., Belachew, M., 2010. Active passive margins. *Nat. Geosci.* 3, 670–671. <https://doi.org/10.1038/ngeo972>.
- Espurt, N., Callot, J.-P., Totterdell, J., Stuckmeyer, H., Vially, R., 2009. Interactions between continental breakup dynamics and large-scale delta system evolution: insights from the Cretaceous Ceduna delta system, Bight Basin, Southern Australian margin. *Tectonics* 28, TC6002. <https://doi.org/10.1029/2009TC002447>.
- Falvey, D.A., 1974. The development of continental margins in plate tectonic theory. *J. Aus. Petrol. Prod. Explor. Assoc.* 14, 95–106. <https://doi.org/10.1071/AJ73012>.
- Fernández, M., Afonso, J.C., Ranalli, G., 2010. The deep lithospheric structure of the Namibian volcanic margin. *Tectonophysics* 481, 68–81. <https://doi.org/10.1016/j.tecto.2009.02.036>.
- França, R.L., del Rey, A.C., Tagliari, C.V., Brandão, J.R., Fontanelli, P.R., 2007. Bacia do Espírito Santo. *Buletim de Geociências da Petrobras* 15, 501–509.
- Franke, D., 2013. Rifting, lithosphere breakup and volcanism: comparison of magma-poor and volcanic rifted margins. *Mar. Petrol. Geol.* 43, 63–87. <https://doi.org/10.1016/j.marpetgeo.2012.11.003>.
- Franke, D., Ladage, S., Schnabel, M., Schreckenberger, B., Raichert, Ch., Hinz, K., Paterlini, M., de Abellera, J., Siciliano, M., 2010. Birth of a volcanic margin off Argentina, South Atlantic. In: *In: Meyer, R., van Wijk, J., Breivik, A., Tegner, C.*

- (Eds.), *Magma-Rich Extensional Basins*. *Geochemistry, Geophysics, Geosystems*, vol. 11. pp. Q0AB04. <https://doi.org/10.1029/2009GC002715>.
- Gac, S., Klitzke, P., Minakov, A., Faleide, J.I., Scheck-Wenderoth, M., 2016. Lithospheric strength and elastic thickness of the Barents Sea and Kara sea region. *Tectonophysics* 691, 120–132. <https://doi.org/10.1016/j.tecto.2016.04.028>.
- Gabrielsen, R.H., Kyrkjebø, R., Faleide, J.I., Fjeldskaar, W., Kjennerud, T., 2001. The Cretaceous post-rift basin configuration of the northern North Sea. *Petrol. Geosci.* 7, 137–154. <https://doi.org/10.1144/petgeo.7.2.137>.
- Gamboa, D., Alves, T.M., Cartwright, J., Terrinha, P., 2010. MTD distribution on a 'passive' continental margin: the Espírito Santo Basin (SE Brazil) during the Palaeogene. *Mar. Petrol. Geol.* 27, 1311–1324. <https://doi.org/10.1016/j.marpetgeo.2010.05.008>.
- Geissler, W.H., Gaina, C., Hopper, J.R., Funck, T., Blischke, A., Arting, U., Horni, J.A., Peron-Pinvidic, G., Abdelmalak, M.M., 2016. In: Peron-Pinvidic, G., Hopper, J.R., Stoker, M.S. (Eds.), *Seismic Volcanostratigraphy of the NE Greenland Continental Margin*, vol. 447. Geological Society, London, Special Publications, pp. 149–170. <https://doi.org/10.1144/SP447.11>.
- Geoffroy, L., Burv, E.B., Werner, P., 2015. Volcanic passive margins: another way to break up continents. *Sci. Rep.* 5, 14828. <https://doi.org/10.1038/srep14828>.
- Gouiza, M., Hall, K., Welford, J.K., 2017. Tectono-stratigraphic evolution and crustal architecture of the Orphan basin during North Atlantic rifting. *Int. J. Earth Sci.* 106, 917–937. <https://doi.org/10.1007/s00531-016-1341-0>.
- Groupe Galice, 1979. The continental margin off Galicia and Portugal: acoustical stratigraphy, dredge stratigraphy and structural evolution. *Deep Sea Drill. Proj.* 47, 633–662.
- Hall, L.S., Gibbons, A.D., Bernardel, G., Whittaker, J.M., Nicholson, C., Rollet, N., Müller, R.D., 2013. Structural architecture of Australia's southwest continental margin and implications for early cretaceous basin evolution. In: *West Australian Basins Symposium*, Perth, 18–21 August 2013, pp. 1–22.
- Hand, H., Sandiford, M., 1999. Intraplate deformation in central Australia, the link between subsidence and fault reactivation. *Tectonophysics* 305, 121–140. [https://doi.org/10.1016/S0040-1951\(99\)00009-8](https://doi.org/10.1016/S0040-1951(99)00009-8).
- Hartz, E.H., Medvedev, S., Schmid, D.W., 2016. Development of sedimentary basins: differential stretching, phase transitions, shear heating and tectonic pressure. *Basin Res.* 29, 591–604. <https://doi.org/10.1111/bre.12189>.
- Heidbach, O., Rajabi, M., Reiter, K., Ziegler, M., WSM Team, 2016. World Stress Map Database Release 2016. GFZ Data Services <https://doi.org/10.5880/WSM.2016.001>.
- Heine, C., Muller, R.D., 2005. Late Jurassic rifting along the Australian North West Shelf margin geometry and opening ridge configuration. *Aust. J. Earth Sci.* 52, 27–39. <https://doi.org/10.1080/08120090500100077>.
- Hillis, R.R., Sandiford, M., Reynolds, S.D., Quigley, M.C., 2008. Present-day stresses, seismicity and Neogene-to-Recent tectonics of Australia's 'passive' margins: intraplate deformation controlled by plate boundary forces. In: Johnson, H., Doré, A.G., Gatiloff, R.W., Holdsworth, R., Lundin, E.R., Ritchie, J.D. (Eds.), *The Nature and Origin of Compression in Passive Margins*, vol. 306. Geological Society, London, Special Publications, pp. 71–90. <https://doi.org/10.1144/SP306.3>.
- Hiscott, R.N., Wilson, R.C.L., Gradstein, F.M., Pujalte, V., Garcia-Mondejar, J., Boudreau, R.R., Wishart, H.A., 1990. Comparative stratigraphy and subsidence history of Mesozoic rift basins of North Atlantic. *AAPG (Am. Assoc. Pet. Geol.) Bull.* 74, 60–76.
- Holford, S.P., Hillis, R.R., Duddy, I.R., Green, P.F., Tassone, D.R., Stoker, M.S., 2011. Paleothermal and seismic constraints on late Miocene–Pliocene uplift and deformation in the Torquay sub-basin, southern Australian margin. *Aust. J. Earth Sci.* 58, 543–562. <https://doi.org/10.1080/08120099.2011.565074>.
- Holford, S.P., Tuit, A.K., Hillis, R.R., Green, P.F., Stoker, M.S., Duddy, I.R., Sandiford, M., Tassone, D.R., 2014. Cenozoic deformation in the Otway Basin, southern Australian margin: implications for the origin and nature of post-breakup compression at rifted margins. In: Alves, T.M., Bell, R.E., Jackson, C.A.-L., Minshull, T.A. (Eds.), *Deep Water Continental Margins: Geological and Economic Frontiers*, vol. 26. Basin Research, pp. 10–37. <https://doi.org/10.1111/bre.12035>.
- Horsthemke, E., Ledendecker, S., Porada, H., 1990. Depositional environments and stratigraphic correlation of the Karoo Sequence in northwestern Damaraland. *Commun. Geol. Surv. Namibia* 6, 67–77.
- Howarth, V., Alves, T.M., 2016. Fluid flow through carbonate platforms as evidence for deep-seated reservoirs in Northwest Australia. *Mar. Geol.* 380, 17–43. <https://doi.org/10.1016/j.margeo.2016.06.011>.
- Hudec, M.R., Jackson, M.P.A., 2007. Terra infirma: understanding salt tectonics. *Earth Sci. Rev.* 82, 1–28. <https://doi.org/10.1016/j.earscirev.2007.01.001>.
- Huisman, R., Beaumont, Ch., 2011. Depth-dependent extension, two-stage breakup and cratonic underplating at rifted margins. *Nature* 473, 74–78. <https://doi.org/10.1038/nature09988>.
- Illsley-Kemp, F., Keir, D., Bull, J.M., Gernon, T.M., Ebinger, C., Ayele, A., Hammond, J.O.S., Kendall, J.-M., Goitom, B., Belachew, M., 2017a. Seismicity during continental breakup in the Red Sea rift of northern Afar. *J. Geophys. Res.* 123, 2345–2362. <https://doi.org/10.1002/2017JB014920>.
- Illsley-Kemp, F., Savage, M.K., Keir, D., Hirschberg, H.P., Bull, J.M., Gernon, T.M., Hammond, J.O.S., Kendall, J.-M., Ayele, A., Goitom, B., 2017b. Extension and stress during continental breakup: seismic anisotropy of the crust in Northern Afar. *Earth Planet. Sci. Lett.* 477, 41–51. <https://doi.org/10.1016/j.epsl.2017.08.014>.
- Indrevær, K., Gabrielsen, R.H., Faleide, J.I., 2016. Early Cretaceous synrift uplift and tectonic inversion in the Loppa High area, southwestern Barents Sea, Norwegian shelf. 174. *Journal of the Geological Society, London*, pp. 242–254. <https://doi.org/10.1144/jgs2016-066>.
- Ingersoll, R.V., 2011. Tectonics of sedimentary basins, with revised nomenclature. In: Busby, C., Azor, A.A. (Eds.), *Tectonics of Sedimentary Basins: Recent Advances*. Blackwell Publishing Ltd., pp. 3–43. <https://doi.org/10.17850/njg97-3-03>.
- Janutyte, I., Lindholm, C., 2017. Earthquake source mechanisms in onshore and offshore Nordland, northern Norway. *Norw. J. Geol.* 97, 227–239. <https://doi.org/10.17850/njg97-3-03>.
- Jeannot, L., Kuszniir, N., Mohn, G., Manatschal, G., Cowie, L., 2016. Constraining lithosphere deformation modes during continental breakup for the Iberia–Newfoundland conjugate rifted margins. *Tectonophysics* 680, 28–49. <https://doi.org/10.1016/j.tecto.2016.05.006>.
- Jiménez-Munt, I., Sabadini, R., Gardi, A., Bianco, G., 2003. Active deformation in the Mediterranean from Gibraltar to Anatolia inferred from numerical modeling and geodetic and seismological data. *J. Geophys. Res.: Solid Earth* 108. <https://doi.org/10.1029/2001JB001544>. ETG 2-1-ETG 2-24.
- Jovane, L., Figueiredo, J.J.P., Alves, D.P.V., Iacopini, D., Giorgioni, M., Vannucchi, P., Moura, D.S., Bezeraa, F.H.R., Vital, H., Rios, I.L.A., Molina, E.C., 2016. Seismostratigraphy of the Ceará plateau: clues to Decipher the Cenozoic evolution of Brazilian equatorial margin. *Front. Earth Sci.* <https://doi.org/10.3389/feart.2016.00090>.
- Kaki, C., d'Almeida, G.A.F., Yalo, N., Amelina, S., 2013. Geology and petroleum systems of the offshore Benin basin (Benin). *Oil Gas Sci. Technol. – Rev. IFP* 68, 363–381.
- Keeley, M.L., Light, M.P.R., 1993. Basin evolution and prospectivity of the Argentine continental margin. *J. Petrol. Geol.* 16, 451–464. <https://doi.org/10.1111/j.1747-5457.1993.tb00352.x>.
- Keir, D., 2014. Magmatism and deformation during continental breakup. *Astron. Geophys.* 55, 5.18–5.22. <https://doi.org/10.1093/astrogeo/atu213>.
- Khutorski, Polyak, 2017. Special features of heat flow in transform faults of the North Atlantic and Southeast Pacific. *Geotectonics* 51, 152–162. <https://doi.org/10.1134/S0016852117010022>.
- Klitgord, K.D., Schouten, H., 1986. In: Vogt, P.R., Tucholke, B.E. (Eds.), *Plate Kinematics of the Central Atlantic M.* pp. 351–378. <https://doi.org/10.1130/DNAG-GNA-M.351>.
- Koptev, A., Burov, E., Calais, E., Leroy, S., Gerya, T., Guillou-Frottier, L., Cloething, S., 2016. Contrasted continental rifting via plume-craton interaction: applications to central East African rift. *Geosci. Front.* 259, 221–236. <https://doi.org/10.1016/j.gsf.2015.11.002>.
- Kukla, P.A., Strozyk, F., Mohriak, W.U., 2018. South Atlantic salt basins – witnesses of complex passive margin evolution. *Gondwana Res.* 53, 41–57. <https://doi.org/10.1016/j.gr.2017.03.012>.
- Kutas, P.S.I., Rusanov, O.M., 2004. Deep faults, heat flow and gas leakage in the northern Black Sea. *Geo Mar. Lett.* 24, 163–168. <https://doi.org/10.1007/s00367-004-0172-3>.
- Kyrkjebø, R., Gabrielsen, R.H., Faleide, J.I., 2004. Unconformities related to the Jurassic–Cretaceous synrift–post-rift transition of the northern North Sea. *J. Geol. Soc. London* 161, 1–17. <https://doi.org/10.1144/0016-764903-051>.
- Langhi, L., Borel, G.D., 2005. Influence of the Neotethys rifting on the development of the Dampier Sub-basin (North West Shelf of Australia), highlighted by subsidence modelling. *Tectonophysics* 397, 93–111. <https://doi.org/10.1016/j.tecto.2004.10.005>.
- Lavier, L., Manatschal, G., 2006. A mechanism to thin the continental lithosphere at magma-poor margins. *Nature* 440, 324–328. <https://doi.org/10.1038/nature04608>.
- Lee, Muirhead J.D., Fischer, T.P., Ebinger, C.J., Kattenhorn, S.A., Sharp, Z.D., Kianji, G., 2016. Massive and prolonged deep carbon emissions associated with continental rifting. *Nat. Geosci.* 9, 145–149. <https://doi.org/10.1038/ngeo2622>.
- Lei, C., Alves, T.M., Ren, J., Pang, X., Yang, L., Liu, J., 2019. Depositional architecture and structural evolution of a region immediately inboard of the locus of continental breakup (Liwan Sub-basin, South China Sea). *Geol. Soc. Am. Bull.* 131, 1059–1074. <https://doi.org/10.1130/B35001.1>.
- Leinfelder, R.R., Wilson, R.C.L., 1998. Third-order sequences in an Upper Jurassic rift-related second-order sequence, central Lusitanian Basin, Portugal. In: Graciansky, P.C. (Ed.), *Mesozoic and Cenozoic Sequence Stratigraphy of European Basins*, vol. 60. Society of Economic Palaeontologists and Mineralogists Special Publication, pp. 507–525. <https://doi.org/10.2110/pec.98.02.0507>.
- Light, M.P.R., Maslany, M.P., Greenwood, R.J., Banks, N.L., 1993. Seismic sequence stratigraphy and tectonics offshore Namibia. In: Williams, G.D., Dobb, A. (Eds.), *Geol. Soc. (Lond.) Spec. Publ.* vol. 71. pp. 163–191. <https://doi.org/10.1144/GSL.SP.1993.071.01.08>.
- Lima, C., 2003. Ongoing Compression across South American Plate: observations, numerical modelling and some implications for petroleum geology. In: Ameen, M. (Ed.), *Fracture and In-Situ Stress Characterization of Hydrocarbon Reservoirs*, vol. 209. Geological Society, London, Special Publications, pp. 87–100. <https://doi.org/10.1144/GSL.SP.2003.209.01.09>.
- Lizarralde, D., Axen, G.J., Brown, H.E., Fletcher, J., González-Fernández, A., Harding, A.J., Holbrook, W.S., Kent, G.M., Paramo, P., Sutherland, F., Umhoefer, P.J., 2007. Variation in styles of rifting in the Gulf of California. *Nature* 448, 466–469. <https://doi.org/10.1038/nature06035>.
- Lundin, E., Doré, A.G., 2002. Mid-Cenozoic post-breakup deformation in the 'passive' margins bordering the Norwegian–Greenland Sea. *Mar. Petrol. Geol.* 19, 79–93. [https://doi.org/10.1016/S0264-8127\(01\)00046-0](https://doi.org/10.1016/S0264-8127(01)00046-0).
- Ma, T., Chen, P., 2015. A wellbore stability analysis model with chemical-mechanical coupling for shale gas reservoirs. *J. Nat. Gas Sci. Eng.* 26, 72–98. <https://doi.org/10.1016/j.jngse.2015.05.028>.
- Ma, T., Chen, P., Yang, C., Zhao, J., 2015. Wellbore stability analysis and well path optimization based on the breakout width model and Mogi–Coulomb criterion. *J. Petrol. Sci. Eng.* 135, 678–701. <https://doi.org/10.1016/j.petrol.2015.10.029>.
- Ma, T., Wu, B., Fu, J., Zhang, Q., Chen, P., 2017. Fracture pressure prediction for layered formations with anisotropic rock strengths. *J. Nat. Gas Sci. Eng.* 38, 485–503. <https://doi.org/10.1016/j.jngse.2017.01.002>.
- Magoon, L.B., Beaumont, E.A., 1999. Chapter 3, "petroleum systems. In: Beaumont, E.A., Foster, N.H. (Eds.), *Exploring for Oil and Gas Traps*, Treatise of Petroleum Geology, Handbook of Petroleum Geology. American Association of Petroleum Geologists, pp. 1150.

- McKenzie, D., 1978. Some remarks on the development of sedimentary basins. *Earth Planet Sci. Lett.* 40, 25–32. [https://doi.org/10.1016/0012-821X\(78\)90071-7](https://doi.org/10.1016/0012-821X(78)90071-7).
- Marfurt, K.J., Alves, T.M., 2015. Pitfalls and limitations in seismic attribute interpretation of tectonic features. *Interpretation* 3 <https://doi.org/10.1190/INT-2014-0122.1>. SB5-SB15.
- Mattos, N.H., Alves, T.M., Omosanya, K.O., 2016. Crestal fault geometries reveal late halokinesis and collapse of the Samson Dome, Northern Norway: implications for petroleum systems in the Barents Sea. *Tectonophysics* 690, 76–96. <https://doi.org/10.1016/j.tecto.2016.04.043>.
- Manatschal, G., Bernoulli, D., 1998. Rifting and early evolution of ancient ocean basins: the record of the Mesozoic Tethys and of the Galicia-Newfoundland margins. *Mar. Geophys. Res.* 20, 371–381. <https://doi.org/10.1023/A:1004459106686>.
- Mauduit, T., Guerin, G., Brun, J.P., Lecanu, H., 1997. Raft tectonics: the effects of basal slope angle and sedimentation rate on progressive extension. *J. Struct. Geol.* 19, 1219–1230. [https://doi.org/10.1016/S0191-8141\(97\)00037-0](https://doi.org/10.1016/S0191-8141(97)00037-0).
- Meier, T., Rybacki, E., Backers, T., Dresen, G., 2015. Influence of bedding angle on borehole stability: a laboratory investigation of transverse isotropic oil shale. *Rock Mech. Rock Eng.* 48, 1535–1546. <https://doi.org/10.1007/s00603-014-0654-1>.
- Mello, M.R., Azambuja Filho, N.C., Bender, A.A., Barbanti, S.M., Mohriak, W., Schmitt, P., Jesus, C.L.C., 2012. In: Mohriak, W.U., Danforth, A., Post, P.J. (Eds.), *The Namibian and Brazilian Southern South Atlantic Petroleum Systems: Are They Comparable Analogues?*, vol. 369. Geological Society, London, Special Publications, pp. 249–266. <https://doi.org/10.1144/SP369.18>.
- Merle, R., Jourdan, F., Girardeau, J., 2018. Geochronology of the Tore-Madeira Rise seamounts and surrounding areas: a review. *Aust. J. Earth Sci.* 65, 591–605. <https://doi.org/10.1080/0882120099.2018.1471005>.
- Meulenkamp, J.E., 1979. *Field Guide to the Neogene of Crete A32*. Publications of the Department of Geology and Paleontology, Univ. Athens, pp. 1–32.
- Miller, N.C., Lizarralde, D., 2013. Thick evaporites and early rifting in the Guaymas basin, Gulf of California. *Geology* 41, 283–286. doi: 10.1130/G33747.1.
- Minshull, T., 2009. Geophysical characterisation of the ocean–continent transition at magma-poor rifted margins. *Compt. Rendus Geosci.* 341, 382–393. <https://doi.org/10.1016/j.crte.2008.09.003>.
- Miranda, R., Valadares, V., Terrinha, P., Mata, J., Azevedo, M.R., Gaspar, M., Kullberg, J.C., Ribeiro, C., 2009. Age constraints on the Late Cretaceous alkaline magmatism on the west Iberian margin. *Cretaceous Res.* 30, 575–586. <https://doi.org/10.1016/j.cretres.2008.11.002>.
- Mohriak, W.U., Leroy, S., 2012. Architecture of rifted continental margins and break-up evolution: insights from the south atlantic, North Atlantic and Red Sea–Gulf of aden conjugate margins. In: Mohriak (Ed.), *Conjugate Divergent Margins*. Geol. Soc. (Lond.), vol. 369. Spec. Publ., pp. 497–535. <https://doi.org/10.1144/SP369.17>.
- Monteleone, V., Minshull, T.A., Marin-Moreno, H., 2019. Spatial and temporal evolution of rifting and continental breakup in the Eastern Black Sea Basin revealed by long-offset seismic reflection data. *Tectonics*. <https://doi.org/10.1029/2019TC005523>.
- Moore, J., 1992. A syn-rift to post-rift transition sequence in the Main Porcupine Basin, offshore western Ireland. In: Parnell, J. (Ed.), 62. Geological Society (London) Special Publications, pp. 333–349. <https://doi.org/10.1144/GSL.SP.1992.062.01.26>.
- Moreira, J.L.P., Madeira, C.V., Gil, J.A., Machado, M.A.P., 2007. *Bacia de Santos*. *Buletin de Geociências da Petrobras* 15, 531–549.
- Mount, V.S., Suppe, J., 1987. State of stress near the San Andreas fault: implications for wrench tectonics. *Geology* 15, 1143–1146. [https://doi.org/10.1130/0091-7613\(1987\)15<1143:SOSNTS>2.0.CO;2](https://doi.org/10.1130/0091-7613(1987)15<1143:SOSNTS>2.0.CO;2).
- Ndiaye, M., Ngom, P.M., Gorin, G., Villeneuve, M., Sartori, M., Medou, J., 2016. A new interpretation of the deep-part of Senegal-Mauritanian Basin in the Diourbel-Thies area by integrating seismic, magnetic, gravimetric and borehole data: implication for petroleum exploration. *J. Afr. Earth Sci.* 121, 330–341. <https://doi.org/10.1016/j.jafrearsci.2016.06.002>.
- Nemčok, M., Henk, A., Allen, R., Sikora, P.J., Stuart, C., 2012. In: Mohriak, W.U., Danforth, A., Post, P.J., Brown, D.E., Tari, G.C., Nemčok, M., Sinha, S.T. (Eds.), *Conjugate Divergent Margins*. Geological Society, London, Special Publications, pp. 369. <https://doi.org/10.1144/SP369.8>.
- Neres, M., Miranda, J.M., Font, E., 2013. Testing Iberian kinematics at Jurassic-cretaceous times. *Tectonics* 32, 1312–1319. <https://doi.org/10.1002/tect.20074>.
- Neres, M., Terrinha, P., Custódio, S., Silva, S.M., Luis, J., Miranda, J.M., 2018. Geophysical evidence for a magmatic intrusion in the ocean–continent transition of the SW Iberia margin. *Tectonophysics* 744, 118–133. <https://doi.org/10.1016/j.tecto.2018.06.014>.
- Nilsen, T.H., Sylvester, A.G., 1995. Strike–slip basins. In: Busby, C., Ingersoll, R. (Eds.), *Tectonics of Sedimentary Basins*. Blackwell Science, Oxford, pp. 425–456.
- Norcliffe, J.R., Paton, D.A., Mortimer, E.J., McCaig, A.M., Nicholls, H., Rodriguez, K., Hodgson, N., van der Spuy, D., 2018. Laterally Confined Volcanic Successions (LCVS); recording rift-jumps during the formation of magma-rich margins. *Earth Planet Sci. Lett.* 504, 53–63. <https://doi.org/10.1016/j.epsl.2018.09.033>.
- Nova Scotia Department of Energy, 2016. Central Scotian Slope Study - Chapter 3 Stratigraphy. [https://energy.novascotia.ca/sites/default/files/.../Chapter%203%20Stratigraphy\(1\).pdf](https://energy.novascotia.ca/sites/default/files/.../Chapter%203%20Stratigraphy(1).pdf).
- Omosanya, K.O., Eruteya, O.E., Suregar, E.S.A., Zieba, K.J., Johansen, S.E., Alves, T.M., Waldmann, N.D., 2018. Three-dimensional (3-D) seismic imaging of conduits and radial faults associated with hydrothermal vent complexes (Vøring Basin, Offshore Norway). *Mar. Geol.* 399, 115–134. <https://doi.org/10.1016/j.margeo.2018.02.007>.
- Parsons, A.J., Whitham, A.G., Kelly, S.R.A., Vautravers, B.P.H., Dalton, T.J.S., Andrews, S.D., Pickles, C.S., Strogen, D.P., Braham, W., Jolley, D.W., Gregory, F.J., 2017. Structural evolution and basin architecture of the Traill Ø region, NE Greenland: a record of polyphase rifting of the East Greenland continental margin. *Geosphere* 13, 733–770. <https://doi.org/10.1130/GES01382.1>.
- Pascal, Ch., 2015. Heat flow of Norway and its continental shelf. *Mar. Petrol. Geol.* 66, 956–969. <https://doi.org/10.1016/j.marpetgeo.2015.08.006>.
- Pedersen, J.H., Karlsen, D.A., Backer-Owe, K., Lie, J.E., Brunstad, H., 2006. The geochemistry of two unusual oils from the Norwegian North Sea: implications for new source rock and play scenario. *Petrol. Geosci.* 12, 85–96. <https://doi.org/10.1144/1354-079305-658>.
- Peel, F.J., 2014. How do salt withdrawal minibasins form? Insights from forward modelling, and implications for hydrocarbon migration. *Tectonophysics* 630, 222–235. <https://doi.org/10.1016/j.tecto.2014.05.027>.
- Pereira, R., Alves, T.M., Mata, J., 2017. Alternating crustal architecture in West Iberia: a review of its significance in the context of NE Atlantic rifting. *J. Geol. Soc. Lond.* 174, 522–540. <https://doi.org/10.1144/jgs2016-050>.
- Piedade, A., Alves, T.M., 2017. Structural styles of Albian rafts in the Espírito Santo Basin (SE Brazil): evidence for late raft compartmentalisation on a ‘passive’ continental margin. *Mar. Petrol. Geol.* 79, 201–221. <https://doi.org/10.1016/j.marpetgeo.2016.10.023>.
- Pindell, J., Graham, R., Horn, B., 2014. Rapid outer marginal collapse at the rift to drift transition of passive margin evolution, with a Gulf of Mexico case study. *Basin Res.* 26, 701–725. <https://doi.org/10.1111/bre.12059>.
- Pinet, N., 2016. Far-field effects of Appalachian orogenesis: a view from the craton. *Geology* 44, 83–86. <https://doi.org/10.1130/G37356.1>.
- Pinheiro, L.M., Wilson, R.C.L., Reis, R.P., Whitmarsh, R.B., Ribeiro, A., 1996. The western Iberian margin: a geophysical and geological overview. In: Whitmarsh, R.B., Sawyer, D.S., Klaus, A., Masson, D.G. (Eds.), *Proceedings of the ODP, Scientific Results*, vol. 149. Ocean Drilling Program, College Station, TX, pp. 3–23.
- Pitman III, W.C., Andrews, J.A., 1985. Subsidence and Thermal History of Small Pull-Apart Basins, vol. 37. Society of Economic Paleontologists and Mineralogists Special Publication, pp. 45–119.
- Polteau, S., Mazzini, A., Hansen, G., Planke, S., Jerram, D.A., Millett, J., Abdelmalak, M.M., Blischke, A., Myklebust, R., 2019. The pre-breakup stratigraphy and petroleum system of the Southern Jan Mayen Ridge revealed by seafloor sampling. *Tectonophysics* 760, 152–164. <https://doi.org/10.1016/j.tecto.2018.04.016>.
- Postma, G., Drinia, H., 1993. Architecture and sedimentary facies evolution of a marine, expanding outer-arc half-graben (Crete, late Miocene). *Basin Res.* 5, 103–124. <https://doi.org/10.1111/j.1365-2117.1993.tb00060.x>.
- Quirk, D.G., Rüpke, L.H., 2018. Melt-induced buoyancy may explain the elevated rift-rapid sag paradox during breakup of continental plates. *Sci. Rep.* 8, 9985. <https://doi.org/10.1038/s41598-018-27981-2>.
- Rasmussen, E.S., Lomholt, S., Andersen, C., Vejbaek, O.V., 1998. Aspects of the structural evolution of the Lusitanian Basin in Portugal and the shelf and slope area offshore Portugal. *Tectonophysics* 300, 199–255. [https://doi.org/10.1016/S0040-1951\(98\)00241-8](https://doi.org/10.1016/S0040-1951(98)00241-8).
- Reeve, M.T., Jackson, C.A.-L., Bell, R.R., Magee, C., Bastow, I.D., 2015. The stratigraphic record of prebreakup geodynamics: evidence from the Barrow Delta, offshore Northwest Australia. *Tectonics* 35. <https://doi.org/10.1002/2016TC004172>.
- Reston, T.J., McDermott, K., 2011. Successive detachment faults and mantle unroofing at magma-poor rifted margins. *Geology* 39, 1071–1074. <https://doi.org/10.1130/G32428.1>.
- Ribes, C., Ghienne, J.-F., Manatschal, G., DeCarlis, A., Karner, G.D., Figueiredo, P.H., Johnson, C.A., 2019. Long-lived mega fault-scarps and related breccias at distal rifted margins: insights from present-day and fossil analogues. *J. Geol. Soc. Lond.* <https://doi.org/10.1144/jgs2018-181>.
- Ring, U., Brachert, T., Fassoulas, C., 2001. Middle Miocene graben development in Crete and its possible relation to large-scale detachment faults in the southern Aegean. *Terra Nova* 13, 297–304. <https://doi.org/10.1046/j.1365-3121.2001.00359.x>.
- Ritter, U., Zielinski, G.W., Weiss, H.M., Zielinski, R.L.B., Sættem, J., 2004. Heat flow in the Vøring basin, mid-Norwegian shelf. *Petrol. Geosci.* 10, 353–365. <https://doi.org/10.1144/1354-079303-616>.
- Ritzmann, O., Jokat, W., 2003. Crustal structure of northwestern Svalbard and the adjacent Yermak Plateau: evidence for Oligocene detachment tectonics and non-volcanic breakup. *Geophys. J. Int.* 152, 139–159. <https://doi.org/10.1046/j.1365-246X.2003.01836.x>.
- Roberts, D.G., Bally, A.W., 2012. *Regional Geology and Tectonics: Principles of Geologic Analysis*. Elsevier Science, pp. 404. <https://doi.org/10.1016/B978-0-444-53042-4.00070-4>.
- Rodríguez-Salgado, P., Childs, C., Shannon, P.M., Walsh, J.J., 2019. Structural evolution and the partitioning of deformation during basin growth and inversion: a case study from the Mizen Basin Celtic Sea, offshore Ireland. *Basin Res.* <https://doi.org/10.1111/bre.12402>.
- Rosleff-Soerensen, B., Reuning, L., Back, S., Kukla, P.A., 2012. Seismic geomorphology and growth architecture of a Miocene barrier reef, Browse Basin, NW-Australia. *Mar. Petrol. Geol.* 29, 233–254. <https://doi.org/10.1016/j.marpetgeo.2010.11.001>.
- Rosleff-Soerensen, B., Reuning, L., Back, S., Kukla, P.A., 2014. The response of a basin-scale Miocene barrier reef system to long-term, strong subsidence on a passive continental margin, Barcoo Sub-basin, Australian North West Shelf. *Basin Res.* 28. <https://doi.org/10.1111/bre.12100>.
- Rouby, D., Raillard, S., Guillocheau, F., Bouroulec, R., Nalpas, T., 2002. Kinematics of a growth fault/raft system on the West African margin using 3-D restoration. *J. Struct. Geol.* 24, 783–796. [https://doi.org/10.1016/S0191-8141\(01\)00108-0](https://doi.org/10.1016/S0191-8141(01)00108-0).
- Rowan, M., Jackson, M.P.A., Trudgill, B., 1999. Salt-related fault families and fault welds in the Northern Gulf of Mexico. AAPG (Am. Assoc. Pet. Geol.) Bull. 83, 1454–1484. <https://doi.org/10.1306/E4FD41E3-1732-11D7-8645000102C1865D>.
- Ruby, D., Raillard, S., Guillocheau, F., Bouroulec, R., Nalpas, T., 2002. Kinematics of a growth fault/raft system on the West African margin using 3-D restoration. *J. Struct. Geol.* 24, 783–796. [https://doi.org/10.1016/S0191-8141\(01\)00108-0](https://doi.org/10.1016/S0191-8141(01)00108-0).
- Rullkötter, J., Leythaeuser, D., Horsfield, B., Littke, R., Mann, U., Müller, P.J., Radke, M.,

- Schaefer, R.G., Schenck, H.-J., Schwofchou, K., Witte, E.G., Welte, D.H., 1988. Organic matter maturation under the influence of a deep intrusive heat source: a natural experiment for quantitation of hydrocarbon generation and expulsion from a petroleum source rock (Toarcian shale, northern Germany). *Org. Geochem.* 13, 847–856. [https://doi.org/10.1016/0146-6380\(88\)90237-9](https://doi.org/10.1016/0146-6380(88)90237-9).
- Salomon, E., Koehn, D., Passchier, C., Hackspacher, P.C., Glasmacher, U.A., 2015. Contrasting stress fields on correlating margins of the South Atlantic. *Gondwana Res.* 28, 1152–1167. <https://doi.org/10.1016/j.gr.2014.09.006>.
- Sandiford, M., Egholm, D.L., 2008. Enhanced intraplate seismicity along continental margins: some causes and consequences. *Tectonophysics* 457, 197–208. <https://doi.org/10.1016/j.tecto.2008.06.004>.
- Scheck-Wenderoth, M., Maystrenko, Y.P., 2008. How warm are passive continental margins? A 3-D lithosphere-scale study from the Norwegian margin. *Geology* 36, 419–422. <https://doi.org/10.1130/G24545A.1>.
- Scheck-Wenderoth, M., Maystrenko, Y.P., 2013. Deep control on shallow heat in sedimentary basins. *Energy Procedia* 40, 266–275. <https://doi.org/10.1016/j.egypro.2013.08.031>.
- Schettino, A., Turco, E., 2009. Breakup of Pangaea and plate kinematics of the central Atlantic and Atlas regions. *Geophys. J. Int.* 178, 1078–1097. <https://doi.org/10.1111/j.1365-246X.2009.04186.x>.
- Schmidt, S., 2014. *The Petroleum Potential of the Passive Continental Margin of South-Western Africa – A Basin Modelling Study*. Unpublished PhD Thesis, Wilhelmshaven, pp. 182.
- Schmitt, A.K., Martín, A., Weber, B., Stockli, D.F., Zou, H., Shen, C.C., 2013. Oceanic magmatism in sedimentary basins of the northern Gulf of California rift. *Geol. Soc. Am. Bull.* 125, 1833–1850. <https://doi.org/10.1130/B30787.1>.
- Schulte, S.M., Mooney, W.D., 2005. An updated global earthquake catalogue for stable continental regions: reassessing the correlation with ancient rifts. *Geophys. J. Int.* 161, 707–721. <https://doi.org/10.1111/j.1365-246X.2005.02554.x>.
- Segev, A., Avni, Y., Shahar, J., Wald, R., 2017. Late Oligocene and Miocene different seaways to the Red Sea–Gulf of Suez rift and the Gulf of Aqaba–Dead sea basins. *Earth Sci. Rev.* 171, 196–219. <https://doi.org/10.1016/j.earscirev.2017.05.004>.
- Segev, A., Sass, E., Schattner, U., 2018. Age and structure of the levant basin, eastern mediterranean. *Earth Sci. Rev.* 182, 233–250. <https://doi.org/10.1016/j.earscirev.2018.05.011>.
- Sengor, A.M.C., Burke, K., 1978. Relative timing of rifting and volcanism on Earth and its tectonic implications. *Geophys. Res. Lett.* 6, 419–421.
- Serié, Ch., Huse, M., Schødt, N.H., Brooks, J.M., Williams, A., 2017. Subsurface fluid flow in the deep-water Kwanza Basin, offshore Angola. *Basin Res.* 29, 149–179. <https://doi.org/10.1111/bre.12169>.
- Shipboard Scientific Party, 1979. Site 398. In: In: Sibuet, J.C., Ryan, W.B.F. (Eds.), *Initial Reports of the DSDP*, vol. 47. U.S. Government Printing Office, Washington, pp. 25–233.
- Shipboard Scientific Party, 2004. Leg 210 summary. In: In: Tucholke, B.E., Sibuet, J.-C., Klaus, A. (Eds.), *Proc. ODP, Init. Repts.*, vol. 210. Ocean Drilling Program, College Station, TX, pp. 1–78. <https://doi.org/10.2973/odp.proc.ir.210.101.2004>.
- Sibson, R.H., 1982. Fault zone models, heat flow, and the depth distribution of earthquakes in the continental crust of the United States. *Bull. Seismol. Soc. Am.* 72, 151–163.
- Sibson, R.H., 1994. Crustal stress, faulting and fluid flow. In: In: Parnell, J. (Ed.), *Geofluids: Origin, Migration and Evolution of Fluids in Sedimentary Basins*, vol. 78. Geological Society Special Publication, pp. 69–84.
- Sibuet, J.-C., Yeh, Y.-C., Lee, C.-S., 2016. Geodynamics of the south China sea. *Tectonophysics* 692, 98–119. <https://doi.org/10.1016/j.tecto.2016.02.022>.
- Sigal, J., 1979. Chronostratigraphy and eocrostratigraphy of Cretaceous formations recovered on DSDP Leg 47B. Site 398. In: *Initial Reports of the Deep-Sea Drilling Project*, vol. 47. U.S. Govt. Printing Office, Washington, pp. 287–326 2.
- Sinclair, I.K., 1995. In: In: Scrutton, R.A. (Ed.), *Sequence Stratigraphic Response to Aptian–Albian Rifting in Conjugate Margin Basins: a Comparison of the Jeanne d'Arc Basin, Offshore Newfoundland, and the Porcupine Basin, Offshore Ireland*, vol. 90. Geological Society, London, Special Publication, pp. 29–49. <https://doi.org/10.1144/GSL.SP.1995.090.01.02>.
- Skogseid, J., Planke, S., Faleide, J.I., Pedersen, T., Eldholm, O., Neverdal, F., 2000. NE Atlantic continental rifting and volcanic margin formation. In: In: Nøttvedt, A. (Ed.), *Dynamics of the Norwegian Margin*, vol. 167. Geological Society, London, Special Publications, pp. 295–326. <https://doi.org/10.1144/GSL.SP.2000.167.01.12>.
- Soares, D.M., Alves, T.M., Terrinha, P., 2012. The breakup sequence and associated lithospheric breakup surface: their significance in the context of rifted continental margins (West Iberia and Newfoundland margins, North Atlantic). *Earth Planet Sci. Lett.* 355–356, 311–326. <https://doi.org/10.1016/j.epsl.2012.08.036>.
- Soares, D.M., Alves, T.M., Terrinha, P., 2014. Contourite drifts on distal margins as indicators of established lithospheric breakup. *Earth Planet Sci. Lett.* 401, 116–131. <https://doi.org/10.1016/j.epsl.2014.06.001>.
- Soares, E.F., Zalán, P.V., Figueiredo, J.J.P., Trostdorf Jr., I., 2007. Bacia do Pará-Maranhão. *Buletin de Geociências da Petrobras* 15, 321–329.
- Souche, A., Schmid, D.W., Ruepke, L., 2017. Interrelation between surface and basement heat flow in sedimentary basins. *AAPG (Am. Assoc. Pet. Geol.) Bull.* 101, 1697–1713. <https://doi.org/10.1306/12051615176>.
- Stapel, G., Cloething, S., Pronk, B., 1996. Quantitative subsidence analysis of the Mesozoic evolution of the Lusitanian basin (western Iberian margin). *Tectonophysics* 266, 493–507. [https://doi.org/10.1016/S0040-1951\(96\)00203-X](https://doi.org/10.1016/S0040-1951(96)00203-X).
- Steckler, M.S., Watts, A.B., 1978. Subsidence of the Atlantic-type continental margin off New York. *Earth Planet Sci. Lett.* 41, 1–13. [https://doi.org/10.1016/0012-821X\(78\)90036-5](https://doi.org/10.1016/0012-821X(78)90036-5).
- Stein, S., Liu, M., Camelbeeck, Th., Merino, M., Landgraf, A., Hintersberger, E., Kübler, S., 2017. Challenges in assessing seismic hazard in intraplate Europe. In: In: Landgraf, A., Kübler, S., Hintersberger, E., Stein, S. (Eds.), *Seismicity, Fault Rupture and Earthquake Hazards in Slowly Deforming Regions*, vol. 432. Geological Society, London, Special Publications, pp. 13–28. <https://doi.org/10.1144/SP432.7>.
- Stephenson, A.E., Cadman, S.J., 1993. Browse Basin, Northwest Australia: the evolution, palaeogeography and petroleum potential of a passive continental margin. *Palaeogeogr. Palaeoclimatol. Palaeoecol.* 111, 337–366. [https://doi.org/10.1016/0031-0182\(94\)90071-X](https://doi.org/10.1016/0031-0182(94)90071-X).
- Storti, F., Holdsworth, R.E., Salvini, F., 2003. Intraplate strike-slip deformation belts. In: In: Storti, F., Holdsworth, R.E., Salvini, F. (Eds.), *Intraplate Strike-Slip Deformation Belts*, vol. 210. Geological Society, London, Special Publications, pp. 1–14. <https://doi.org/10.1144/GSL.SP.2003.210.01.01>.
- Sun, Q., Alves, T., Lu, X., Chen, C., Xie, X., 2019. True Volumes of Slope Failure Estimated From a Quaternary Mass-Transport Deposit in the Northern South China Sea. *Geophys. Res. Lett.* 45, 2642–2651. <https://doi.org/10.1002/2017GL076484>.
- Sun, Q., Alves, T., Xie, X., He, J., Li, W., Ni, X., 2017. Free gas accumulations in basal shear zones of mass-transport deposits (Pearl River Mouth Basin, South China Sea): An important geohazard on continental slope basins. *Mar. Petrol. Geol.* 81, 17–32. <https://doi.org/10.1016/j.marpetgeo.2016.12.029>.
- Svennevig, K., Guarnieri, P., Stemmerik, L., 2016. Tectonic inversion in the Wandel sea basin: a new structural model of Kilen (eastern north Greenland). *Tectonics* 35, 2896–2917. <https://doi.org/10.1002/2016TC004152>.
- Sykes, L., 1978. Intraplate seismicity, reactivation of preexisting zones of weakness, alkaline magmatism, and other tectonism postdating continental fragmentation. *Rev. Geophys. Space Phys.* 16, 621–688. <https://doi.org/10.1029/RG016i004p00621>.
- Tamanna, M.S., Hansen, Th., Borsato, R., Greenhalgh, J., Moussavou, M.R., Essongue, L.O., 2013. *Deepwater Hydrocarbon Prospectivity Analysis of Offshore North and South Gabon Basin*. PGS interim report, pp. 5.
- Tao, Z., Alves, T.M., 2016. The role of gravitational collapse in controlling the evolution of crestal fault systems (Espírito Santo Basin, SE Brazil). *J. Struct. Geol.* 92, 79–98. <https://doi.org/10.1016/j.jsg.2016.09.011>.
- Tari, G., Jabour, H., 2013. Salt tectonics along the Atlantic margin of Morocco. In: In: Mohriak, W.U., Danforth, A., Post, P.J. (Eds.), 369. Geological Society, London, Special Publications, pp. 337–353. <https://doi.org/10.1144/SP369.23>.
- Taugourdeau-Lantz, J., Azema, C., Hasenboehler, B., Masure, E., Moron, J., 1982. Évolution des domaines continentaux et marins de la marge portugaise (Leg 47B, site 398D) au cours du Crétacé; Essai d'interprétation par l'analyse palynologique compare S7-XXIV. *Bulletin de la Société Géologique de France*, pp. 447–459. <https://doi.org/10.2113/gssgfbull.S7-XXIV.3.447>.
- Teske, A., Lizarralde, D., Höfig, T.W., 2018. Expedition 385 Scientific Prospectus: Guaymas Basin Tectonics and Biosphere. *International Ocean Discovery Program* <https://doi.org/10.14379/iodp.sp.385.2018>.
- Trumbull, R.B., Reid, D., de Beer, C., van Acken, D., 2007. Magmatism and continental breakup at the west margin of southern Africa: a geochemical comparison of dolerite dikes from northwestern Namibia and the Western Cape. *S. Afr. J. Geol.* 110, 477–502. <https://doi.org/10.2113/gssajg.110.2-3.477>.
- Tucholke, B.E., Sibuet, J.-C., 2007. Leg 210 synthesis: tectonic, magmatic, and sedimentary evolution of the Newfoundland-Iberia rift: a synthesis based on ocean drilling through ODP Leg 210. In: In: Tucholke, B.E., Sibuet, J.-C., Klaus, A. (Eds.), *Proceedings of the ODP, Scientific Results*, vol. 210. Ocean Drilling Program, College Station, TX, pp. 1–56. <https://doi.org/10.2973/odp.proc.sr.210.101.2007>.
- Ulvrova, M.M., Brune, S., Williams, S., 2018. Breakup without borders: how continents speed up and slow down during rifting. *Geophys. Res. Lett.* 46. <https://doi.org/10.1029/2018GL080387>.
- Ward, N., Alves, T.M., Blenkinsop, T.G., 2018a. Differential compaction over Late Miocene submarine channels in SE Brazil: implications for trap formation. *Geol. Soc. Am. Bull.* 130, 208–221. <https://doi.org/10.1130/B31659.1>.
- Ward, N.I.P., Alves, T.M., Blenkinsop, T.G., 2018b. Submarine sediment routing over a blocky mass-transport deposit in the Espírito Santo Basin, SE Brazil. *Basin Res.* 30. <https://doi.org/10.1111/bre.12282>.
- Watts, A.B., Ryan, W.B.F., 1976. Flexure of the lithosphere and continental margin basins. *Tectonophysics* 36, 25–44. [https://doi.org/10.1016/0040-1951\(76\)90004-4](https://doi.org/10.1016/0040-1951(76)90004-4).
- Weijermars, R., Jackson, M.P.A., Vendeville, B., 1993. Rheological and tectonic modeling of salt provinces. *Tectonophysics* 217, 143–174. [https://doi.org/10.1016/0040-1951\(93\)90208-2](https://doi.org/10.1016/0040-1951(93)90208-2).
- White, N., McKenzie, D., 1988. Formation of the “steer’s head” geometry of sedimentary basins by differential stretching of the crust and mantle. *Geology* 16, 250–253. [https://doi.org/10.1130/0091-7613\(1988\)016<0250:FOTSSH>2.3.CO;2](https://doi.org/10.1130/0091-7613(1988)016<0250:FOTSSH>2.3.CO;2).
- White, N., Thompson, M., Barwise, T., 2003. Understanding the thermal evolution of deep-water continental margins. *Nature* 426, 334–343. [10.1038/nature02133](https://doi.org/10.1038/nature02133).
- Whitman, A.G., Price, S.P., Kelly, S.R.A., Koraini, A.M., 1999. Cretaceous (post-Valanginian) sedimentation and rift events in northeastern Greenland (71°–77°N). In: Fleet, A.J., Boldy, S.A.R. (Eds.), *Petroleum Geology of Northwest Europe: Proceedings of the 5th Conference*. Geological Society, London, pp. 325–336. <https://doi.org/10.1144/0050325>.
- Whitmarsh, R.B., Minshull, T.A., Russell, S.M., Dean, S.M., Loudon, K.E., Chian, D., 2001. The role of syn-rift magmatism in the rift-to-drift evolution of the West Iberia continental margin: geophysical observations. In: In: Wilson, R.C.L., Whitmarsh, R.B., Taylor, B., Frotzheim, N. (Eds.), *Non-Volcanic Rifting of Continental Margins: A Comparison of Evidence from Land and Sea*, vol. 187. Geological Society, London, Special Publications, pp. 107–124. <https://doi.org/10.1144/GSL.SP.2001.187.01.06>.
- Whitney, B.B., Clark, D., Hengesh, J.V., Bierman, P., 2016. Paleoseismology of the Mount Narryer fault zone, Western Australia: a multistrand intraplate fault system. *Geol. Soc. Am. Bull.* 128, 684–704. <https://doi.org/10.1130/B31313.1>.
- Wilkinson, M., Hazzeldine, R.S., 2011. Oil charge preserves exceptional porosity in deeply buried, overpressured, sandstones: central North Sea, UK. *J. Geol. Soc.* 168, 1285–1295. <https://doi.org/10.1144/0016-76492011-007>. London.

- Wilson, D.S., 1992. Focused mantle upwelling beneath mid-ocean ridges: evidence from seamount formation and isostatic compensation of topography. *Earth Planet Sci. Lett.* 113, 41–55. [https://doi.org/10.1016/0012-821X\(92\)90210-M](https://doi.org/10.1016/0012-821X(92)90210-M).
- Wilson, R.C.L., Hiscott, R.N., Willis, M.G., Gradstein, F.M., 1989. The Lusitanian Basin of West-Central Portugal: Mesozoic and Tertiary Tectonic, Stratigraphy, and Subsidence History, vol. 46. *Memoir of the American Association of Petroleum Geologists*, pp. 341–361. <https://doi.org/10.1306/M46497C22>.
- Wilson, R.C.L., Manatschal, G., Wise, S., 2001. In: Wilson, R.C.L. (Ed.), *Rifting along Non-volcanic Passive Margins: Stratigraphic and Seismic Evidence from the Mesozoic Successions of the Alps and Western Iberia*, vol. 187. Geological Society, London, Special Publication, pp. 429–452. <https://doi.org/10.1144/GSL.SP.2001.187.01.21>.
- Wolin, E., Stein, S., Pazzaglia, F., Meltzer, A., Kafka, A., Berti, C., 2012. Mineral, Virginia, earthquake illustrates seismicity in a passive-aggressive margin. *Geophys. Res. Lett.* 39, L02395. <https://doi.org/10.1029/2011GL050310>.
- Wygrala, B.P., 1989. *Integrated study of an oil field in the southern Po Basin, northern Italy*. Ber. Kernforsch. Julich 2313, 217 ISSN 0366–0885.
- Xie, X., Heller, P.L., 2009. Plate tectonics and basin subsidence history. *Geol. Soc. Am. Bull.* 121, 55–64. <https://doi.org/10.1130/B26398.1>.
- Zachariah, A.-J., Gawthorpe, R., Dreyer, T., Corfield, S., 2009. Controls on early post-rift physiography and stratigraphy, lower to mid-Cretaceous, North Viking Graben, Norwegian North Sea. *Basin Res.* 21, 189–208. <https://doi.org/10.1111/j.1365-2117.2008.00371.x>.
- Zhao, F., Alves, T.M., Li, W., Wu, S., 2015. Recurrent slope failure enhancing source rock burial depth and seal unit competence in the Pearl River Mouth Basin, offshore South China Sea. *Tectonophysics* 643, 1–7. <https://doi.org/10.1016/j.tecto.2014.12.006>.
- Zhao, F., Alves, T.M., Wu, S., Li, W., Huuse, M., Mi, L., Sun, Q., Ma, B., 2016. Prolonged post-rift magmatism on highly extended crust of divergent continental margins (Baiyun Sag, South China Sea). *Earth Planet Sci. Lett.* 445, 79–91. <https://doi.org/10.1016/j.epsl.2016.04.001>.
- Zobach, M.L., Zobach, M.D., 1989. Chapter 24: tectonic stress field of the continental United States. In: Pakiser, L.C., Mooney, W.D. (Eds.), *Geophysical Framework of the Continental United States*, Boulder, Colorado. Geological Society of America Memoir 172, pp. 523–540. <https://doi.org/10.1130/MEM172-p523>.